UNIVERSITY OF OKLAHOMA

GRADUATE COLLEGE

COMBUSTION CHARACTERISTICS OF THREE-COMPONENT FUEL BLENDS IN A POROUS MEDIA BURNER AT LEAN CONDITIONS

A THESIS

SUBMITTED TO THE GRADUATE FACULTY

in partial fulfillment of the requirements for the

Degree of

MASTER OF SCIENCE

By

FLAVIO I. MORENO OVALLE
Norman, Oklahoma
2017

COMBUSTION CHARACTERISTICS OF THREE-COMPONENT FUEL BLENDS IN A POROUS MEDIA BURNER AT LEAN CONDITIONS

A THESIS APPROVED FOR THE
SCHOOL OF AEROSPACE AND MECHANICAL ENGINEERING

BY

_____
Dr. R. N. Parthasarathy, Co-chair

_____
Dr. S. R. Gollahalli, Co-chair

_____
Dr. W. E. Merchan-Merchan

Para Francisco, Anabella y Diego.

"Combustion is without exaggeration the most important [chemical] reaction to humanity. […] The first real progress [humankind] made in [its] ascent or descent from the anthropomorphic missing link depended upon [its] control of fire or combustion; and in many ways our further progress depends upon more intelligent and efficient control of combustion."

George G. Brown
Proceedings of the First Symposium on Combustion

Acknowledgments

I would like to express my immeasurable and deepest gratitude to my thesis advisors Dr. Ramkumar N. Parthasarathy and Dr. Subramanyam R. Gollahalli for their guidance, patience, and support throughout this entire process. I have no doubt that I would not have been able to complete this challenge without their constant encouragement and motivation. I am sure that the knowledge that we were able to share, and the lessons they taught me (inside and outside the classroom) will stay with me for life and will help me become a better engineer and a better person. I thank Dr. Parthasarathy for being a guide, a mentor, and a great role model from the earliest moments of my life at OU until this very moment. I owe him for always believing in me, and for helping me find reaches of my potential that I never knew I had. The passion with which he engages in his craft and his impeccable way of teaching will always be an inspiration to pursue excellence. I thank Dr. Gollahalli for his wisdom and his willingness to share it. I will never be able to repay the science, engineering and life lessons that I directly or indirectly learned from him. There is no question that without his guidance I would not have treasured my field of study the way I do. I thank them both for financially supporting me during my graduate studies, allowing me to focus solely on the completion of this degree.

I thank Dr. Wilson E. Merchan-Merchan for his advice, and for the knowledge he shared with me inside and outside the classroom. I am in deep appreciation for his willingness to be a part of my thesis defense committee and cannot assign a value to his commitment and his contributions to improve my work.

I would like to recognize the help received by the school of Aerospace and Mechanical Engineering at the university of Oklahoma, and the administrative staff. Special thanks to Mrs. Kate O'Brien, Mrs. Melissa Foster, Mrs. Rebecca Norris, and Mrs. Debra Mattax for their unconditional support. Additionally, I would like to thank all my teaching assistant supervisors, Dr. K. Nawaz, Dr. J. Baldwin, Dr. C. Dalton, Dr. K. Gramoll, and Mr. Andy Ferguson for their support and all the knowledge I acquired from them.

I would like to express gratitude to the AME Machine Shop team, especially Mr. Billy Mays and Mr. Greg Williams for their expertise which helped me design and modify my experimental setup, for the genuine care, and for the little talks that will always remain as a bond of friendship and appreciation.

I am extremely thankful to my friend, and brother in arms, Dr. Arun Balakrishnan for all the conversations and discussions that took place in the Combustion Lab. which spanned almost every imaginable topic. I am forever grateful for the knowledge he shared with me throughout my graduate studies. I would also like to thank the rest of

the Combustion Lab. team Mohamad Imran, Alex Spens, Jesse Harter, Tonci Maleta and Bach Duong for all the rewarding discussions and conversations that took place in the lab and outside of it.

I would like to extend a recognition to the Davis UWC Scholar foundation, and the Holden family who made this entire project a reality. I would like to highlight the never ending support and friendship that I received from the people in charge of the program at OU; Craig Hayes, Tony Lee, and Vianne Hinsdale. Additionally, I would like to acknowledge all the care, and guidance that I received from my friend and padrino Luis Salvatierra. Many thanks, also, to all the various student associations and their members who made Oklahoma a home; PANAM, TUW, BISA, and the AME Graduate Student Community.

Lastly, I would like to thank my parents Francisco and Anabella and their undying and unconditional love. I am well aware that without their care, and emotional support this journey would have been significantly more difficult. I thank my brother, Diego, for always being there and for bringing a smile to my face even in the hardest times. I thank all of my friends, who never abandoned me, and all of my teachers, who never left me astray. This thesis is for you!

Thank You!

Table of Contents

List of Tables

List of Figures

Abstract

The increasing energy demand and the growing concern over the environmental impact caused by the combustion of fossil fuels require the development of effective alternative fuel sources. Biodiesels and bio-alcohols are attractive alternatives to liquid petroleum-based fuels. Biodiesels, such as soy methyl ester can be produced from renewable resources by transesterification of vegetable oils. Methyl esters have properties similar to those of petroleum-based fuels which allow them to be blended with petroleum fuels and to be used in existing infrastructure with minimal or no modification. Alcohols can be produced from renewable resources through the distillation of sugar, and starch crops. Adding alcohols such as butanol to a biofuel-petroleum blend extends the miscibility limits of the blend, increases the content of renewable components, and the concentration of fuel-bound oxygen in the fuel. The characteristics of the blends of alternative fuels and petroleum-based fuels (up to 20% content of alternative fuels) did not vary significantly with respect to a neat petroleum fuel in terms of performance indicators such as heating value or adiabatic flame temperature.

Porous media combustors offer several unique characteristics and advantages when compared to conventional burners, such as an enhanced heat transfer between the combustion products and the reactants, improved mixing of the unburned mixture, and improved evaporation of liquid fuels. These unique characteristics allows for flame

stabilization at lean and ultra-lean combustion conditions which suppress the formation of pollutants like NOx and CO. Porous media burners have been developed for application such as furnaces, gas turbines, steam generators, and heating systems.

The porous media burner used in this study consisted two different chambers; a flame chamber fixed on top of a spray chamber with the porous media encased between them. The flame chamber (4.3 cm each side, and 27 cm tall) was manufactured out of stainless steel, it was fitted with tempered glass windows in the front and rear sides to allow flame visualization. In addition, it had two lateral 1 cm wide slots to perform probe or thermocouple measurements. The spray chamber had slightly larger dimensions (5 cm square, and 30 cm high) and was located upstream the flame chamber and the porous media casing. It was fitted with four tempered glass windows in order to observe the quality of the spray. Two silicon carbide porous media were used in the burner; an evaporation porous medium (EPM) was the upstream segment of the porous burner. The EPM had pores of diameter 0.75 mm and a pore density of 31 pores per centimeter. The EPM served to enhance the spray evaporation by transferring trapped combustion heat to the fuel/air unburned mixture. It also functioned as a flashback barrier since the pore diameter was small enough to quench the reactions. The second porous medium was a combustion porous medium (CPM). The CPM was characterized by its low pore density (8 pores per cm) and relatively larger pores (diameter >1 mm). The CPM helped to enhance the mixing and stabilize the reactions. In this study, the flame was located downstream of the CPM. The porous media were held together in a two-part stainless steel casing with an inlet and outlet of square dimensions of 3.75 cm. Both halves of the

casing had inner dimensions corresponding to those of the porous media, and outer dimensions of 10 cm on each side.

Fuel was injected into a preheated (463 K) co-flowing environment using an air-blast atomizer upstream of the porous media. The experiments were carried using three different fuels Jet-A, a blend of 10% SME with 90% Jet-A (SA 10), and a 10% butanol-10%SME-80% Jet-A blend (BSA 10-10), and their combustion characteristics were studied at three different equivalence ratios, ϕ=0.5, ϕ=0.6, and ϕ=0.7 which were selected based on the stability of the flames in the fuel lean operation regime. Equivalence ratio was varied by changing the fuel flow rate and keeping the total air flow rate constant. Flame appearance was measured by taking photographs of the flame; exhaust global emissions and in-flame species concentration at 25%, 50% and 75% flame height were performed using a NOVA gas analyzer and a quartz sampling probe of 1mm aperture and a body of 6mm ID and 7.2mm OD; temperature measurements were carried using an in-house built R-type thermocouple at 25%, 50%, and 75% flame height; soot volume fraction was measured using a laser and a power meter, and the integrity of the burner after operation was addressed by measuring the pressure drop through each PM after operation.

The flames generated in the porous media burner were non-luminous, and blue due to the lean combustion conditions, enhanced evaporation of the reactants, and mixing mechanisms. Additionally, the presence of fuel-bound oxygen in the blend affected the luminosity and visible height of the flames as oxidation of the fuel occurred faster when

the concentration of fuel-bound oxygen was higher. The appearance of the flames and the soot volume fraction measurements showed that no measurable amount of soot was being generated by the flames. The emission indices of NOx were comparable for the all the fuel blends at a given equivalence ratio. Peak emission index for NOx was found to occur at ϕ= 0.6. It was concluded that the thermal NOx formation mechanism was the dominant mechanism in all cases studied since the highest peak in-flame temperatures for all fuels were recorded at ϕ=0.6. Radial in flame temperature profiles were uniform through the span of the PM as a consequence of the enhanced mixing, and homogeneous reaction produced by the presence of the porous media. Peak temperatures were similar for all flames, at all conditions, on every flame height recorded. The emission indices of CO were comparable for the all the fuel blends at any given equivalence ratio. Peak emission index for CO was found to occur at ϕ= 0.6. CO emission indices were significantly lower than those of open spray flames, and open flames which demonstrate the effects of the porous media burner in suppressing CO emissions. After 100 hours of operation while using blends the pressure drop across the EPM increased by 59 Pa, while pressure drop increased 2 Pa for the CPM.

Chapter 1: Introduction

It is an undeniable truth that fossil fuels started a revolution in technology that laid the foundations of modern civilization. However, the indiscriminate use of these energy sources has led to the increment in environmental pollution, and greenhouse gas emissions responsible for an accelerated global warming, and climate change. The growing concern over the harmful effects on the environment due to the use of fossil fuels paired with the volatility of the oil market are two top issues that are addressed by the investigation and development of alternative fuel sources.

At a point in history where the demand of energy is increasing at its most accelerated pace, it is crucial to supply such need with sustainable, yet effective sources. Emerging technologies which use wind energy and solar energy form one section of alternative energy utilization; however, there is a large portion of the industrial sector and the vast majority of the transportation sector that heavily rely on safe and easily transported fuel sources, such as liquid fuels. The use of biodiesels, and bio-alcohols (produced from renewable resources), paired with the development of new combustion technologies, offers an attractive alternative to the use of petroleum-based fuels.

1.1 The Addition of Biodiesels (Methyl Esters)

Biodiesels, such as soy methyl ester (SME) present a viable and attractive alternative to petroleum-based fuels in the energy market. These fuels are produced from a variety of sources ranging from organic waste, crops stover, algae, sugar cane, and vegetable oils. Such biofuels derived from vegetable oils and their blends with mineral fuels are already being used in power generation and diesel engines. Since the physical characteristics of these fuels are generally similar to those of petroleum-based fuels, both can be easily blended and used in existing infrastructure with minimal or no modification Aldana et al. (2014), Tsai et al. (2010).

Most vegetable oils are structured as a triglyceride; triglycerides contain three long hydrocarbon chains (fatty acids) which may have up to three double bonds in each chain, with each chain also containing an ester group ($RCO2R'$). The long chains of the triglycerides cause these compounds to have high molecular weights and high viscosities; by processing these compounds through transesterification, the triglycerides are broken up into smaller alkyl esters. Studies on biodiesels have been performed using different combustion methods such as compression ignition engines, gas turbines, spray flames, vaporized flames, etc.

1.2 The Addition of Alcohols

Alcohols present another source of attractive alternate fuels. They can also be produced from renewable sources through the distillation of sugar, starch crops, or from second generation sources such as lumber mill residues, and crops stover.

Short alcohols, such as methanol and ethanol, have been effectively used as fuel blend components. Blends of gasoline and small amounts of ethanol (up to 20%) can be used in internal combustion engines with no modification. The development of new engine technologies that allow higher alcohol concentration blends, and the already large ethanol production in the U.S. (equivalent to 0.6 million barrels of oil a day in 2010) are factors that have resulted in increased usage of alcohols as additives (Renewable fuel association, 2010).

As the cost of production of long-chain alcohols drops, the use of these types of compounds becomes more appealing because they possess more similar characteristics to those of conventional petroleum based fuels. Butanol (C_4H_9OH) can also be produced from renewable feed stocks, and is already considered a better alternative to short-chain alcohols because it has a heating value that is 41% higher than that of methanol, and 20% higher than that of ethanol. Also, butanol is a safer alternative to alcohols that are readily used as additives, such as ethanol, because it is less corrosive and less volatile than methanol and ethanol (Szulczyk, 2010).

1.3 Three-Component Blends

The addition of alcohol to a biodiesel-petroleum blend promises several benefits, such as extending the miscibility limits of the blend, and adding an increased content of the renewable components. Studies in engines with petroleum-biodiesel-methanol blends have shown that the performance characteristics of the engine, and NOx emissions did not change drastically, but the emission concentrations of CO, and unburned hydrocarbons decreased at high loads (Howell et al. 1996).

The addition of butanol to petroleum fuels/ biodiesel blends is an attractive idea due to the benefits provided by blending with butanol as well as the combined beneficial effects of the biofuel and the alcohol (which have oxygen present in them). Some studies have shown that butanol is a good addition to petroleum fuel/vegetable oil because butanol not only improves the blend characteristics such as lowering the cold filtering plugging point, and the kinematic viscosity, but also serves as a solvent for the vegetable oils (Atmanli et al., 2015). Also, engine studies indicate that the use of butanol-petroleum fuel blend results in less NOx emission than that obtained with the use of petroleum fuels (Carter et al. 2015).

1.4 Porous Media Combustion

Porous media burners offer the unique characteristic of enhancing heat transfer between the combustion products and the unburned reactants due to the presence of the porous media. The addition of a porous medium provides an environment in which more

effective mixing occurs. In the case of liquid fuel combustion, the presence of porous media in the combustor provides the conditions for liquid to be better vaporized. Because of the enhanced combustion conditions, porous media burners extend the flammability limits of the mixture, and help obtain higher reaction rates and flame speeds, (Howell et al.,1996). It is also established that due to the thermal interaction between the products, the porous matrix, and the reactants super-adiabatic flame temperatures can be achieved at the reaction zone, because the reactants 'borrow' energy form the burnt mixture Weinberg (1971).

The type and physical configuration of the porous matrix has a big influence on the nature of the reaction. The use of catalytic or non-catalytic porous media would result in different reaction behavior due to the chemical effects caused by the porous media. On the other hand, the use of a foam, a lattice, or a honey comb porous media would actively determine key characteristics of the flame behavior, such as mixing of the reactants, heat transfer properties, or flame temperature. Non-catalytic porous media tend to be seen as a better option for long use burners as they offer the best combination of cost and perceived advantages. Catalytic porous media tend to be manufactured out of costly materials, and due to the fact that the catalytic component is applied as a coating, the probability of blocked pores increases, thereby diminishing the effectiveness of the component. Notably, reticulated foam has been shown to provide a superior mixing and an adequate heat transfer when compared to lattices or honeycombs Gao et al. (2014).

Chapter 2: Literature Review

The contents of this chapter are a summary of previous studies on the use of alternative fuels, its benefits, and drawbacks, as well as studies done on combustion in porous media. The literature presented is mainly focused on studies involving porous media burners, or the addition of vegetable methyl ester, or alcohols, or both to fuel blends. The first section provides information on the blends of petroleum-based fuels with any or both of the aforementioned alternative fuels, and the second section does a similar job regarding porous media combustion.

2.1 Combustion of Petroleum Fuels and Alternative Fuels Blends

Yilmaz (2012) investigated the effects of intake air preheating on the performance and emission characteristics of a diesel engine fueled by a biodiesel-ethanol (85%-15%), and biodiesel-methanol (85%-15%) compared to those of diesel, and neat biodiesel. The experiment was carried out using a two cylinder, 4-cycle water-cooled engine at two different inlet conditions; preheated (85°C), and ambient (30°C). It was observed that biodiesel-alcohol mixtures presented higher brake specific fuel consumption at different load conditions when the inlet air was preheated. The BSFC measured for both biodiesel-alcohol blends was comparable between the two blends at any given air inlet temperature. At ambient temperature, both three-component blends produced 20% higher BSFC than diesel, and 10% higher than neat biodiesel. When the inlet air was

pre-heated, the use of both blends resulted in 38% higher BSFC when compared to neat diesel burned at ambient conditions, and 17% higher BSFC when compared to neat biofuel burned at ambient conditions. The effect of inlet preheating on the combustion emission of the blends was also measured; at 46% load condition, the biodiesel/methanol produced the highest CO concentration at the exhaust (43% higher than diesel) irrespective of the air intake temperature.

Air preheating had a stronger role while the biodiesel/ethanol blend was being used; at ambient condition CO concentration at the exhaust was measured to be 34% higher than with diesel, while at pre-heated conditions emissions were only 5% higher than diesel emissions. At 92% load conditions the CO emissions of biodiesel/methanol at both temperature conditions were comparable to those of diesel; the concentration values measured for the biodiesel/ethanol blend were 30% lower than those of diesel. At higher engine loads, the inlet temperature did not have any effect on CO emissions for any of the blends. NOx emissions measured for the biodiesel/alcohol blends were found to be lower than those of diesel for both engine loads tested, however they increased with increased inlet temperature. For instance, at 46% load, biodiesel/methanol at ambient conditions produced 38% less NOx than diesel while at pre-heated conditions NOx concentration was only 25% lower than diesel; for biodiesel/ethanol at ambient conditions the NOx concentration was 25% lower than the results measured for diesel, while at preheated conditions NOx concentrations were only 12% lower than that of diesel. At 92% engine load the measurements of NOx concentrations for all four study

cases did not vary more than 10% form the ones measured for diesel which implies that at higher loads inlet temperature had little effect on NOx formation.

Armas et al. (2014) documented the gaseous emissions, smoke opacity, and particle concentrations of a turbocharged direct ignition diesel engine running on two blends of diesel with alcohols (10% ethanol, and 16% butanol) tested at road load conditions. The authors found that the alcohol blends had slightly higher NOx emissions. The total mass of NOx [g] produced was recorded through a run of 1200 seconds. Neat diesel produced the least amount of NOx during the trial (2.0 g); followed by the butanol-diesel blend with an increment of 13% with respect to diesel; lastly, the blend with higher recorded emissions was the ethanol-diesel blend with NOx emissions measured at 2.40 g, a 20% increment with respect to neat diesel. The authors suggested that the higher emission of NOx measured for the blends was a result of the high oxygen concentration in the molecules, favoring the formation of these compounds. CO emissions were measured during the same time interval. Neat diesel produced the highest amount of CO [g] at 3.25 g; butanol/diesel, and ethanol/diesel blends produced comparable amounts of CO between each other, both 40% lower than the value measured by neat diesel. Unburned HCs emissions were low and comparable for all fuels measured at the same time interval (0.16 g). On the other hand, alcohol blends produced much lower emissions (40% less than pure diesel) during acceleration conditions. Alcohol blends, particularly ethanol-diesel, resulted in 50% lower smoke opacity values and particle concentrations than those of neat diesel, indicating the effects cause by fuel bound oxygen in the reduction of soot formation. The study points out the potential of alcohol-diesel blends

to reduce CO and particulate emissions, especially if the engines are tuned to burn these type of blends.

Imtenan et al. (2014) performed an experimental investigation that evaluates the comparative improvement of emission and performance characteristics of diesel and a palm methyl ester – diesel blend (20% PME, 80% diesel) when an additive such as ethanol, n-butanol, or diethyl ether is included in the blend. When the additional component is included in the blend, the resultant blend composition is 80% diesel, 15% PME, and 5% additive. The authors' findings include qualitative observations on the improved atomization of the three-component fuel (independent of the additive) supported by the improved combustion characteristics when compared to neat diesel or a two component blend. N-butanol was the additive with the highest calorific value (34.33 kJ/g), followed by diethyl ether (33.89 kJ/g) and ethanol (27.33 kJ/g). The resultant calorific value of the of the blends did not vary significantly between blends, diesel had a calorific value of 44.66 kJ/g, where the calorific value of the blends lied within 5% of an average value of 43.4 kJ/g. The power output [kW] of the engine while running on blends when the additive was butanol or diethyl ether was comparable to that of diesel. Power did not vary more than 5% between the diesel output and the blends output for a set range of speeds (1250rpm – 2500 rpm). Power outputs for the ethanol blend, and the two-component blend were 8% and 17% respectively less than that with diesel. For a given speed, diesel produced the highest emission concentration of CO at the exhaust, the CO concentration for the two component blend was typically 13% lower than that of diesel for the range of speed specified earlier. Among the three-

component blends, the blend containing diethyl ether produced the highest CO concentration (15% lower than diesel), followed by the butanol blend (25% lower than diesel), and lastly the ethanol blend (38% lower than diesel); this behavior was consistently observed through the range of speed used in the experiment. NOx emissions also were reduced by the presence of the additive, probably due to the lower calorific value of the blends. Diesel and the two-component blend had comparable NOx emission values throughout the range of speeds used during the experiment. NOx concentrations measured for the blends containing butanol and ethanol as additives were comparable among each but consistently lower than the NOx concentration of diesel (typically 10% lower). The three-component blend containing diethyl ether produced the least amount of NOx at the exhaust, typically 13% lower than the values given for diesel.

Tuccar et al. (2014) used diesel-microalgae biodiesel-butanol blends to characterize the performance and emission of a compression ignition engine. The ternary blends used for these study were 80% diesel, 20% biodiesel; 70% diesel, 20% biodiesel, 10% butanol; 60% diesel, 20% biodiesel, 20% butanol. The physical properties of the blends were not significantly different than those of pure diesel, density for example, ranged from 833 kg/m^3 for diesel, to 843 kg/m^3 corresponding to the 80% diesel, 20% biodiesel blend. The largest difference between cetane numbers was 9% which corresponded to the 60%-20%-20% blend with a CN of 51.6 and diesel which has a CN of 56.46. Maximum torque output decreased monotonically with the addition of alternative fuels, the maximum output was achieved with pure diesel (237 Nm), and the lowest output

was obtained with the 60%-20%-20% blend at 222 Nm, 6% lower than the maximum. On the other hand, the brake specific fuel consumption showed an opposite trend, with the lowest value corresponding to pure diesel, and the highest corresponding to the 60%-20%-20% blend (30% higher than diesel).

NOx emissions appeared to increase with the addition of microalgae biodiesel probably due to the better quality of combustion, and the higher temperatures achieved. The two-component blend produced the highest NOx concentration at the exhaust; NOx concentration for the blend was consistently 10% higher than that of diesel for a wide range of engine speeds (1200 rpm – 2800 rpm). The NOx measurements for the two three-component blends were comparable between each other (they did not vary more than 5% between blends), the measurements with these fuels were 15% lower than those with neat diesel through most of the speeds tested for the experiment. The reduced values of NOx concentration in blends in which butanol was present is presumably due to the lower heating values of butanol. CO emissions were reduced as the amount of alternative fuels increased in the blend, particularly for the blends containing butanol as these blends had a higher concentration of molecular bound oxygen. For the given range of speeds tested, the D80B20 blend consistently generated 12% less CO than neat diesel. The CO emissions for the D70B20But10 blend were comparable to the emission values recorded for the two component blend, however while increasing the butanol content (D60B20But20) the CO emissions were 19% lower than those measured for neat diesel. A similar trend to that of CO was observed in the measurement of smoke

opacity, as the blend with higher fuel-bound oxygen concentration (D60B20But20) had 50% lower smoke opacity than diesel.

Atmanli et al. (2015) analyzed the effects of n-butanol addition to diesel-vegetable oil blends on performance and emission characteristics of a diesel engine running at standard room conditions. The tests carried were conducted at full load, at eight different speeds between 1800 and 4400 rpm. The blends used were 70% diesel, 20% vegetable oil, and 10% butanol; the vegetable oils used for the experiment included canola, soy, sunflower, corn, olive and hazelnut. All the blends had similar lower heating values, which were on average 5% lower than that of diesel (43.38 MJ/kg), similarly the cetane number values of the blends were similar between each other, and were (on average) 11% lower than that of diesel (55.5). The three-component fuels consistently produced comparable (less than 5% variation) BSFC values between them across the range of speed specified for the experiment. While running on ternary blends, the engine had an average BSFC 43% higher than while running on diesel for most of the engine speeds chosen for the experiment. Brake power, however, did not vary more than 10% between the ternary blends and diesel at any given speed.

In terms of exhaust gases, ternary blends produced around 25% more NOx emissions than diesel throughout the entire range of speeds; blends containing canola and soy oil produced NOx values consistently lower (10% on average) than the rest of the ternary blends. Ternary blends also produced higher concentrations of CO at the exhaust, particularly at low engine speeds. CO emissions were comparable between ternary blends, at low engine speeds CO concentrations are on average 30% higher than the

values recorded for diesel, whereas at the higher end of the tested speeds the difference decreases to around 15%. Exhaust gas temperature was consistently 8% lower when the engine was running with ternary blends as compared to with diesel; the temperature of the exhaust gas for all ternary blends was comparable between the blends across the testing envelope.

Gómez et al. (2016) studied the blends of diesel and three groups of oxygenated and paraffinic alternative fuels and their soot tendencies taking pure low-sulphur diesel as the baseline. A standardized Smoke Point Lamp was used to find the smoke point of binary blends between (group 1) diesel and an animal fat biodiesel, non-oxygenated alternatives; (group 2) diesel and a hydro-threated vegetable oil (HVO); and (group 3) diesel and ethanol, or butanol. Different blend ratios were used in the experiment, ranging from 5% content of alternative fuel up to 80%. In order to summarize the authors' findings regarding blends with 10% alternative fuel only will be discussed in this section. At a blend ratio of 90% diesel with 10% alternative fuel content the heating value and the cetane number did not vary significantly (less than 7% difference) with respect to diesel. At the specified blend ratio, group 1 blends did not have any molecular-bound oxygen; the group two fuel had 1% (by mass) of molecular bound oxygen; where group three had 2%, and 4% (by mass) for butanol and ethanol respectively. The increase in fuel-bound oxygen concentration in the blend decreased the sooting tendency of the flame. The blends of diesel-alcohol (either ethanol or butanol) effectively suppressed soot formation (measured as smoke opacity) to a value 40% lower than that of diesel; the diesel/HVO blend which presented a value 10%

lower than the measured value for diesel; and group 1 additive blends had similar sooting tendencies to diesel. The authors attributed the different sooting profiles to the aromatic content of the fuel, fuel-bound oxygen concentration, unsaturation, and branching of the molecules.

2.2 Combustion in Porous Media

Jugjai et al. (2002) investigated the combustion of liquid fuels using a porous medium burner. The investigation was carried out by burning kerosene without the use of a spray atomizer, the fuel was supplied dropwise into the top surface of the evaporation porous medium and the combustion reaction took place on the lower surface of the porous medium where swirling air was supplied. The combustor was also equipped with a packed bead emitter downstream of the flame. Observations on the evaporation mechanisms, as well as the combustion process were made by measuring axial and radial temperature profiles of the flames, and emission characteristics without the pack emitter installed. It was determined that evaporation was enhanced by the presence of the porous medium to the point where kerosene (T_{evap}= 250°C) completely evaporated inside the solid porous matrix; the temperature at the top surface of the porous media was measured to be 200°C, and 400°C at the bottom surface. Stable combustion was obtained for equivalence ratios ranging between 0.38 and 0.86. The equivalence ratio was altered by changing the amount of swirling air entering the combustion chamber. The authors qualitatively describe complete combustion at the lower surface of the PM with no soot, or odor. For equivalence ratio between 0.4 and 0.7 the emission of CO does not significantly vary from an average value of 150 ppm, however at higher

equivalence ratios (ϕ = 0.86) the CO emissions increased drastically by 160% to values around 400 ppm presumably due to incomplete combustion. NOx emissions increase monotonically with equivalence ratio, at ϕ = 0.4 the NOx concentration was recorded as 100 ppm, whereas for the highest equivalence ratio such value was close to 160 ppm. Higher NOx values occurred at higher combustion temperatures, which suggest the dominance of thermal NOx formation.

Keramiotis et al. (2012) carries and experimental study on flame stability and combustion emissions on a two phase porous media using methane and liquefied petroleum gas (LPG) as fuels. A rectangular (130 x 185 mm) porous burner was used, the downstream section, or mixing chamber, was made out of high pore density alumina foam, and the upstream most section, or combustion zone made out of 10 ppi silicon carbide (SiC) foam. The burner was tested over a range of nominal thermal loads from 200 to 1000 kW/m^2 under various lean combustion conditions, while keeping the reaction stabilized inside the combustion foam. The study revealed stable operation within flashback and blowout limits for a wide range of thermal loads (200 to 1000 kW/m^2) and stoichiometry (excess air ratio, λ = 1.2, 1.4, 1.6). At the center of the burner CO emissions of LPG were found to be similar for all excess air ratios, and thermal load of 200 kW/m^2, maximum value was recorded for λ= 1.2 at 20 ppm, whereas the minimum was found to be 15 ppm corresponding to λ= 1.4. A similar behavior was observed for higher thermal loads. At the center of the burner, NOx emissions increased monotonically with the decrease of excess air. For LPG combustion and a thermal load of 200 kW/m^2 the lowest NOx concentration corresponded to λ= 1.6 with a value of 3

ppm, whereas the maximum was found to be 17 ppm corresponding to λ=1.2. The authors found that NOx emissions consistently increased by 20% with a 100% increment in thermal load. Temperature measured 1 mm above the PM burner varied within 20°C of the median (850°C for 200 kW/m^2, and 1200°C for 400 kW/m^2) for all excess air ratios; the temperature profiles where practically uniform across the width, and length of the porous media burner suggesting a thorough mixing of reactants during combustion. Almost identical results were obtained while using methane as fuel, concluding that such burner configuration has a good fuel interchangeability concerning emissions and burner operation. The burner also kept the capability of running at lean combustion regimes while providing constant thermal output.

Gao et al. (2014a) analyzed the effects that different foam materials had in a two-layer porous media burner for methane/air premixed combustion. The objective of the study was to determine the stability limits, flame temperature, and emissions of for a burner equipped with porous media of different materials. The porous media burner for this study used an upstream section packed with 3 mm alumina (Al_2O_3) beads, and cellular foam of different materials in the downstream section. The foam materials investigated were alumina, zirconia (ZrO_2), iron-chromium-aluminum (FeCrAl), and silicon carbide (SiC). The pore density was the same for all foams, 10 pores per inch (ppi), except for SiC foams for which different pore densities were studied (10, 20, 25, 30 ppi). The flames studied were stabilized inside the upstream section and it was determined by the authors that flame temperature was jointly controlled by heat release, heat loss, and heat transmission. The minimum stable flame velocity was found to be similar for all foams

with a recorded value close to 15 cm/s. FeCrAl was the material with the largest stability envelope, the highest flame velocity for this foam was measured to be 80 cm/s. SiC foams maximum speed varied with porosity; the 10 ppi foam generated flame speeds up to 70 cm/s, the 20 ppi foam up to 65 cm/s, 35 ppi up to 60 cm/s, and the 30 ppi foam maximum stable flame speed was 35 cm/s. Al_2O_3 and ZrO_2 foams produced stable flames at speeds 44% lower than those of FeCrAl. At a given flame speed (40cm/s), FeCrAl, and 10 ppi SiC produced the highest flame temperatures at a value of 1220°C; Al_2O_3 and ZrO_2 foams produced flame temperatures 100°C lower. CO emissions were not sensitive to the material and remained below 50 ppm for all tests. Unburned HC concentrations for the Al_2O_3, ZrO_2, and FeCrAl foams were almost constant for their stability envelope; however, flames generated with the ZrO_2 foams had an HC concentration of about 1300 ppm, which was twice more unburned HC than FeCrAl, and three times higher concentration than Al_2O_3. The HC concentration in the flame with SiC foam decreased with an increase in flame speed ,from 2500 ppm at 15 cm/s down to 500 ppm at 80 cm/s. NOx emission remained low (below 3 ppm) for all four materials. The authors concluded that flame stability limits expanded with increased foam conductivity, and pore density.

In another study Gao et al. (2014b) made a comparison study on the effects of different porous media shapes in a two-layer porous burner for the combustion of methane/air mixtures. Flame stability limits, flame temperature, flame speeds, and emissions were recorded for premixed flames stabilized over 13 mm alumina beads, 10 ppi (pores per inch) alumina foams, and 100 cpsi (combs per square inch) alumina honeycombs. The

study revealed that foams have the largest stability range with stable flame speeds ranging from 15 cm/s to 45cm/s, followed by beads (10 cm/s to 30 cm/s, and honeycombs with the narrowest (15 cm/s to 25 cm/s). The difference in stability range was directly attributed to the intricate path network that characterizes foams as well as the thin optical layer associated with them. For a given flame speed (25 cm/s), the packed beads produced the highest flame temperature (1150°C), honeycomb combustor flames generated flame temperatures 5% smaller than those produced by the packed beads combustor, foams generated flame temperatures that were 11% lower than those generated by the packed beads. The authors concluded that the foam burner generated lower temperatures due to the strong radiative heat transfer of the foam structure. The structure of the burner also affected emissions; CO emissions did not vary significantly across the stability range of all combustor types; however, the magnitude decreased in the order of foams (400 ppm), beads (120 ppm) and honeycombs (50 ppm). Honeycombs, however, presented the highest concentration of unburned hydrocarbons (20000 ppm), HC emissions for beads, and foams did not exceed 700 ppm. NO_x concentration was unaffected by the porous media configuration as the emissions for all three burners were found to be lower than 4 ppm at all conditions.

Pan et al. (2015) documented the premixed combustion characteristics of hydrogen/oxygen mixtures in a micro porous media combustor of different materials using numerical simulation. The study was carried out with the objective of designing a micro porous media burner to be used in a thermo-photovoltaic generator. The objective of the study was to investigate the effects that different parameters had on the

temperature of the porous media, emitter efficiency of the combustor, and temperature distribution through the porous matrix. The investigation was carried out by changing several crucial parameters such as porous media material (SiC, Si_3N_4, and Al_2O_3), equivalence ratio (0.6, 0.8, 1.0), and porosity of the porous media. The heat capacities for SiC, Si_3N_4, and Al_2O_3 are 275 J/kg*K, 690 J/kg*K, and 1000 J/kg*K respectively, The thermal conductivity values of SiC, Si_3N_4, and Al_2O_3 are 92 W/m*K, 31 W/m*K, and 25 W/m*K respectively. The simulation results showed that for equivalence ratio of 0.8 the temperature gradient for SiC was 175 K, for Si_3N_4 was 405 K, and for Al_2O_3 was 682 K from which it can be concluded that SiC would have a more uniform temperature distribution through the porous matrix allowing for intensified and more stable combustion.

Using the SiC porous matrix at an equivalence ratio of 1.0, the wall temperature of the porous medium was found to be 1400 K, with an emitter efficiency of 15.9%; At ϕ = 0.8, the temperature at the porous medium wall was recorded at 1350 K with an emitter efficiency of 18.2%; whereas for ϕ = 0.6 the simulated temperature at the wall was close to 1350 K, with an emitter efficiency of 14.1%. Optimal porosity was important for the micro combustor, as too high or too low porosities can influence the combustion behavior. The effects of porositiy were explored at ϕ=0.8 with a SiC porous foam. Porosities of 30%, 50%, and 70% were explored in the simulation. For a flow velocity of 9 m/s the pressure drop for 70%, 50%, and 30% porosities were 134 Pa, 140 Pa, and 45Pa respectively. The temperature gradients through the combustor (for the same conditions) were given as 510 K, 413 K, and 251 K for porosities of 70%, 50%, and

30% respectively. 50% porosity was the optimal balance between temperature distribution and pressure drop through the combustor. The simulation concluded that the best porous media for the the TPV micro combustor would be a SiC, 50% porous matrix at ϕ=0.8.

Mustafa et al. (2016) presented an experimental evaluation on the effects of several cooking oil-kerosene fuel blends for the combustion process used in thermoelectric (TE), and thermo-photovoltaic (TPV) power systems. Three different blends of vegetable cooking oil (VCO) and kerosene (K) were tested, 95%-05% VCOK, 90%-10% VCOK, 80%-20% VCOK. All three blends were used in both of the combustors, and the temperature distribution and emission profiles were recorded. TE electrical power output was especially sensitive to richer fuel mixtures as 400% increase in power output was achieved by increasing ϕ = 0.1 to ϕ = 1.1, and not too affected by the blend composition as the power output of one blend was within 5% of each other blend for a given condition. Temperature measured at the center of the burner had a peak at equivalence ratio ϕ = 0.7, the peak temperature measured above the burner (850°C) did not vary significantly with the fuel composition for this burner configuration. For this burner configuration, CO emissions had a non-monotonic variation with increase of equivalence ratio. The lowest measured concentration (350 ppm) occurred at equivalence ration 0.6; in the other hand the maximum recorded concentration reached 600 ppm at ϕ = 1.1. For a given equivalence ratio the blends with higher kerosene concentration produced as much as 18% more CO than that with the lowest amount of kerosene (95-05 VCOK). NOx monotonically decreased with the increase of

equivalence ratio from emission concentrations as high as 19 ppm for 95-05 VCOK at ϕ = 0.1 to 10 ppm for the same fuel at ϕ = 1.1. NOx emissions were consistently lower when the fuel had higher concentrations of kerosene. For instance, 80-20 VCOK produced 30% less NOx than 95-05 VCOK at any equivalence ratio. The TPV system was more influenced by the mixture composition, with the mixture with highest kerosene concentration yielding higher electrical output; 95-05 VCOK on average produced twice more power than the blend with lowest kerosene concentration. The axial temperature of the flame did not have a significant change with change of mixture, the peak temperature measured in this burner was close to 700°C for ϕ = 0.6. CO emissions had a non-monotonic variation with increase of equivalence ratio. The lowest measured concentration (230 ppm) occurred at equivalence ration 0.35; in the other hand the maximum recorded concentration reached 350 ppm at ϕ = 0.8. For a given equivalence ratio the kerosene concentration on the blends did not produce significant effect in the emission measurements as they were within 5% of each other. NOx monotonically decreased with the increase of equivalence ratio from emission concentrations as high as 13 ppm for 95-05 VCOK at ϕ = 0.1 to 4 ppm for the same fuel at ϕ = 1.1. NOx emissions were consistently lower when the fuel had higher concentrations of kerosene. For instance, 80-20 VCOK produced 30% less NOx than 95-05 VCOK for most of the combustion conditions.

Lapirattanakun and Charoensuk (2017) designed a cooking stove with a porous media burner operating in waste vegetable oil (WVO) and steam mixture as fuel. The porous region was created by packing 2 cm diameter ceramic balls in a 20cm OD, 10 cm ID, 15 cm height annular burner. The porous media region was used as a heat recirculation region, as well as a flame stabilizer. The vegetable oil was atomized using a high pressure nozzle, and the steam fuel-mixture was supplied into the porous media from the center cylinder. The steam supply was generated by vaporizing water using the heat recovered by the porous media region. Well-distributed temperatures throughout the porous media were achieved even if the firing rate was varied (345-1475 kW/m^2). Combustion performance was not negatively affected by the addition of steam at flow rates between 0.16-0.22 kg/min as the thermal efficiency did not vary more than 5% between different water flow rates at any given nominal firing rate. However, thermal efficiency varied drastically with the increase of firing rate (27% at 300 kW/m^2, and 7.5% for 1400 kW/m^2). At any given firing rate, the CO concentration increased with an increase in water flow rate; in the case of maximum thermal efficiency, CO concentrations measured with an added water flow rate of 0.16 kg/min were 50% lower than those measured with a water flow rate of 0.22 kg/min, similar magnitudes were observed at any given firing rate. On the other hand, NOx concentrations peaked when the flow rate of water added was 0.20 kg/min. At a firing rate of 300 kW/m^2, NOx concentration was measured to be 22 ppm when the water flow rate was 0.16 kg/min; 40 ppm was measured for 0.20 kg/s and 26 ppm for a water flow rate of 0.22 kg/min, similar trends were observed through the operational envelope; however, magnitudes decreased at higher firing rates.

In conclusion, the use of alternative fuels paired to petroleum-based fuels provides an alternative that does not compromise the performance of the combustion devices used due to the similar physical characteristics of the blend compounds, as well as a similar heating value of the blends and the pure fuels. The use of fuel blends paired with a porous media combustor generally yields lower NOx due to the reduced flame temperature obtained as a consequence of the fuel lean burning conditions that porous media allows carrying. CO emissions are generally reduced by the use of blends due to the increased presence of fuel-bound oxygen which allows for a quicker and more effective oxidation of the fuel.

Porous media burners appear to be advantageous while paired with alternative fuel blends since they provide the ability to stabilize a reaction at leaner conditions, and provide a better evaporation profile for any given fuel used. Due to these unique characteristics, porous media burners seem to be ideal to carry the combustion of liquid fuels, especially those with high boiling points such as vegetable methyl esters.

2.3 Problem Definition and Objective

The current study is primarily focused on the combustion characteristics of a ternary blend of Jet-A, SME, and butanol (80%-10%-10% by volume). Previous studies focused mainly on the performance of ternary blend fuels while used in internal combustion engines. Studies like that made by Imran (2015) focused only on the use of Jet-A/butanol blends on a porous media burner, while others like Barajas (2009) only focused on the combustion of petroleum based fuels/vegetable methyl esters on porous media. The present study is focused on investigating the effects on performance and emission characteristics of ternary blends flames, as well as the effects that such fuel will have on the burner.

The following specific objectives were set in order to study the combustion characteristics of a ternary blend fuel in a two-phase porous media burner at different equivalence ratios and controlled preheated co-flow environment.

- Measure and compare the global emissions of the fuels studied.
- Measure the radial in-flame concentration profiles of CO, NOx, CO_2, and O_2, at different flame heights.
- Measure the radial in-flame temperature profiles at different flame heights.
- Measure the relative soot volume fraction at the flame axis.

- Assess the effects of the blends on the injector, and the porous media burner.

  The fuels used in this study were Jet-A, Jet-A 90%-SME 10%, and Jet-A 80%-SME 10%- butanol 10%; at equivalence ratios 0.5, 0.6, 0.7, in a co-flow environment preheated to 463 K.

Chapter 3: Experimental Setup & Instrumentation

A description of the appropriate experimental setup is presented in the following chapter. The selection of the instrumentation was essential to adequately address the previously set objectives. The facility described, and a similar setup was used on previous studies by Periasamy (2007), Barajas (2009), Dahifale (2010) and Imran (2015).

3.1 Porous Media Combustion Setup

All experiments were carried at the Combustion and Flame Dynamics Laboratory located in the University of Oklahoma main campus. The experiments were conducted in a large steel combustion chamber (76cm on each side, and 163cm height) fitted with four pyrex glass windows, and connected to an exhaust duct, as seen in Figure 3.1. The ambient pressure of the laboratory was maintained at slightly higher than atmospheric in order to provide a positive draft in the laboratory combustion chamber so that flue gases did not leak into the laboratory installations.

The setup consisted of two different chambers; a flame chamber fixed on top of a spray chamber with the porous media encased between them. The flame chamber was manufactured out of stainless steel (4.3 cm each side, and 27 cm tall), it was fitted with

tempered glass windows in the front and rear sides to allow flame visualization. In addition, it had two lateral 1 cm wide slots to perform probe or thermocouple measurements. The spray chamber had slightly larger dimensions (5 cm square, and 30 cm high) and was located upstream the flame chamber, and the porous media casing. It was fitted with four tempered glass windows in order to observe the quality of the spray. The spray chamber would remain insulated to the environment if the spray was not being surveyed.

3.1.1 Porous Media

Two different non-catalytic porous reticulated foams were used in the study. Both matrices were made out of silicon carbide (SiSiC), with dimensions (4.0 x 4.0 x 2.5) cm each.

The evaporation porous media, EPM, was the upstream most segment of the burner. This segment of the burner had a relatively high pore density (31 ppcm, pores per centimeter), the pores were characterized by their small diameter (<0.75mm). The EPM was the section of the burner which served to enhance evaporation by transferring part of the heat generated during combustion to the unburned fuel/air mixture. Furthermore, the EPM also functioned as a flashback barrier, since the pore diameter was small enough to quench the reactions. A photograph of the EPM is displayed in Figure 3.3.

The combustion porous media, CPM, was characterized by its low pore density (8 ppcm) and the relatively large diameter of its pores (>1mm). This section had the purpose of enhancing the mixing process even further, as well as to stabilize the reaction, either at the section surface, or within the porous segment. In this study, the flames were located downstream the CPM. The CPM was the burner segment that recuperated the waste heat generated by the combustion reaction and transferred upstream to the EPM. All three heat transfer mechanisms played an important role in the CPM performance. A photograph of the CPM is displayed in Figure 3.4.

The porous media matrices were held together in a two-part stainless steel casing with inlet and outlet of square dimensions of 3.75cm. Both halves of the casing had inner dimensions corresponding to those of the porous media, and outer dimensions of 10 cm on each side. The porous media casing was insulated to the environment by a layer of fiber glass insulation. A schematic diagram of the enitre porous media burner setup is presented in Figure 3.5.

3.1.2 Preheated Co-Flow Air Supply

The co-flow air was supplied by the University of Oklahoma physical plant. In order to treat the air, the flow passed through a condenser on an ice bath to remove moisture. Downstream, the air was further dried by passing the flow through a packed bed of drierite (calcium sulphate 98%-cobalt chloride 2%) to dry it even further. Before being directed into the heating system, the air passed through a 0.1 micron filter to remove

any solid particles. The co-flow air supply was regulated with a calibrated rotameter. The details of the rotameter can be found in Table 3.1.

In order to pre-heat the co-flow supply the stream was split into two streams that were heated by two individual 120V ETS 52088-6 air process heaters which suplied 400W each. The two streams were reunited at a rectangular settling chamber (4cm x 4cm x 27cm) where the flow was straightened by a series of screens prior to entering the evaporation chamber. For the present experiments , the co-flow air was preheated to 463K. The setup was able to reach steady-state thermal conditions in 40 minutes, however prior to any experiment run the setup was let to heat for 90 minutes in order to ensure steady-state conditions. The settling chamber was insulated to the environment by a layer of fiber glass insulation in order to prevent excecive heat loss.

The temperature inside the settling chamber was meassured by two different 1mm diameter K-type (chromel-alumel) thermocouples placed at different sides of the chamber to monitor temperature uniformity. The power output of the heaters was regulated using an Omega CN79000 controller, and two solid state relays were fed with the output from the thermocouples .

3.1.3 Fuel Supply

The fuels were stored in a 3000ml stainless steel tank from which they were drawn and metered by a calibrated rotameter (the details of the rotameter can be found in Table 3.1). The fuel tank was pressurized to 1.4 atm by suppliying compressed nitrogen into the tank.

The fuel spray was generated inside of the spray chamber, and was directed towards the upstream face of the evaporation porous media. The fuel was atomized directly into the co-flow air stream which carried the vapour downstream.

A Delavan swirl model No. 3060-1 air blast atomizer served as the injector. It was attached to a 0.42 inner diameter, 0.63 cm outer diameter stainless steel tube. Atomizing air for the spray passed through a 1.28 ID, 1.90 cm OD pipe that was mounted concentrically around the fuel tube. The atomizing air supply was drawn out of a compressed air cylinder, and regulated with a calibrated rotameter (the details of the rotameter can be found in table 3.1). The atomizing air and the fuel were kept apart prior to the nozzle exit.

3.1.4 Fuels

Three fuels were the main components for the blends used in the study: aviation-grade kerosene (Jet-A), soy methylester (SME), and n-butanol. The experiments were carried using pure Jet-A, a blend of 10% SME with 90% Jet-A (SA 10), and a 10% butanol-

10%SME-80% Jet-A blend (BSA 10-10). Important properties of the neat component fuels, and the blends are summarized in Table 3.2.

Neat Jet-A had the highest heating value, followed by SME with a heating value 10% lower than that of Jet-A, and lastly n-butanol with a heating value about 25% lower than that of Jet-A. The considerably large difference in heating values between Jet-A and butanol was a limiting factor while deciding the blend fractions. Among the fuels used in this study Jet-A had the highest heating value, followed by SA 10, and BSA 10-10 with 1% and 4% lower heating values relative to Jet-A.

The amount of oxygen bound to the fuel molecules is a key factor in the combustion behavior of each blend. The parent fuel with the highest ammount of fuel-bound oxygen was n-butanol, in which the mass percentage of molecule-bound oxygen is 21%. Butanol is followed by SME with 11%, and Jet-A which has no oxygen in its chemical composition. The highest ammount of fuel-bound oxygen for the fuels used in this study corresponds to BSA 10-10 which has a 3% content by mass, followed by SA 10 with 0.9% content by mass.

The boiling point of butanol (390 K) is lower compared to that of Jet-A (418 K-573 K), and SME (619 K-678 K). The range of boiling points enabled butanol to evaporate before Jet-A, and SME. which allowed for the combustion reaction to start earlier when the blends contained butanol compared to the other fuels .

3.1.5 Test Conditions

Flame characteristics were measured at equivalence ratio (ϕ) conditions 0.5, 0.6, 0.7, for each of the fuel blends. The detailed description of the test conditions is displayed in Tables 3.3a-c.

The different exit equivalence ratios were achieved by varying the fuel flow rate while keeping the total air flow rate (co-flow + atomizing air) constant at 125 l/min. The ratio between the fuel, and atomizing air flow rates was kept approximately the same across fuels and equivalence ratio conditions to ensure that the drop velocity and size distribution, (measured with a phase-Doppler analyzer PDPA), was approximately the same for all fuels at all conditions, as measured by Ratul (2012). In addition, the carbon input rate for each equivalence ratio condition was kept approximately constant for all fuels, as seen in Tables 3.3a-c.

3.2 Experimental Apparatus and Procedure

3.2.1 Flame appearance

Digital images of the flames were obtained using a Canon EOS 350-D camera. The photographs were taken with an f-stop of f/3.5, an ISO of 100, and an exposure time of 0.2 seconds. The camera was located outside the laboratory combustion chamber, 1 meter from the flame in order to capture the entire flame diemnsions. The flame heights were determined by correlating the amount of pixels occupied by a known distance and

scaling the flame height based on the established correation. Four photographs were taken with each fuel at each equivalence ratio condition.

3.2.2 Global emissions

The combustion byproducts meassured during this experiment were oxygen, carbon dioxide, carbon monoxide, and nitric oxide.

The flue emissions were collected using a Pyrex gas collector and sampled by a 1 mm tip un-cooled 6 mm ID, 7.1 mm OD quartz probe. The collector cone was placed 2cm. directly above the visible flame, the gas sample was then treated by passing it through a water trap condenser submerged in an ice bath, and through fiber filters to prevent moisture and solid particles to reach the gas analyzers.

Carbon monoxide concentration measurements were acquired using a NOVA 376WP gas analyzer, while Nitric oxides, carbon dioxide, and oxygen concentrations were obtained with a NOVA 7466K analyzer. CO_2 concentrations were collected using a non-dispersive infrared detector, O_2, CO, and NO_X were made with electrochemical sensors.

Emissions indices were calculated and documented to account for the dilution due to air entrainment. Emissions indices were calculated using the method described by Turns (2011).

$$EI_i = \left(\frac{X_i}{X_{CO}+X_{CO_2}}\right) * \left(x * \frac{MW_i}{MW_F}\right) \quad (3.1)$$

Where EI_i, is the emission index for the species being recorded in [$g_{species}/kg_{fuel}$], X_i is the mole fraction of the species being measured, X_{CO}, and X_{CO2} are the mole fractions of carbon monoxide, and carbon dioxide respectively, x is the number of moles of carbon in a mole of fuel, MW_i [g/mol], and MW_F [kg/kmol] are the molar weights of the measured species and the fuel, respectively. Figure 3.9 shows a schematic diagram of the global emissions measurement setup.

3.2.3 In-Flame Species Concentration

Local concentrations of the reaction products were measured at three different axial locations (25%, 50%, 75% flame height), and across the radial direction at 2 mm intervals using a two-dimensional manual traverse. The gas was sampled using the same quartz probe used for the global emissions measurements. The collected gas sample was then treated by using the same methods described before in the global emission measurements in order to remove prevent moisture, and solid particles to reach the gas analyzers.

Carbon monoxide concentration measurements were acquired using a NOVA 376WP gas analyzer, while Nitric oxides, carbon dioxide, and oxygen concentrations were obtained with a NOVA 7466K analyzer. CO_2 concentrations were collected using a non-dispersive infrared detector, O_2, CO, and NO_X were made with electrochemical sensors. Especial caution was taken to ensure that the insides of the flame chamber were

sealed to the environment except for an aperture big enough for the probe to enter. Figure 3.10 shows a schematic diagram of the in-flame species concentration measurement setup.

3.2.4 In-Flame Temperature

Temperature measurements were taken at three different axial locations (25%, 50%, 75% flame height), and across the radial direction at 2mm intervals using the same setup used in the in-flame species measurements. Temperature data was collected using an R-type (Platinum/Platinum-Rhodium) thermocouple made with wires of 0.05mm in diameter. The thermocouple bead had a diameter of 0.2mm, and was coated with a homogeneous silicon dioxide coat in order to suppress the platinum catalytic effects. The coat was created by covering the bead with silicone grease and exposing it to the blue region of a Bunsen burner flame. Especial caution was taken to ensure that the insides of the flame chamber were sealed to the environment except for a small aperture through which the thermocouple was inserted.

The data was collected from the thermocouple through LabVIEW data acquisition software. The sample time at each location was 10 seconds at a sampling rate of 1 Hz. The measured temperature was then corrected for conductive, convective, and radiative heat losses (Ratul 2012). Figure 3.11 shows a schematic diagram of the in-flame temperature measurement setup.

3.2.5 Soot Volume Fraction

The path integrated soot volume fraction measurement was made by using the relationship established from the application of Beer's law, and Mie's theory as presented by Yagi and Iino (1962) for a propane air flame. The relationship has been used by various authors including Romero, Imran, who have similarily studied the soot distrubution in laminar partially premixed flames in palm methyl ester with diesel, and Jet-A with butanol, respectively. Ultimately soot voulme fraction, $F_{v,}$ [ppm] is calculated by:

$$F_v = -\frac{\ln\left(\frac{I_o}{I_s}\right)\lambda}{k_\lambda \delta} \tag{3.2}$$

Where I_s is the incident laser intensity [mW], I_o the attenuated laser intensity [mW], k_λ the spectral extinction coefficient based on the refractive indices of the soot, λ the laser wavelength [m], and δ the laser beam path (flame thickness) [m].

The flame thickness was measured in a similar fashion to the flame height, using a digital image processor to correlate a known length to the amount of pixels occupied by it, and applying that correlation to the pixels occupied by the flame. For all the soot volume fraction calculations the flames were assumed axisymmetric. A 5mW Helium-Neon laser of wavelength λ=632.8nm was used as the light source coupled with a Coherent Field Mate laser power detector. Both the laser and the detector were mounted in such a way that the laser beam will pass through the flame before striking the

detector. The laser beam intensity was measured prior, and after starting the flame in order to record the change in power measured.

The laser intensity got attenuated while passing through the flame due to the presence of soot; the beam attenuation, I_o, was obtained by measuring the intensity of the beam together with the power output of the flame field ($I_o + I_f$) as measured by the detector. The power intensity measured due to the flame, I_f, was determined by documenting the power output measured with the flame running and no incident laser beam. Especial caution was taken to ensure that the flame chamber was sealed to the environment except for a 1x1 cm aperture through which the laser beam passed. The measurements were taken for all fuels, at all three different equivalent ratio conditions, at three different axial locations (25%, 50%, and 75% flame height). Figure 3.13 shows a schematic diagram of the soot volume fraction measurement setup.

3.2.6 Pressure Drop across the Porous Media

Pressure drop across the porous media was measured with new porous media prior to starting any experiments, after 100 hours of operation to document the degradation suffered by the porous media due to the interaction with the fuels, and after maintenance was done on each porous medium. To measure the pressure drop, the porous medium and its casing (same used in the burner) were attached at the end of a square stainless steel pipe (4cm x 4cm x 27cm). Compressed air supplied from the university physical plat was passed through the steel chamber at a flow rate comparable to the total airflow rate used in the experiments (130 l/min). A static pressure port was

located upstream of the steel chamber by installing a T-joint at the inlet of the chamber, then flow was released to the environment. The difference in pressure between the inlet and the outlet was documented using a U-tube manometer (filled with water) with one end attached to the T-joint, and the other open to atmospheric pressure. Pressure drop measurements were performed individually on both porous media; Figure 3.14 shows a schematic diagram of the pressure drop setup.

3.2.7 Experimental Uncertainty

Experimental uncertainties were calculated using 95% confidence intervals, assuming t-distribution for all tests. Random error (R), and biased error (B) were considered while calculating the overall uncertainties. Experimental uncertainty values for all tests are presented in Table 3.4.

3.3 Experimental Procedure

3.3.1 Startup Procedure

- The co-flow air condenser was placed in into an ice bath, immediately after that the co-flow air supply was opened to the required flow rate as specified by the test conditions.
- The heaters were turned on and set to 463 K. The setup took approximately one hour to reach a steady temperature.
- The fuel tank was then pressurized (1.4 atm) using a compressed nitrogen cylinder.
- The atomizing air was initiated, and set to a desired flow rate value.
- A propane pilot flame was ignited downstream of the porous media burner.
- The flow rate of fuel was opened and set to a desired value.
- Once the fuel supply was continuous and the vapors started burning the pilot flame was shut down.

3.3.2 Shutdown

- The fuel flow rate was closed.
- Immediately after the flow was stopped, the fuel tank was depressurized.
- Atomizing airflow was left open for a period of 15 minutes to prevent fuel residues to deposit on the spray nozzle. After that period the atomizing air was shut.
- The heaters were shut off.
- Co-flow air was left running for approximately one hour to allow the setup to cool down. After that period the co-flow stream was closed.

Table 3.1: Physical properties of the parent fuels and blends.

Fuel	Jet-A	SA 10	BSA 10-10	SME	n-Butanol
Chemical Formula	$C_{13}H_{23}$	$C_{13.4}H_{23.8}O_{0.1}$	$C_{11.3}H_{20.8}O_{0.3}$	$C_{18.8}H_{34.6}O_2$	$C_4H_{10}O$
H/C Ratio	1.77	1.78	1.84	1.84	2.50
Molecular Weight [kg/kmol]	179	186.9	161.2	292.2	74
Density [kg/m^3]	795	804	814	881	805
Oxygen % (by mass)	0	0.9	3	11	21.6
Heating Value [MJ/kg]	43.28	42.9	41.6	39.7	33.1
Adiabatic Flame Temperature [K]	2264	2264	2258	2262	2251
Boiling Point [K]	418-573			619-678	390
Enthalpy of Vaporization [kJ/kg]	335			350[1]	550

[1] (Zhang, 2011)

Table 3.2: Nominal flow conditions for equivalence ratio 0.5, 0.6, and 0.7.

ϕ	Fuel	Co-flow Temperature [K]	Coflow Air [l/min]	Atomizing Air [l/min]	Fuel [ml/min]	Carbon input rate $\bullet 10^{-5}$[kg/s]
0.5	Jet-A	463	120.2	3.9	6.54	7.55
	SA 10	463	120.2	3.9	6.56	7.56
	BSA 10-10	463	120.1	4.0	6.63	7.54
0.6	Jet-A	463	119.4	4.7	7.84	9.06
	SA 10	463	119.4	4.7	7.87	9.08
	BSA 10-10	463	119.3	4.8	7.95	9.05
0.7	Jet-A	463	118.6	5.5	9.15	10.60
	SA 10	463	118.6	5.5	9.18	10.60
	BSA 10-10	463	118.5	5.6	9.28	10.60

Table 3.3: Experimental uncertainties for the test meassurements.

Measurement	**Uncertainty**
EI_{NOx} [g/kg_{fuel}]	0.6
EI_{CO} [g/kg_{fuel}]	0.2
CO_2 Concentration [%]	1.7
O_2 Concentration [%]	1.0
CO Concentration [%]	0.5
CO Concentration [ppm]	120
NOx Concentration [ppm]	57
Temperature [K]	26
Soot Volume Fraction [ppm]	0.07

Table 3.4 : List of instruments used in the experimental measurements.

Measurement	Instrument	Manufacturer	Model	Least Count	Notes
Flame imaging	digital SLR camera	Canon	EOS Rebel XT EF-S 18-55	N/A	
Co-flow temperature [K]	K-type Thermocouple	Omega	N/A	0.1	
Flame temperature [K]	R-type Thermocouple	Omega	N/A	0.1	0.2mm bead diameter
NOx concentration [ppm]	electrochemical Sensor	NOVA	7466K	1	
CO concentration [ppm]	electrochemical Sensor	NOVA	376WP	1	
CO concentration [%]	electrochemical Sensor	NOVA	376WP	0.1	
O_2 concentration [%]	electrochemical Sensor	NOVA	7466K	0.1	
CO_2 concentration [%]	non-dispersive infrared detector	NOVA	7466K	0.1	
Distance [mm]	two-dimensional traverse	Velmex	A1500	1	
Laser Intensity [mW]	laser power detector	Coherent	Field Mate	0.01	5mW laser, λ=632.8nm
Liquid Height [cm]	water U-tube manometer	Dyer	N/A	0.1	

Table 3.5: Rotameter manufacturer specifications.

Application	Rotameter	Tube	Float	Maximum Flow Rate (l/min)
Co-Flow Air	Ametek		42-J	565 (air)
Atomizing Air	Lo-Flo	SK 1/4"-27-G-5	Red Sapphire	20 (air)
Fuel	Lo-Flo	SK 1/8"-25-G-5	Black Glass	0.03 (water)

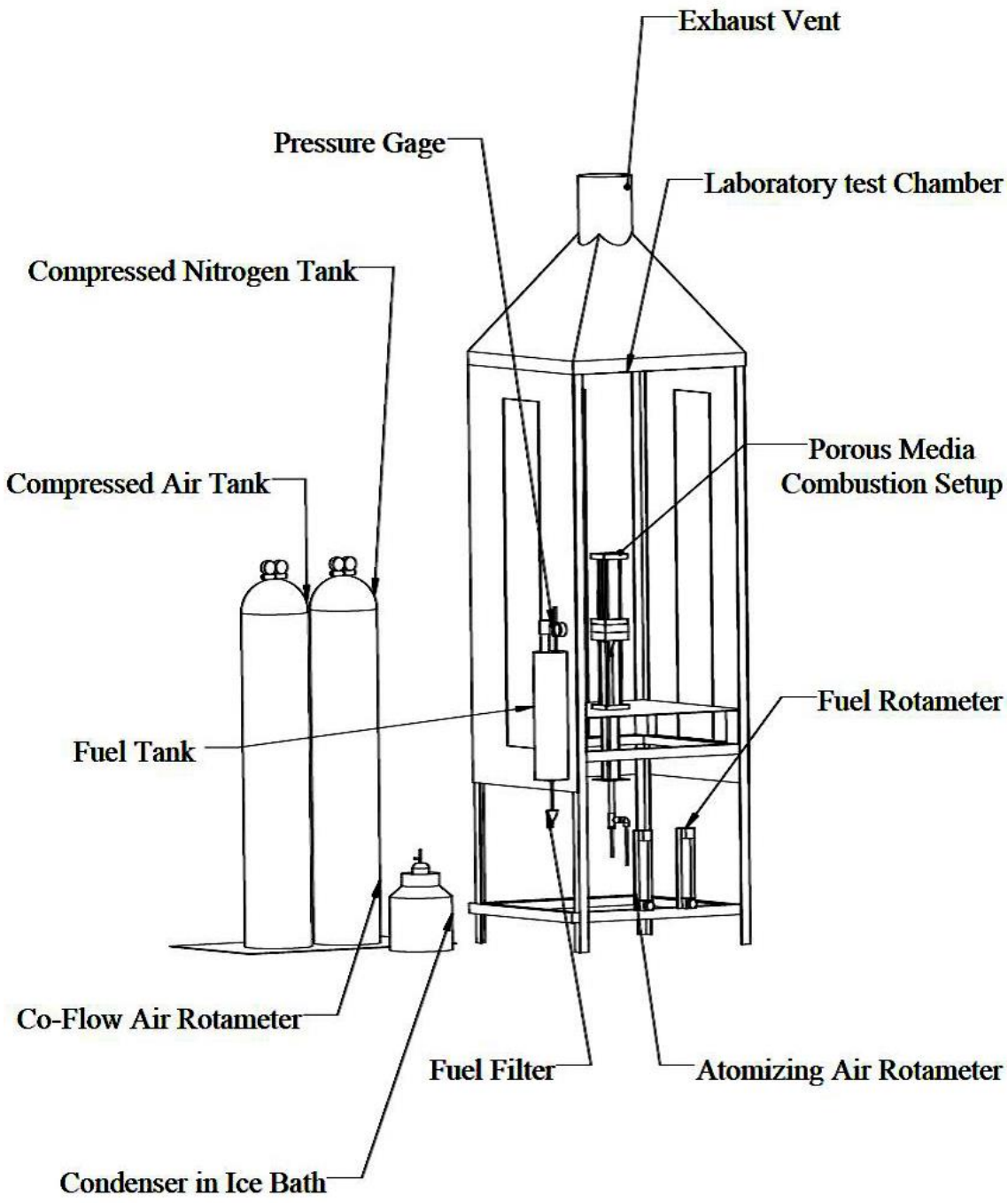

Figure 3.1: Schematic diagram of the combustion chamber.

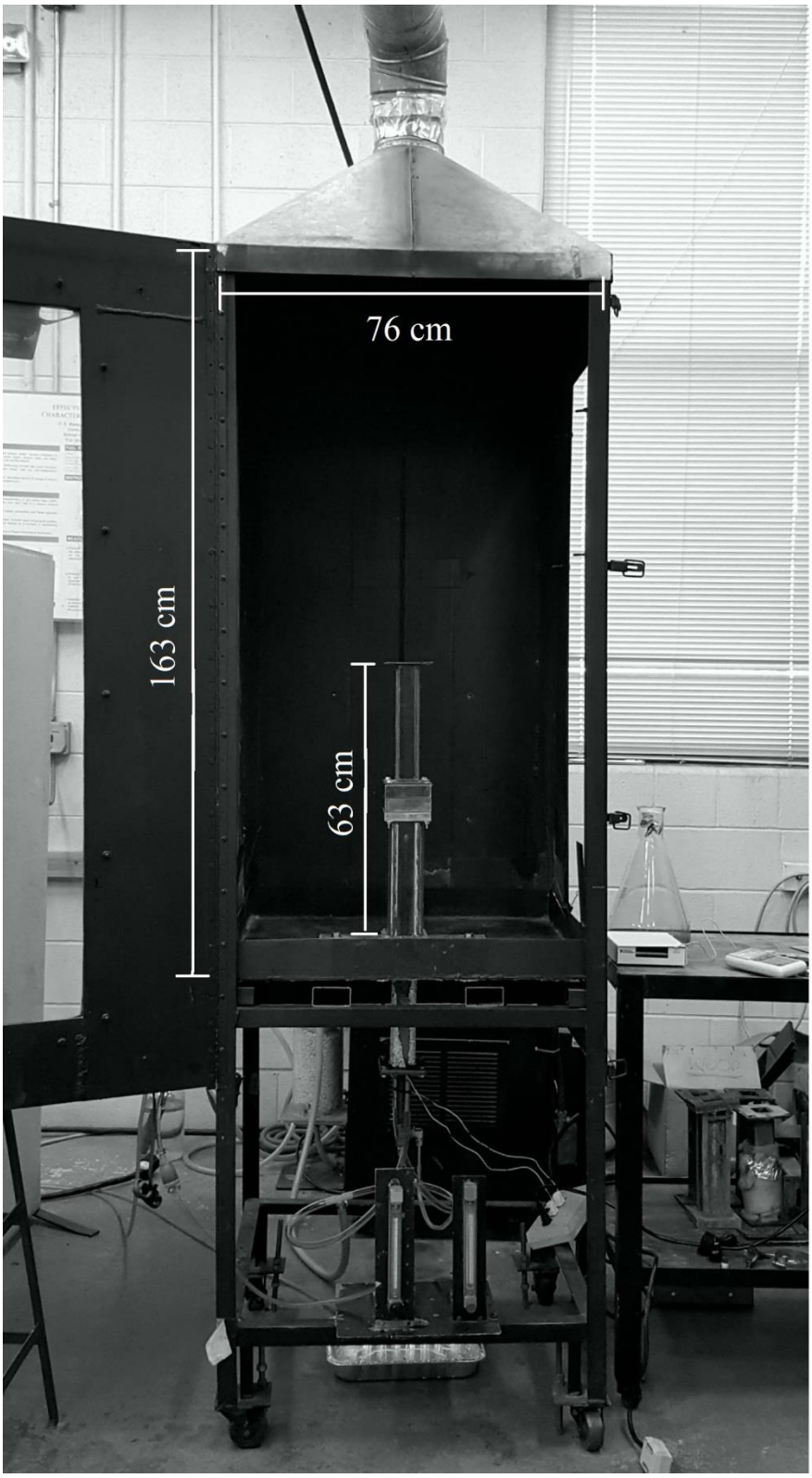

Figure 3.2: Photograph of the combustion chamber.

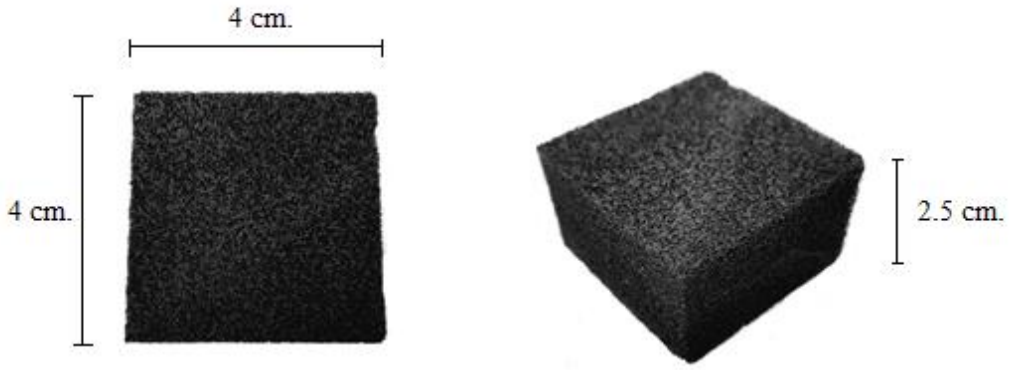

Figure 3.3: Evaporation porous medium photograph.

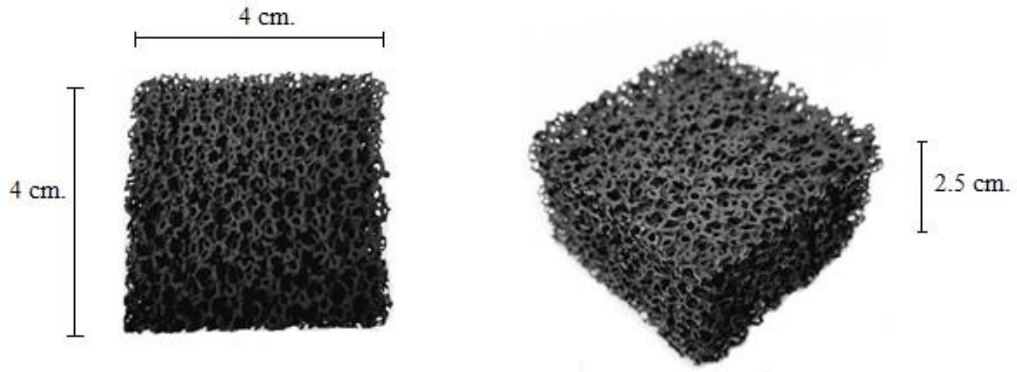

Figure 3.4: Combustion porous media photograph.

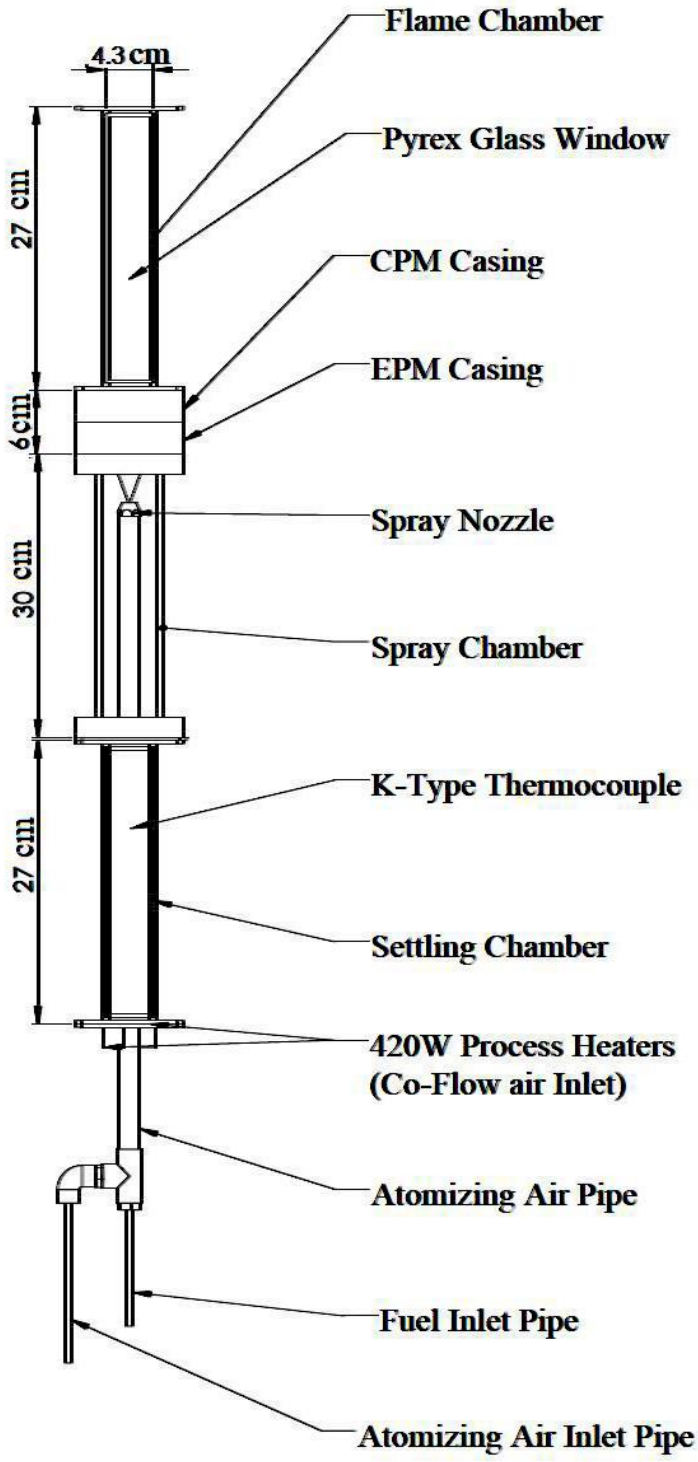

Figure 3.5: Schematic diagram of the porous media burner.

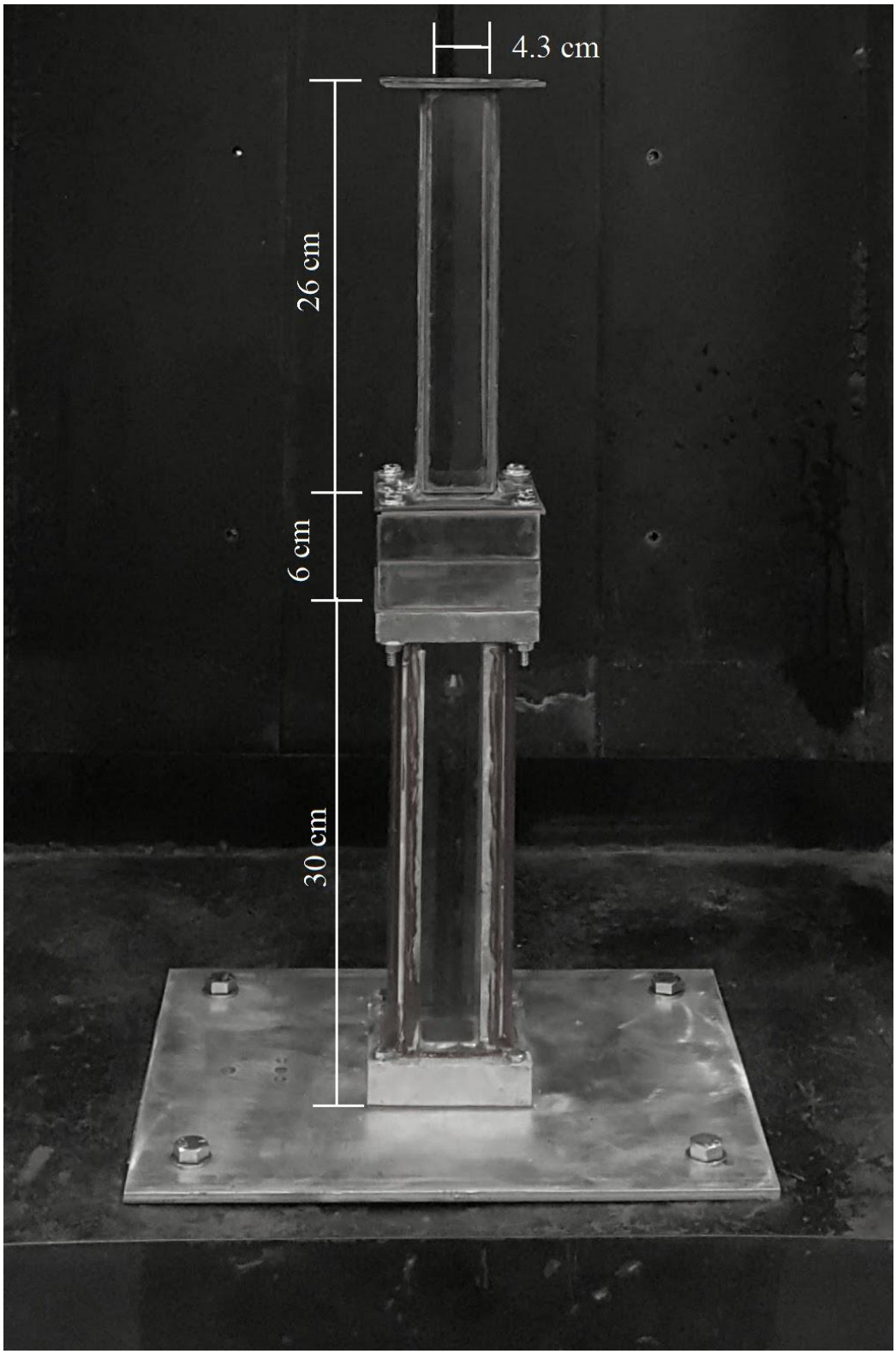

Figure 3.6: Photograph diagram of the porous media burner.

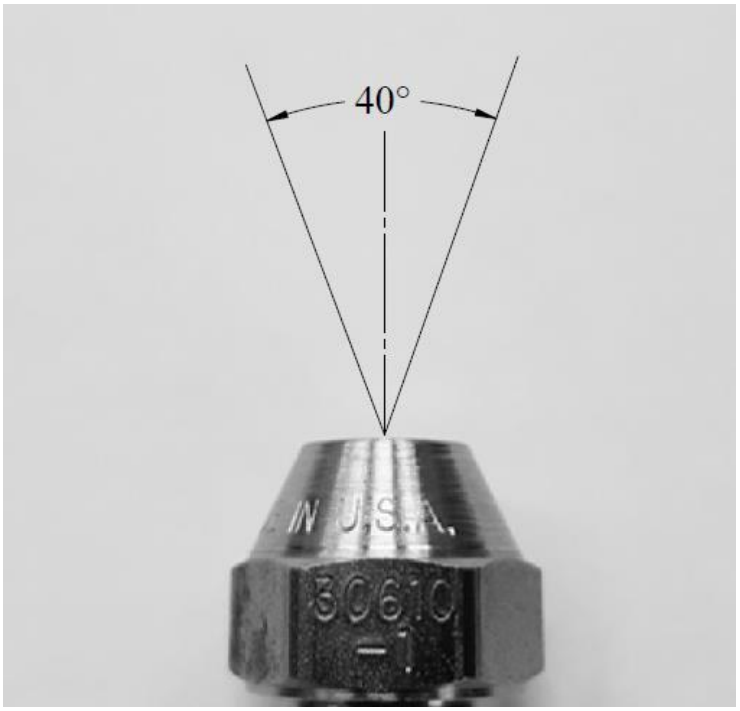

Figure 3.7: Photograph of the fuel atomizer nozzle, and spray.

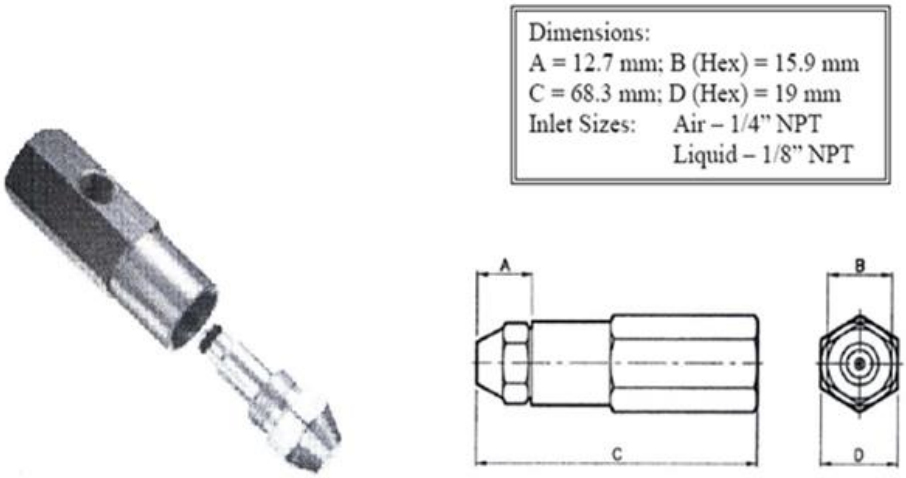

Figure 3.8: Dimensions of the Delavan air blast atomizer.

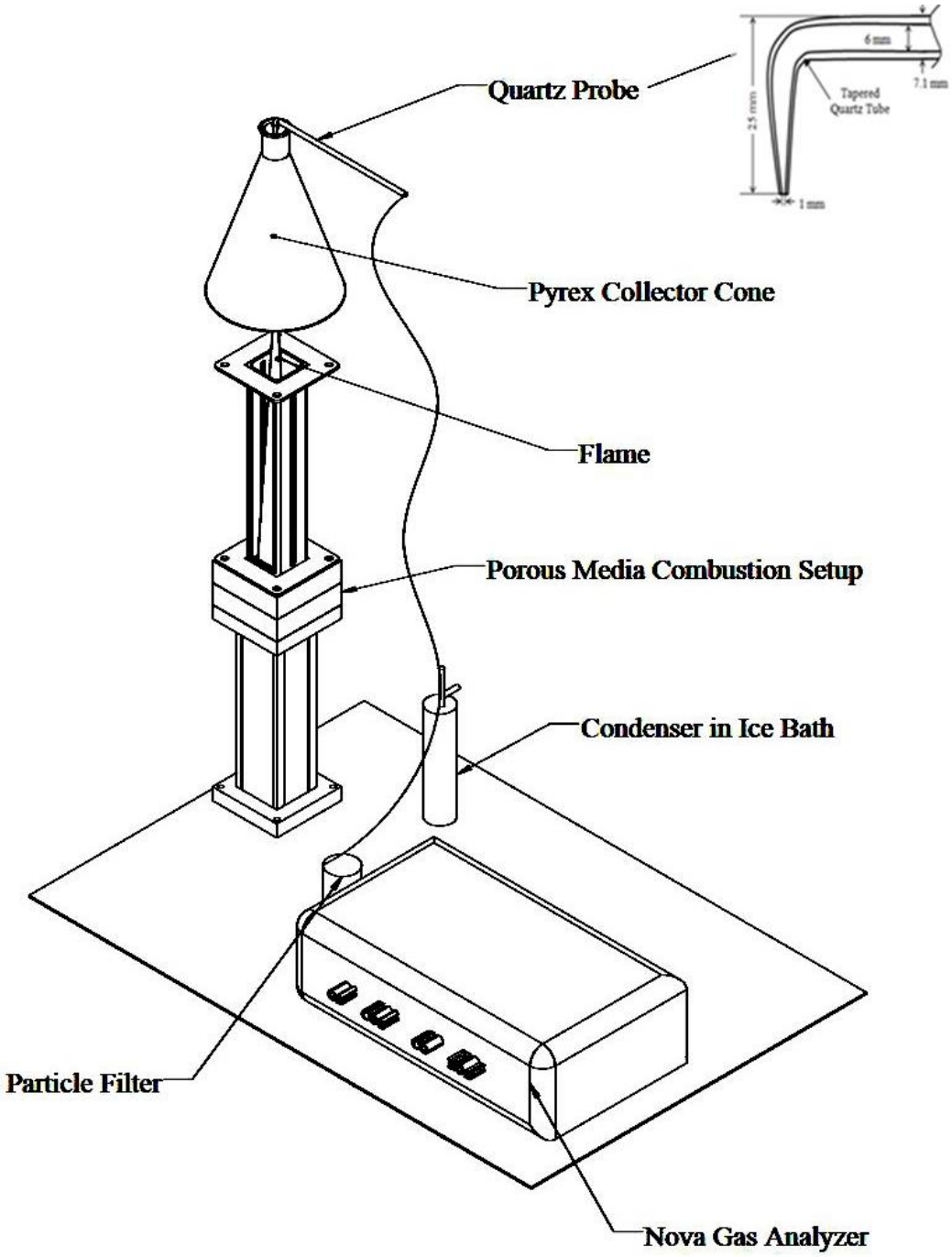

Figure 3.9: Schematic diagram of the global emissions measurement setup.

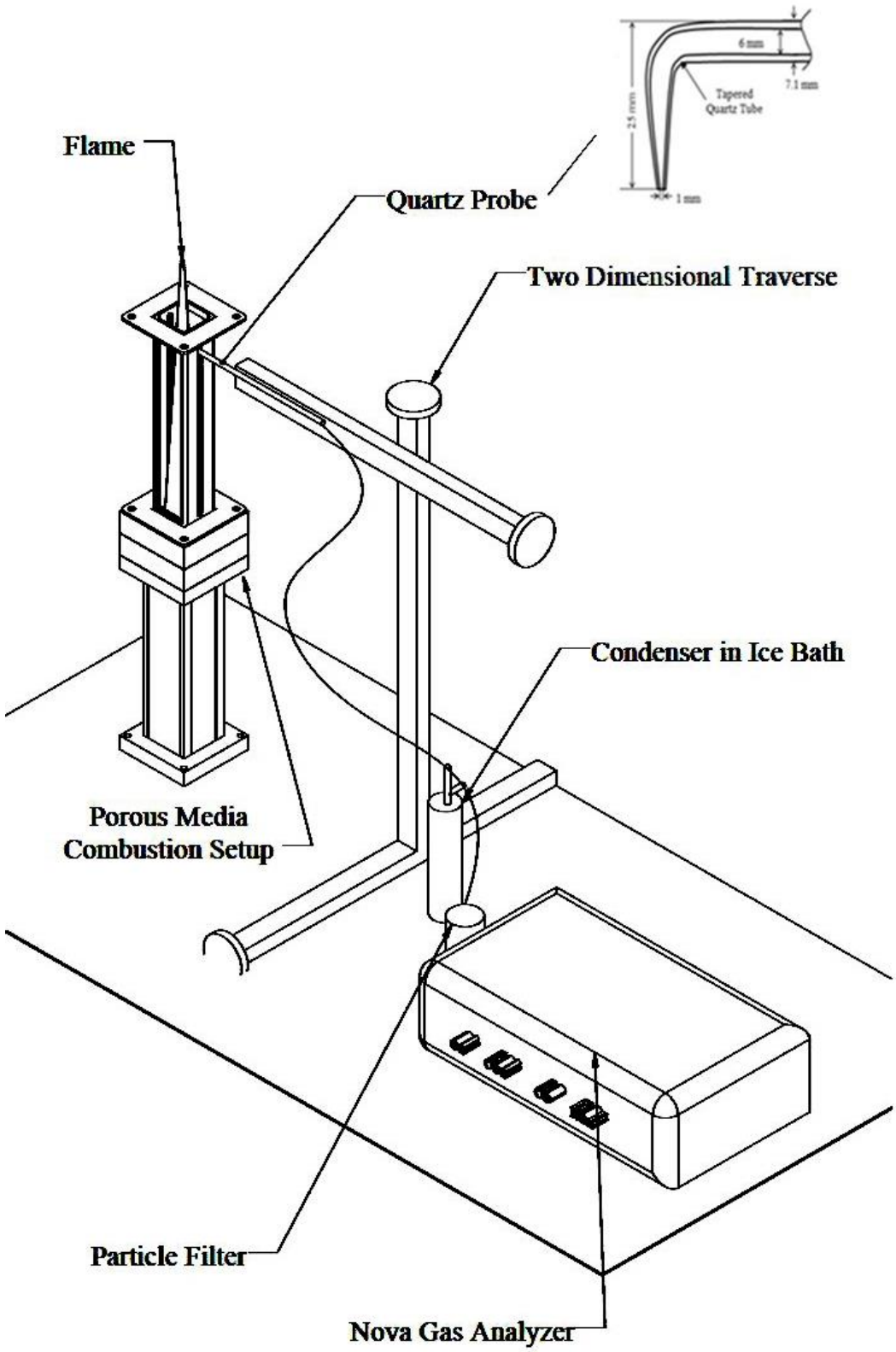

Figure 3.10: Schematic diagram of the in-flame species concentration measurement setup.

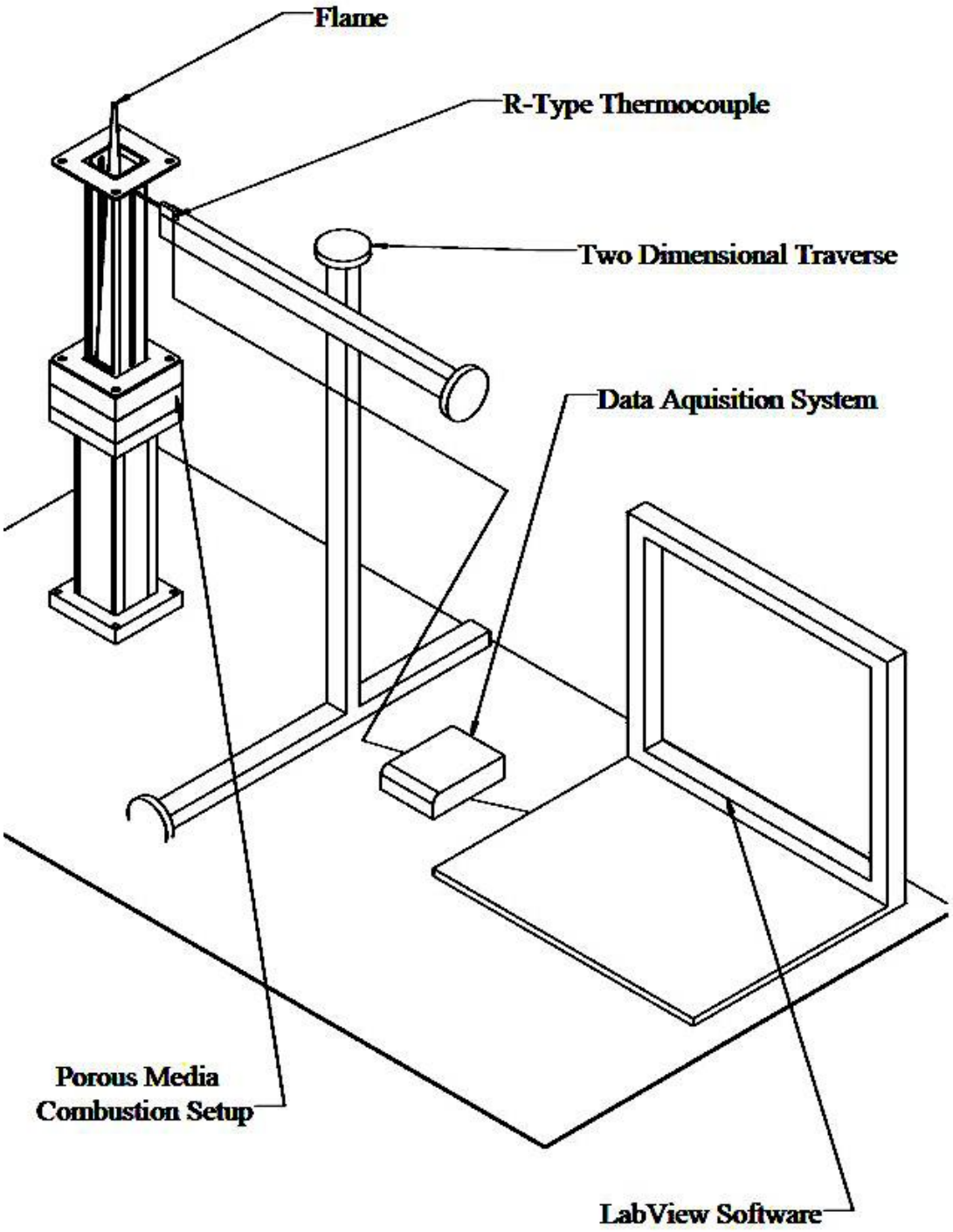

Figure 3.11: Schematic diagram of the in-flame temperature measurement setup.

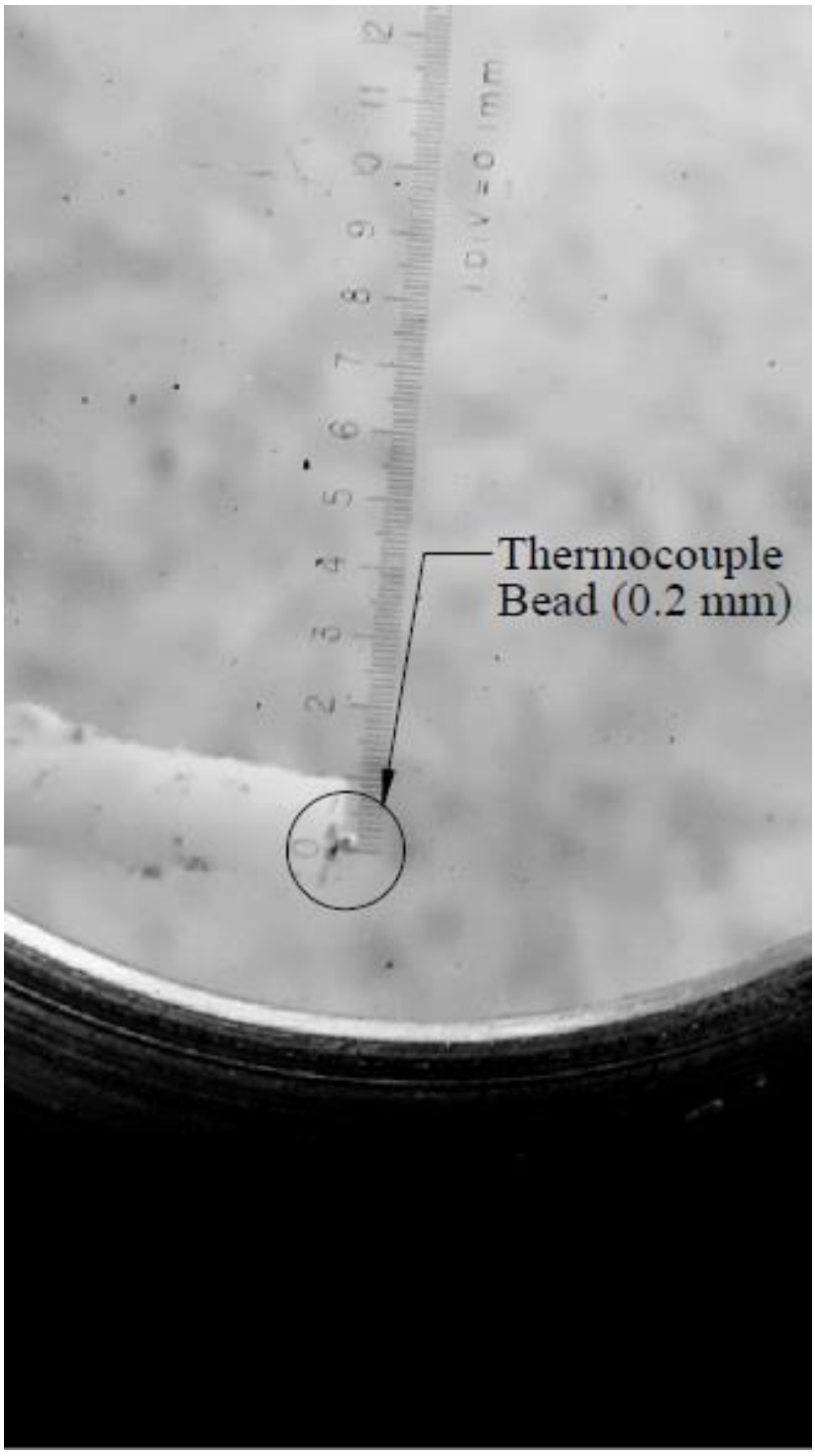

Figure 3.12: Photograph of the thermocouple bead used in the in-flame temperature measurement setup.

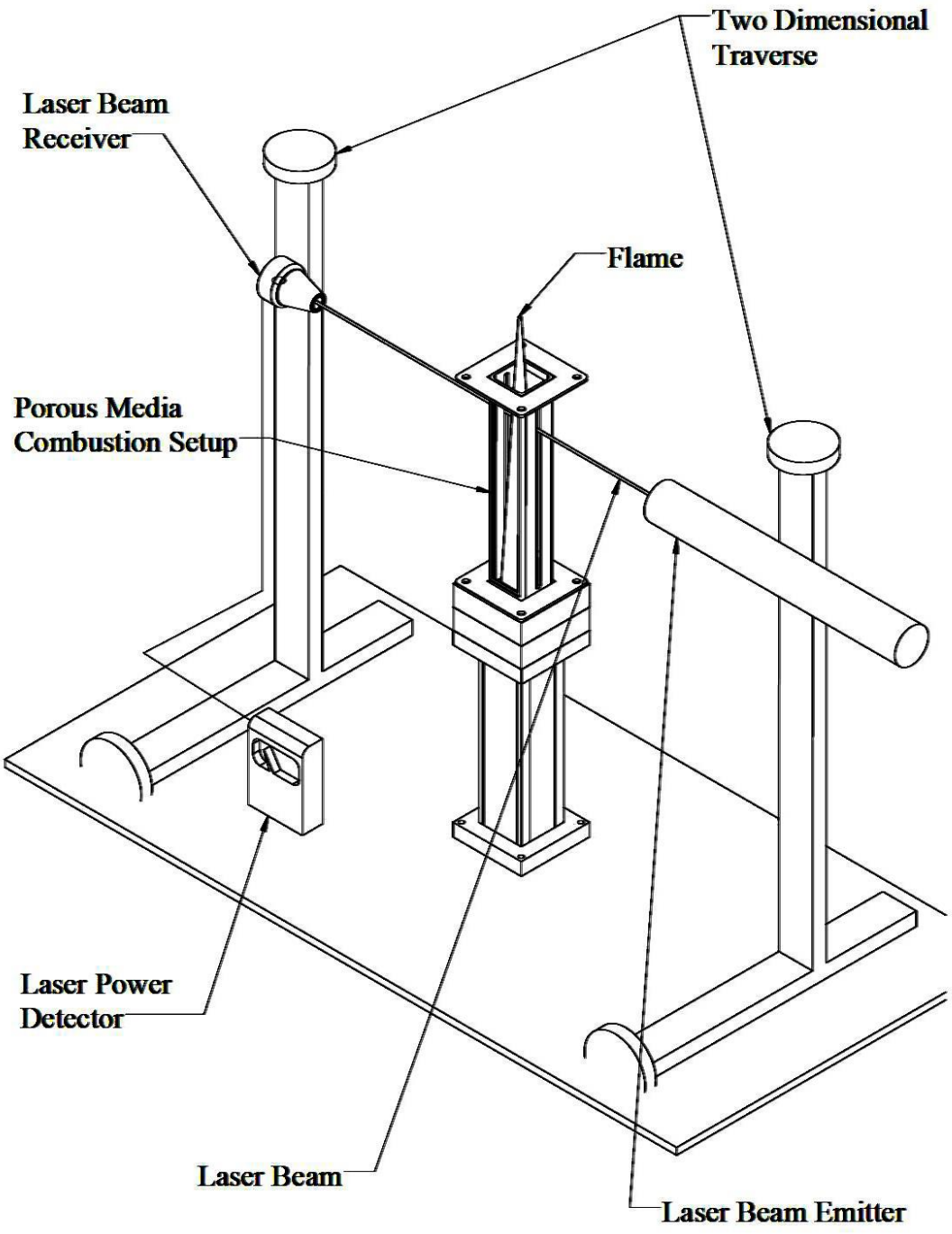

Figure 3.13: Schematic diagram of the axial soot volume fraction measurement setup.

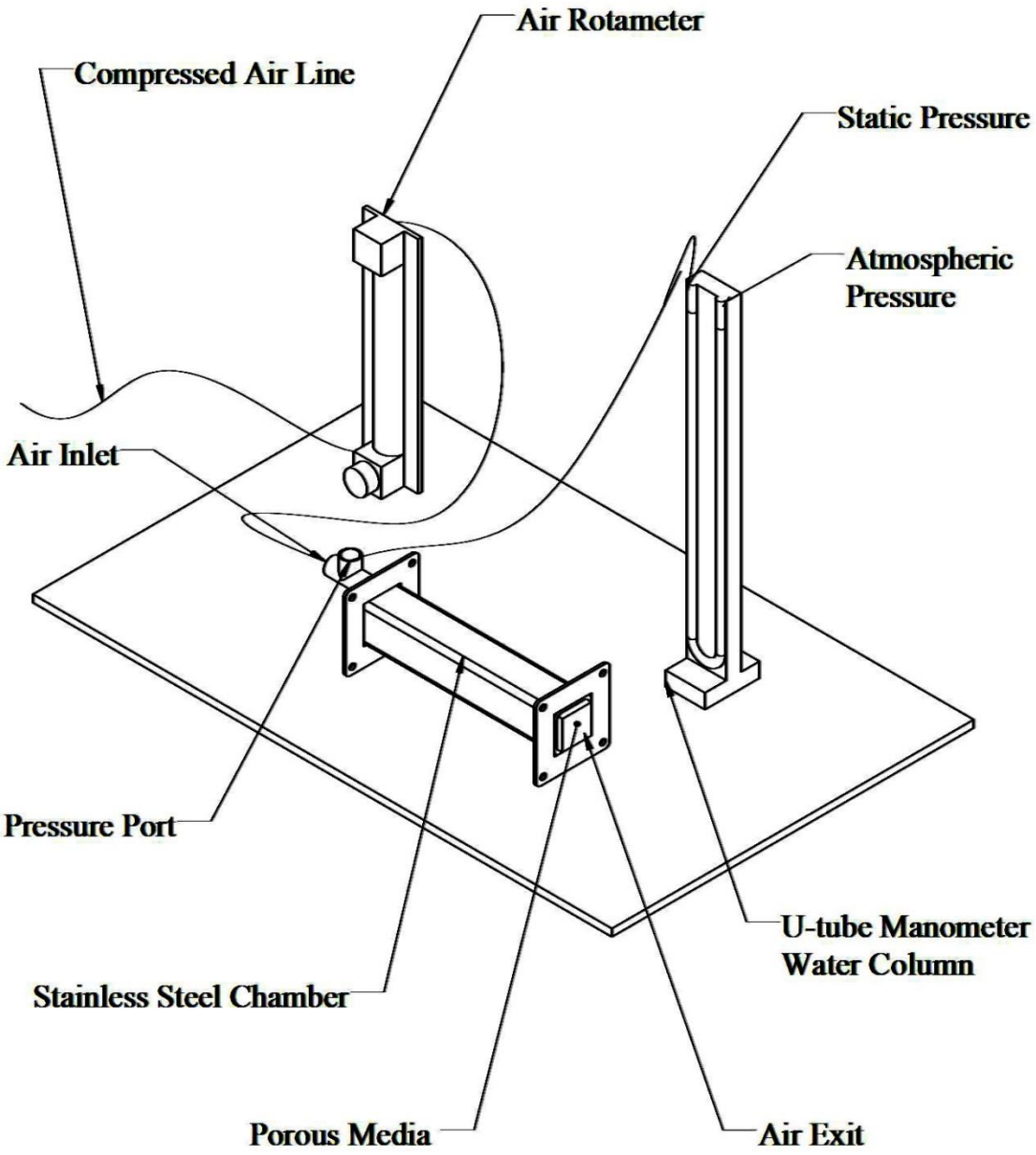

Figure 3.14: Schematic diagram of the pressure drop across the porous media measurement setup.

Chapter 4: Experimental Results & Discussion

The measured results are documented in the following chapter. Detailed descriptions of flame structure, global emissions, in-flame concentration profiles, in-flame temperature profiles, soot volume fraction, and porous media status before and after extended use are presented and discussed.

4.1 Flame Appearance and Flame Dimensions

As described in the experimental procedure (chapter 3), the flame chamber was equipped with front and rear tempered glass windows to allow for flame visualization. A Canon EOS 350D digital camera was placed outside the laboratory chamber in which the flame chamber was located, 1 meter away from the flame axis in order to capture the entire flame height. Color photographs of the flames were taken for each fuel (Jet-A, SA 10, BSA 10-10) at each equivalence ratio (ϕ = 0.5, 0.6, 0.7) chosen for this study. The photographs were obtained with an exposure time of 0.2 seconds, which allowed for capturing an average image of the flames, and the original color of the flames.

The photographs taken for the flames at an equivalence ratio 0.5 are presented in Figure 4.1. The recorded flames had low luminosity with a blue hue present immediately downstream of the porous media. The flames generated from the blended fuels presented a fainter and bluer plume compared to those with Jet-A fuel. This decrease in

luminosity can be directly correlated to the increasing amount of oxygen present in the fuel molecules (0% by mass for Jet-A, 0.9% by mass for SA 10, and 3% by mass for BSA 10-10). The change in flame configuration evidences the effectiveness of fuel-bound oxygen in fuel oxidation. The presence of molecular oxygen suppressed soot precursor formation significantly.

The tallest flame for these combustion conditions was the Jet-A flame with height of 37 cm. The addition of SME to the fuel blend reduced the visible flame height to 35 cm, while the three component blend had the smallest flame with a visible height of 34 cm. The smallest height (BSA 10-10) can be attributed to the increased amount of fuel bound oxygen, as well as the low boiling point of butanol.

A similar trend can be seen in the flames recorded at ϕ=0.6 which are presented in Figure 4.2. The flames had low luminosity and a blue hue immediately downstream of the porous media. For these combustion conditions also, the increase in molecule-bound oxygen concentration in the blends resulted in a reduction in the luminosity of the flames, due to the reduced production of soot precursors. As a consequence, the blended fuel flames appeared bluer than Jet-A flames. The tallest flame for ϕ=0.6 was the Jet-A flame at a flame height of 42 cm. The combustion of SA 10 yielded a reduced visible flame height of 39 cm, while the three component blend presented the smallest flame with a visible height of 38 cm. The decrease in flame height is a result of the increased presence of oxygen in the fuel molecules. The flame heights for all three

fuels increased with the increase of equivalence ratio, due to the increased carbon input rate (Table 3.2).

Finally, the photographs of flames at an equivalence ratio 0.7 are presented in Figure 4.3. The blue hue color of the flames suggests little or no soot formation. As with the flames of the previously described combustion conditions, blended fuels with increased content of molecular bound oxygen resulted in bluer flames. The flames were taller than those corresponding to the equivalence ratio of 0.6. The tallest flame corresponded to pure Jet-A with 47 cm, followed by SA 10 with 42 cm, and lastly the shortest flame height corresponded to the BSA 10-10 blend with 41 cm.

4.2 Global Emissions

4.2.1 Emission Indices of Nitrogen Oxides (NOx)

The concentration of NOx [ppm] in the exhaust emissions was measured using the gas sample collected by the quartz probe and the NOVA 7466K gas analyzer described in Chapter 3. Emission indices, EI_{NOx} [g_{NOx}/kg_{fuel}], were then calculated from Equation 3.1 to quantify the amount of pollutant generated by a unit amount of fuel burned. Figure 4.4 presents the calculated NOx emission indices for Jet-A, SA 10, and BSA 10-10 at equivalence ratios ϕ=0.5, 0.6, and 0.7.. The corresponding experimental uncertainty was found to be ± 0.6 g_{NOx}/kg_{fuel}.

The results in Figure 4.4 showed that for this burner configuration, the NOx emission indices for all fuels studied varied non-monotonically with equivalence ratio. The NOx emission index reached a peak value at ϕ=0.6 for all fuels studied. The NOx emission indices for all flames were comparable at a given equivalence ratio; at ϕ=0.6 all fuels yielded an EI_{NOx} of around 6 g/kg_{fuel} (Jet-A = 6.69 g/kg_{fuel}, SA 10 = 5.98 g/kg_{fuel}, BSA 10-10 = 5.92 g/kg_{fuel}). At the equivalence ratio of 0.5, the NOx emission indices values were again within experimental uncertainties of each other for all fuels at around 3.5 g/kg_{fuel}; (Jet-A = 3.32 g/kg_{fuel}, SA 10 = 4.11 g/kg_{fuel}, BSA 10-10 = 3.66 g/kg_{fuel}). Similarly, the measurements documented for equivalence ratio 0.7 did not show a significant difference among them; the average value for this condition was 3.4 g/kg_{fuel} (Jet-A = 3.20 g/kg_{fuel}, SA 10 = 2.90 g/kg_{fuel}, BSA 10-10 = 3.96 g/kg_{fuel}).

Periasamy (2007) investigated the effects porous media has on the combustion of kerosene, n-heptane, and methanol. Periasamy found that the presence of the porous media burner made EI_{NOx} variation insensitive to equivalence ratio between 0.4 and 0.7. Dahifale (2010) studied the combustion of blends of canola methyl ester and Jet-A in a porous media burner, similar to the present configuration. The author found that EI_{NOx} for the blends decreased monotonically with equivalence ratio between ϕ=0.73 and ϕ=0.96. At ϕ=0.96, the EI_{NOx} for the blends was, on average, 30% lower than the emission indices results measured at ϕ=0.73. This behavior is different from that observed in conventional combustor configurations in which the NOx emission index increases with equivalence ratio in the lean regime. This non-monotonic behavior was attributed to the formation of locally rich regions due to the fuel vaporizing closer to the

porous media. In addition it was noted that for ϕ=0.7 flames, a large fraction (40%) of the observable flame height was located outside the flame chamber. The unexpected decrease between ϕ=0.6 and ϕ=0.7 flames found in this study can be attributed to a combination of the effects described by Dahifale (2010), and effects of air entrainment on the reactions at the fractions of the ϕ=0.7 flames located outside the flame chamber.

There are three major mechanisms that describe the formation of nitric oxides in combustion systems; thermal or Zeldovich mechanism, Fenimore or prompt mechanism, and N_2O intermediate mechanism. The thermal mechanism describes the formation of NO in high temperature regions (typically above 1500 K) in combustion systems over a wide span of equivalence ratios. Thermal mechanism depends not only on high temperatures, but also the residence time of the reactants at the high temperature region. The prompt mechanism describes the formation of NO, and NO_2 from the interaction of atmospheric nitrogen with CH radicals. Prompt mechanism is usually prevalent in fuel-rich systems. Lastly, the N_2O intermediate mechanism describes the NO formation in fuel lean, low-temperature conditions (Periasamy, 2007).

At the present conditions, it appears that the thermal mechanism was dominant. This is discussed when comparing the emission indices to the in-flame peak temperatures (section 4.4), and in-flame NOx concentration (section 4.3.4).

4.2.2 Emission Indices of Carbon Monoxide (CO)

The concentration of CO in the exhaust [ppm] was obtained using the quartz probe described in Chapter 3, and a NOVA 376 WP analyzer. The emission indices, EI_{CO}, [g_{CO}/kg_{fuel}] were calculated using Equation 3.1. The EI_{CO} results for all fuel blends at all equivalence ratios studied are plotted in Figure 4. 5. The corresponding experimental uncertainty found for CO emission index was ±0.2 $g_{CO}/kg_{fuel.}$

The results displayed in Figure 4.5 show that CO emissions also reach a peak at ϕ=0.6, with a non-monotonic variation with equivalence ratio. For a given equivalence ratio, CO emission indices showed a slight peak for the SA 10 flames, EI_{CO} values for BSA 10-10 and Jet-A were comparable; the variation for any given equivalence ratio was within experimental uncertainty. At ϕ=0.5, all values for EI_{CO} were found to be around 4.0 g_{CO}/kg_{fuel} (Jet-A = 3.59 g/kg_{fuel}, SA 10 = 4.44 g/kg_{fuel}, BSA 10-10 = 3.62 g/kg_{fuel}). When the equivalence ratio was increased to 0.6, the CO emission index values increased an average of 70%. The CO emission index for all three fuel blends peaked at equivalence ratio 0.6, and all were within uncertainty range around 6.0 g_{CO}/kg_{fuel} (Jet-A = 6.02 g/kg_{fuel}, SA 10 = 6.38 g/kg_{fuel}, BSA 10-10 = 5.59 g/kg_{fuel}). At the highest equivalence ratio studied (ϕ=0.7) the values for EI_{CO} decreased around 20% with respect to those of ϕ=0.6. Similarly to the other results, the measurements for all fuel blends were comparable in size, all lying within uncertainty around 4.75 g_{CO}/kg_{fuel} (Jet-A = 4.71 g/kg_{fuel}, SA 10 = 5.17 g/kg_{fuel}, BSA 10-10 = 4.51 g/kg_{fuel}).

Periasamy (2007) investigated the effect that porous media has on the combustion of kerosene, n-heptane, and methanol. Periasamy found that for the EI_{CO} of kerosene had a non-monotonic variation with respect to equivalence ratio, peaking at ϕ=0.55. Imran (2015) studied the emission characteristics of Jet-A/butanol in a porous media burner. The author concluded that the global emission index of CO decreased with an increase in concentration of butanol in the blends. Compared to Jet-A, the blend with highest content of butanol (70% Jet-A – 30% butanol) produced 30% less CO; in addition, the results showed an increase in EI_{CO} with equivalence ratio as a consequence of the increased carbon input rate.

Carbon monoxide is usually the result of incomplete combustion (Baukal, 2013). In order to enhance reaction completion and lower CO emissions, combustion systems are operated at fuel lean conditions with premixed or partially premixed flames. Moreover, the addition of fuel bound oxygen to the blends would produce shorter oxidation times for the fuels, making for more complete combustion.

The use of a porous media burner provides an environment which enhances mixing and vaporization, consequently improving the quality and completion of the combustion reaction, hence reducing CO emissions. The effect of the porous media burner can be clearly seen while comparing the emission indices calculated for this, and similar studies to those obtained on open flame studies. The magnitude of EI_{CO} for a porous media burner is often 60%-75% lower than the EI_{CO} measured for open flames, such

was the case when compared to studies performed on open spray flames by Aldana et al. (2014) and Ratul (2012).

In the case of the fuels studied here, the comparable values recorded can be attributed to the similar H/C ratio of the fuels. It can be observed that the effect molecular bound oxygen is compensated by the evaporation, and premixing enhancement propitiated by the porous media as the EI_{CO} of BSA 10-10 and Jet-A are almost equal in magnitude. The slight peak of emissions measured for SA 10 might be due to the chemical properties of the individual components of SME with higher H/C ratios. The unexpected CO emission decrease between ϕ=0.6, and ϕ=0.7, could be due to the fact that a large portion (about 40% of the flame height) of the ϕ=0.7 flames was located outside the flame chamber which increased the availability of oxygen in the reaction zone due to air entrainment. This behavior needs to be studied further with the entire flame entirely enclosed in order to completely understand it.

4.2.3 Exhaust Concentration of Carbon Dioxide (CO_2)

Measurements of exhaust carbon dioxide concentration were performed at the same point where NOx, and CO samples were taken. CO_2 is one of the products of complete combustion, and values of CO_2 amount closer to the value established by the complete reaction equation indicate a more complete use of energy contained in the fuel (Periasamy, 2007).

Figure 4.6 shows the carbon dioxide concentration measured at the exhaust plotted against equivalence ratio for all fuel blends studied. The levels of CO_2 were comparable across the different blend flames (3.75%). Previous studies such as those realized by Dahifale (2010) and Imran (2015) suggest that CO_2 concentration levels would increase as the equivalence ratio increases due to an increased carbon input rate; however, there was no significant increase observed on the CO_2 concentration with equivalence ratio; it is possible that the amount of air entrained after the combustion chamber masked the equivalence ratio variation. Flue concentration of CO_2 was not expected to vary significantly between fuels, as their theoretical product mole fractions do not show a substantial variation. Tables 4.1 a-c show the complete combustion mole percentage of CO_2 with moisture removed from the sample for all fuels at all equivalence ratios studied. The maximum value of CO_2 concentration was 3.96% corresponding to SA 10, at ϕ=0.5; the minimum value corresponded to BSA 10-10 at ϕ= 0.7 (3.55%). The experimental uncertainty corresponding to CO_2 concentration measurement based on the t-distribution assumption was ± 0.19%.

4.2.4 Exhaust Concentration of Oxygen (O_2)

The same quartz probe used to measure the concentrations of NOx and CO coupled with a NOVA 376 WD was used to measure the O_2 concentration [%] in the exhaust. Since the study is carried under lean combustion conditions, there is a finite amount of oxygen expected with the combustion products. Low Concentrations of O_2 at the exhaust are evidence of a more complete combustion.

Figure 4.4 displays the concentration of O_2 measured in the exhaust plotted against equivalence ratio, for all blends in the study. The concentrations measured in the exhaust showed that fuel composition, and the amount of fuel-bound oxygen present in the fuel did not have a significant impact on O_2 consumption. The average concentration value for all fuel blends at all equivalence ratios was 15.4 %; the values for each fuel at each condition deviated within uncertainty range from the average value, with a maximum value of 15.67% corresponding to the BSA 10-10, ϕ=0.7 flame, and a minimum measured of 15.07%, for the BSA 10-10, ϕ=0.5 flame. The experimental uncertainty associated with these measurements was ±0.32%.. Like for CO_2, O_2 was not expected to substantially vary among fuels since the complete combustion values are comparable (Table 4.1a-c).

4.3 In-Flame Species Concentration Measurements

In-flame concentration radial profiles for O_2, CO_2, NOx, and CO were created by inserting a quartz sampling probe to measure the local species concentrations and traversing it along the diameter at three different axial locations (25%, 50%, 75% height of the visible flame) for all fuels (Jet-A, SA 10, BSA 10-10) at each equivalence ratio (ϕ=0.5, 0.6, 0.7). As described in Chapter 3, a 1 mm diameter aperture tapered quartz probe was used to collect gas samples inside the flame. The sampling probe was mounted on a two-dimensional traverse and data were collected at 2 mm intervals across the entire width of the flame. The sample was then treated using an ice bath condenser to remove moisture from the exhaust gas sample and a particle filter to trap solid particles before reaching the 376 WP NOVA gas analyzer.

4.4.1 O_2 In-Flame Concentration Profiles

The concentration values for O_2 for each fuel are plotted against radial distance [mm] at every axial location measured in Figures 4.8-4.16. The experimental uncertainty associated with the measurements was 1.2% and it is presented as error bars in the figures.

Oxygen concentration reached a minimum at the centerline of the flame with lower concentrations measured at higher equivalence ratios (0% for the ϕ=0.6, and ϕ=0.7, and 2% for the ϕ=0.5 flame). It is evident from the in-flame profiles concentrations that with an increased fuel flow rates (ϕ=0.6, ϕ=0.7) more of the oxygen present was being consumed by the reactions in the near-burner region.

Overall in the BSA 10-10 flame, concentrations of oxygen were consistently higher than those of Jet-A and SA 10 flames; this effect resulted as a consequence of BSA 10-10 having a much higher concentration of fuel-bound oxygen which reduces the consumption of free oxygen in the reaction due to the preliminary oxidation of the fuel. Oxygen concentration levels increased as the flame height increased; the increase in concentration was especially noticeable at 75% flame height as two out of three flames extended outside of the flame chamber, which allowed for a more vigorous air entrainment.

4.4.2 CO_2 In-Flame Concentration Profiles

The concentration values for CO_2 for each fuel are plotted against radial distance at every axial location measured in Figures 4.17-4.25. The experimental uncertainty associated with the measurements was 1.2% and it is presented as error bars in the figures.

For an equivalence ratio 0.5, the carbon dioxide concentrations for all flames were comparable; all peaked close to the centerline at about 13%; the concentration profiles did not vary significantly as the flame height at which they were measured increased. This behavior is different from that observed in spray flames without porous media, in which the reaction zone is located off-axis in the near-burner region. CO_2 emissions profiles peaks corresponded to the O_2 emission profiles minimum values. At ϕ=0.6 the concentration profiles look very similar to those found at ϕ=0.5. The peaks were still located close to the axis of the flame, and the maximum value increased to 14%.

The peaks at ϕ=0.7 did not differ in magnitude to those found for lower equivalence ratios; however their locations shifted radially outward between 8 mm and 12 mm. The shift in the peak positions is probably due to the limited amount of oxygen inside the flame cone and the need of entrained air to complete the oxidation of CO at the outside cone flame front.

4.4.4 CO In-Flame Concentration Profiles

Carbon monoxide formation mechanisms are determined by the amount of oxygen available during the reaction, at lean conditions CO concentrations are expected to be low, however they are expected to be found at the location of the reaction, since CO is an intermediary species in the formation of CO_2. The CO gas concentration profiles for all flames, measured at 25%, 50%, and 75% flame height for each equivalence ratio are presented in figures 4.26-4.34.

At equivalence ratio 0.5 and 25% flame height the peak concentrations of all flames are comparable. The peak concentration of around 1% is found to occur close to the centerline of the flame. At larger flame lengths (50%, 75%) the CO concentrations were lower than 1% indicating that most carbon had been fully oxidized by that point.

At ϕ=0.6, similar profiles are observed throughout the flame, the higher concentrations were found closer to the porous media, and they decreased to almost zero in the downstream sections of the flame. The peaks at all flame heights were comparable for all fuel blends, throughout all flame heights. At 25% the peak was found to be around 4% and it was located close to the axis of the flame. At 50% and 75% the peak concentrations were measured to be lower than 1% for all the flames.

For the conditions given at equivalence ratio 0.7, the peak concentrations were comparable for all fuel blend flames, and the concentrations were found to peak at around 6%. For 50% flame height, the peaks for SA 10, and BSA 10-10 were found to be close to 6%, whereas that of Jet-A increased to almost 8%. The same trend was found at 75% percent, with the only difference that the BSA 10-10 peak concentration reduced to 3%. In contrast to previous equivalence ratios, at ϕ=0.7 the peak concentrations did not decrease significantly with flame height, this phenomenon has to be studied further in order to determine the observed trend.

4.4.3 NOx In-Flame Concentration Profiles

The NOx gas concentration profiles for all flames, measured at 25%, 50%, and 75% flame height for each equivalence ratio are presented in figures 4.35-4.43. For ϕ=0.5 at 25% flame height the peak NOx concentration peak (400) was located close to the axis. At 50% flame height the peak concentration was still close to the axis; the peak concentration of NOx in all Jet-A and BSA 10-10 flames increased by about 50 ppm, and that for SA 10 increased up to 600 ppm. The NOx profile for SA 10 was consistently higher than those of Jet-A and BSA 10-10 at this height. As the measurements were taken at 75% flame height, the NOx profile shifted higher for all fuels; however, the emissions for SA 10 were still evidently higher than those of Jet-A and BSA 10-10.

For an equivalence ratio of 0.6, the peak concentrations were located close to the axis, and were about 100 ppm higher than the peak concentrations found in the ϕ=0.5 flames. At 25% flame height, the SA 10 flame had a higher peak (700 ppm) than those of Jet-A and BSA 10-10 (both at about 450 ppm). At 50% flame height SA 10 peak reduced (600 ppm) but it was still consistently higher than the peaks of the other two fuels, despite the peak of BSA 10-10 being higher at this flame height than at 25% height (500 ppm). At 75% flame height the same trend as in 50% height is observed with a slight increase in peak values.

At ϕ=0.7, the NOx concentration peaks shifted about 10 mm outwards, this effect possibly due to less oxygen availability of oxygen in the center of the flame, and more availability on the outside flame. The peaks at 25% height were comparable for all flames at about 300 ppm. At 50% of the flame height, there was a significant increase in the NOx concentration observed from the SA 10 flame of about 100 ppm while the other two flames kept a concentration similar to that of 25% flame height. At 75% flame height, the peak of BSA 10-10 flame remained about the same magnitude as that found in 50% flame height whereas the peak corresponding to the SA 10 flame decreased from 400 ppm to 300 ppm, and that of Jet-A from 300 to about 200.

Peak NOx concentration values at 75% percent flame height showed a similar variation to that found for the EI_{NOx} results, hence the inflame measurements are in agreement with the global emission results. The measured NOx profiles have a strong correlation to the in-flame temperature profiles, which supports the claim that the thermal

mechanism dominates NOx formation at these conditions. Zeldovich mechanism is prevalent at lean combustion conditions when the temperatures are greater than 1500 K (Turns, 2011).

4.4 In-Flame Temperature Measurements

In-flame temperature radial profiles were created by measuring local temperature along a diameter at three different axial locations (25%, 50%, 75% height of the visible flame) for all fuels (Jet-A, SA 10, BSA 10-10), and at each equivalence ratio (ϕ=0.5, 0.6, 0.7). As described in Chapter 3, a silica-coated R-type thermocouple with a bead of 0.2 mm diameter was used to collect the temperature data in the flame with a data acquisition system. The thermocouple was mounted to a two-dimensional traverse and data were collected at 2 mm radial intervals across the entire span of the flame. The temperatures recorded by the thermocouple were corrected to account for radiation and conduction heat losses at the flame-bead interface; the methodology for this correction is described in Appendix B.3. The corrected values for temperature [K] for each fuel are plotted against radial distance [mm] at every axial location measured in Figures 4.44-4.52. The experimental uncertainty associated with the measurements was ±26 K.

Flame peak temperatures for all flames were found close to the centerline at 25% flame height, which suggests that the diffusion controlled interface combustion was not dominant, and that the reactants were in a premixed burning condition. Also, higher temperatures were expected closer to the porous media surface where the reaction zone

was presumed to stabilize. The peak temperature measured at an equivalence ratio ϕ=0.5 was 1726 K corresponding to the Jet-A flame, for ϕ= 0.6 it was 1828 K corresponding to the SA 10 flame, and for ϕ= 0.7 it was 1758 K corresponding to the BSA 10-10 flame. The flame temperatures at each location and the peak temperatures for a given equivalence ratio did not vary more than 100 K between the three fuels. The measured peak temperatures agree with the calculated adiabatic flame temperatures for all three flames. Adiabatic temperatures displayed minimal difference for a given equivalence ratio (less than 15 K). Table 4.2 displays a comparison between the peak temperatures measured, and the calculated adiabatic flame temperatures. Adiabatic flame temperatures were calculated at the experimental conditions (T=463 K, and P=101 kPa) using the method described in Appendix B.4.

In-flame temperature profiles were practically uniform throughout the span of the flame, giving clear evidence of the enhanced mixing due to the presence of the porous media. It was observed that at higher flame locations, the temperature gradient near the axis was higher, due to mixing with surrounding air.

According to the study by Barajas (2009) on a similar setup, pure SME flames had a peak temperature 8% smaller than that of Jet-A flames. The results found in the study suggest that the blends between SME and Jet-A would not yield a peak temperature that exceeds 8% difference. In another study, Imran (2015) concluded that the blends of Jet-A and butanol yielded lower peak temperatures compared to that of Jet-A as the

concentration of butanol in the blends increased. The highest difference from Jet-A flame (12%) found by that author was measured with a 70% Jet-A – 30% butanol blend.

The results found for the SA-10 and BSA 10-10 flames agree with the studies mentioned previously; the maximum variation among the three blends studied did not exceed 5% at any equivalence ratio. These results are expected as the adiabatic flame temperatures calculated also show a minimal (< 3%) variation among them.

Peak temperatures measured in the porous media burner flames were slightly lower (difference less than 100 K) than those measured for open spray flames by Ratul et al. (2012), and Aldana (2010) probably due to heat transfer between the flame and the porous media; however spray flames showed a diffusion temperature profile with temperature peaks away from the flame axis, and lacked the uniformity of the porous media burner temperature profiles.

4.5 Soot Volume Fraction

Soot is mainly composed of carbon solid particles formed from the incomplete combustion of hydrocarbons. Incandescent soot particles within a flame are responsible for the flame's luminosity, as well as most of the heat loss due to radiation; soot particles radiate with peak wavelengths located in the infrared region of the spectrum. (Turns, 2011). As described in the experimental procedures (chapter 3) the path

integrated soot volume fraction was determined by measuring the difference of laser beam intensity with and without the presence of a flame.

From studies such as Ratul et al. (2012), Aldana (2010), and Imran (2015), it was expected that the soot volume fraction increased with equivalence ratio, as the availability of free oxygen decreased. A sharp decrease in soot formation was also expected when using fuel blends with higher molecular-bound oxygen concentration as the soot precursor production was limited by a more effective and faster fuel oxidization mechanism due to the presence of oxygen in the fuel molecules.

Soot volume fraction measurements performed on the flames studied in the current project yielded 0 ppm of soot in the flames for most cases, or quantities that were not able to be resolved from experimental uncertainty (for this experiment, uncertainty corresponded to 0.07 ppm. The minimal formation of soot directly agrees with what is seen in the physical appearance of the flames (Figures 4.1-4.3) as all of them have low luminosities, exhibit a blue hue on the entirety of the flame, and lack the luminous yellow hues characteristic of radiating soot.

Open spray flame studies such as those performed by Aldana (2010), who performed flame characterization studies of open spray flames using diesel and its blends with CME, and SME, and Ratul (2013), who performed a similar study using Jet-A/butanol blends, produced large quantities of soot as observed form the flame appearance. The

spray flames documented by the authors were yellow, and luminous; Open spray flames are dominated by the atomization and the evaporation rate of the droplets, in addition, diffusion flame front effects heavily affect the reaction mechanisms that allow the formation of soot particles in the flame. The physical appearance of these flames can be attributed to soot presence, as incandescent soot within a flame is the primary source of this type of flames' luminosity and color (Turns, 2011). Aldana (2010) determined that blends with higher biodiesel content produced less soot, attributing the effect to the increased concentration of fuel bound oxygen. Ratul (2013) reported a similar trend when the content of butanol was increased in the blends, this effect can also be attributed to the increase in molecule bound oxygen, as well as the lower H/C ratio of butanol compared to Jet-A. From these studies it can be concluded that the increased concentration of molecular bound oxygen effectively reduces soot production in a flame.

Imran (2015) performed a similar study using Jet-A/butanol blends on a spray flame with a porous media burner. The flames have lower luminosity than the ones produced in an open spray burner, which is already an indicator of different combustion mechanisms. While using a porous media burner, the fuel is fully evaporated, and partially premixed at the time of the reaction, which suppresses the diffusion effects seen on spray flames, hence limiting soot production. Soot concentration found by Imran (2015) show lower soot concentrations than the concentrations measured using open spray flames, suggesting the effectiveness of porous media burners on reducing

soot formation. Additionally, soot concentration decreased with increasing concentration of butanol in the blends agreeing with previously published results

In conclusion, several factors drive the formation of soot in a flame, most of which are suppressed by the combustion technique, and the blends used for this study. The use of a two-phase porous media combustor enhances evaporation and mixing, which as a result leads to a complete homogeneous partially premixed reaction downstream of the porous media.

Lean combustion conditions paired with improved mixing mechanisms allow free oxygen to become more readily available to the already evaporated fuel, which in turn suppress soot precursors formation. Additionally, in the case of SA 10, and BSA 10-10 the presence of fuel-bound oxygen increases the effectiveness of fuel oxidation mechanisms, as a result shorter, less luminous flames are formed.

The method described by Yagi and Iino (1962) is still a valid method to measure soot volume fraction, in order to attest to its validity the soot volume fraction at 60% flame height was meassured for a Jet-A flame at equivalence ratios 1.0 and 1.2. The ϕ=1.0 yielded a soot volume fraction of 0.096 ppm, while the ϕ=1.2 flame yielded 0.110 ppm. An extensive description of these measurements is provided in Appendix B.5.

4.6 Pressure Drop across the Porous Media

The pressure drop across each individual porous medium was documented for a new set of porous media (EPM and CPM) prior to any experiments. Measurements were repeated after 100 hours of operation to account for the degradation suffered by the porous media due to the interaction with the fuels after. After the measurements, pressurized air was blown into the porous media with the intention of reducing pore blockage. The pressure drop across the porous media was documented after this was performed.

The results for the pressure drop across the PM are displayed in Figure 4.53. The pressure drop across the new evaporation porous medium was found to be 105 Pa. After 100 hours of operation, the pressure drop across the EPM increased by 56% to a value of 164 Pa. The increase of pressure drop across the EPM is the result of pores becoming clogged due to the contact with liquid fuel, and solid residues accumulation. Solid residues were especially noticeable in the blends that contained SME presumably because of the components of SME with higher boiling points. After blasting air through the porous media the pressure drop across the EPM was reduced to 140 Pa (16% less than the value recorded after 100 hours of operation).

The pressure drop across the new combustion porous medium was found to be 34 Pa. After 100 hours of operation, the pressure drop increased by 6% to a value of 36 Pa. CPM pores are relatively large which made clogging much more difficult, additionally,

most of the fuel passing through the CPM was already vaporized, which allowed for little or no residues to deposit on the CPM. The pressure drop for the CPM remained unaffected after the maintenance procedure.

Considering the operational parameters of the burner, the difference generated by degradation of the porous media is negligible. In conclusion, the use of blends in a similar burner does not represent any major change in performance.

Barajas (2009) performed a similar study in order to determine the effects of solid deposits and pore blockage on the porous media due to the combustion of biofuels-Jet-A blends. Barajas found that after 14 hours of operation the combined pressure drop of the porous media (Pressure EPM + Pressure CPM) increasead 45% on average across three different flow rates (8.1 l/min, 14.6 l/min, 21.2 l\min). The author atributed the increase of pressure drop to the accumulation of solid residues, and the blockage of pores.

Imran (2015) investigated the effects of Jet-A-butanol blends on the porous media after 20 hours of operation at a flow rate of 21.2 l/min. The author found that the pressue drop across the EPM increased by 21% (an increase of 8 Pa), and the CPM pressure drop increased from 2 Pa to 4 Pa.

Table 4.1a: Mole percentage for the dry products of the complete combustion of Jet-A at ϕ=0.5, ϕ=0.6, and ϕ=0.7 at ϕ=1.0

ϕ	CO_2	N_2	O_2
0.5	7.53	81.62	10.85
0.6	9.09	82.17	8.74
0.7	10.68	82.72	6.60
1.0	15.57	84.43	0.00

Table 4.1b: Mole percentage for the dry products of the complete combustion of SA 10 at ϕ=0.5, ϕ=0.6, and ϕ=0.7 at ϕ=1.0

ϕ	CO_2	N_2	O_2
0.5	7.54	81.61	10.85
0.6	9.11	82.15	8.74
0.7	10.71	82.75	6.55
1.0	15.60	84.40	0.00

Table 4.1c: Mole percentage for the dry products of the complete combustion of BSA 10-10 at ϕ=0.5, ϕ=0.6, and ϕ=0.7 at ϕ=1.0

ϕ	CO_2	N_2	O_2
0.5	7.52	81.63	10.85
0.6	9.08	82.17	8.74
0.7	10.69	82.86	6.45
1.0	15.56	84.44	0.00

Table 4.2: Calculated adiabatic flame temperature and peak in flame temperature for the blends at ϕ=0.5, ϕ=0.6, and at ϕ=0.7 with the initial reactant temperature of 463 K.

Fuel	Jet-A	SA 10	BSA 10-10
Adiabatic Flame Temperature $_{(463\ K)}$ [K]	2618	2612	2624
Peak In-Flame Temperature ϕ=0.5 [K]	1726	1725	1719
Peak In-Flame Temperature ϕ=0.6 [K]	1759	1828	1764
Peak In-Flame Temperature ϕ=0.7 [K]	1673	1751	1758

Figure 4.1: Photographs of flames at ϕ=0.5 (exposure time of 0.2 second).

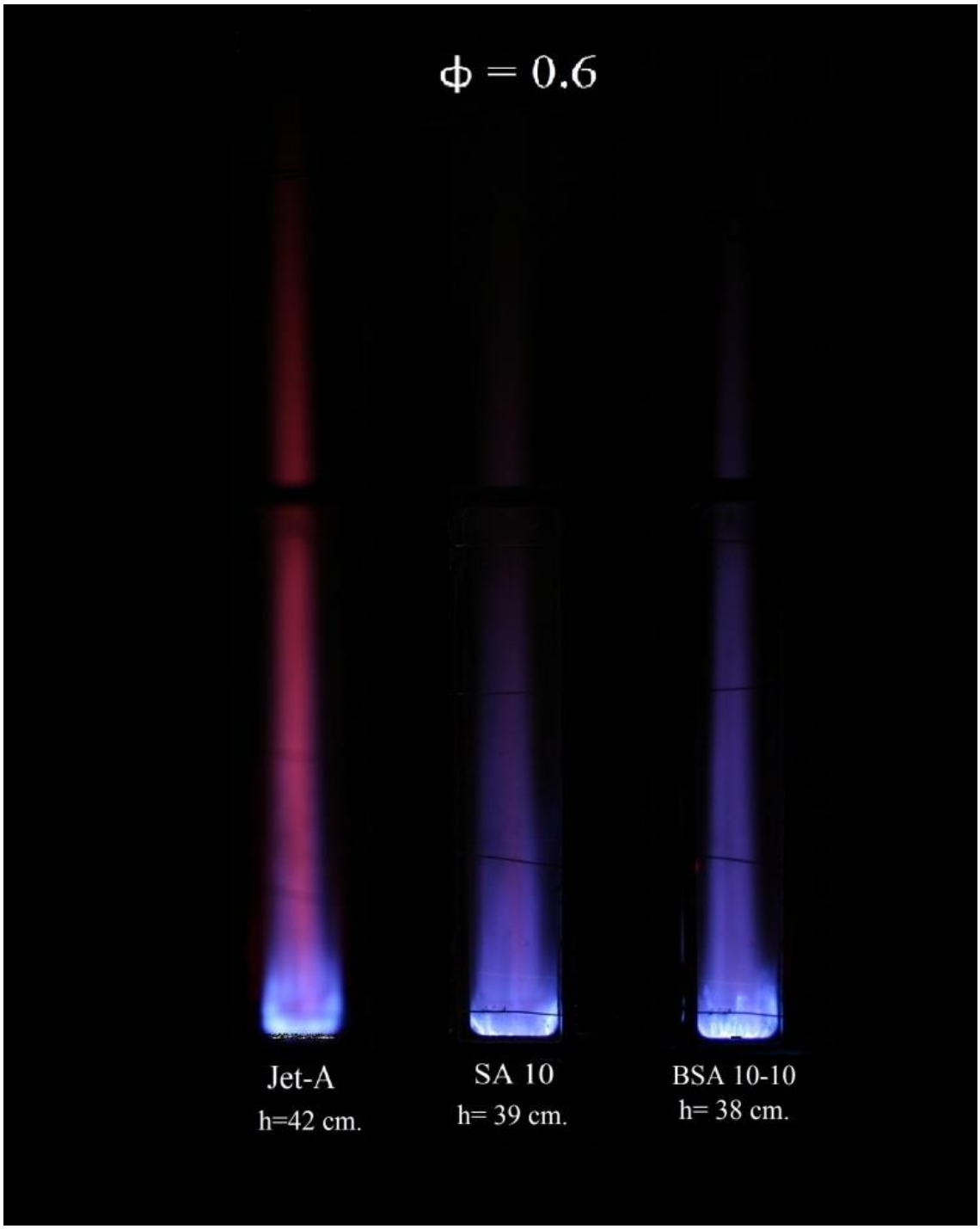

Figure 4.2: Photographs of flames at ϕ=0.6 (exposure time of 0.2 second).

Figure 4.3: Photographs of flames at ϕ=0.7 (exposure time of 0.2 second).

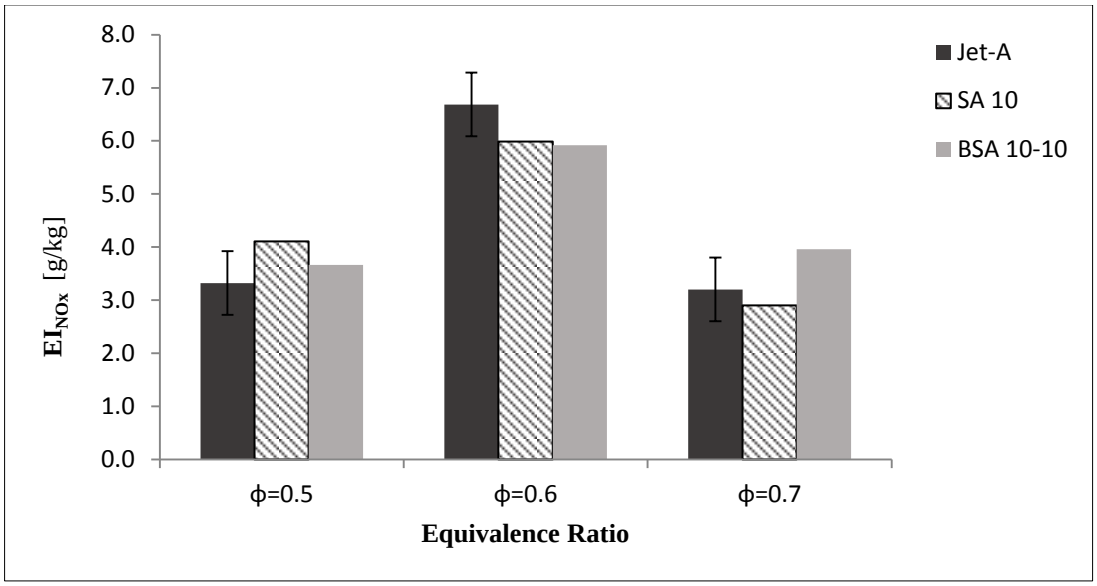

Figure 4.4: NOx global emission indices for all flames for each equivalence ratio.

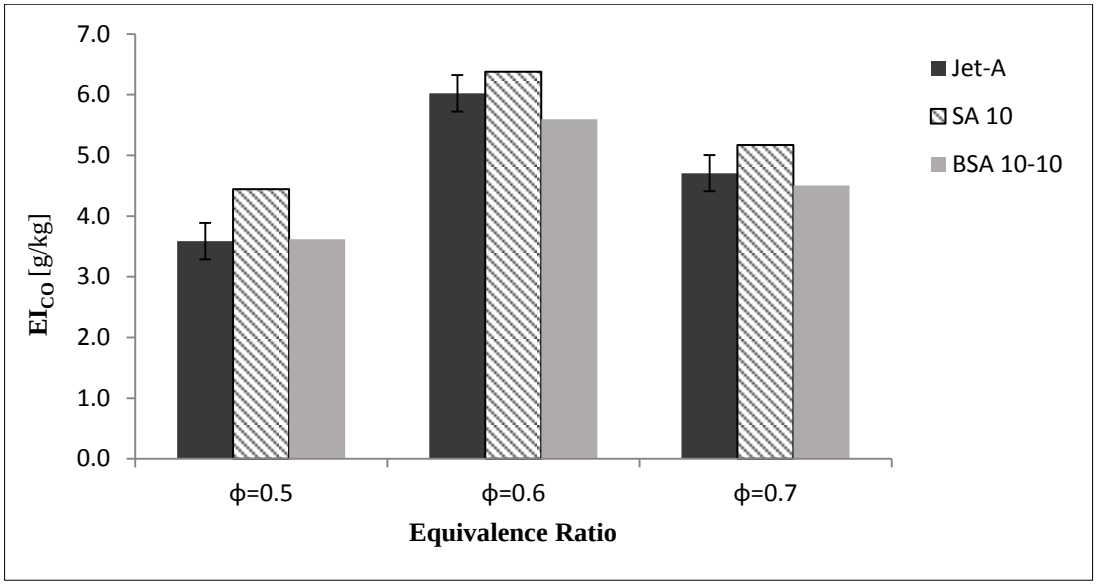

Figure 4.5: CO global emission indices for all flames for each equivalence ratio.

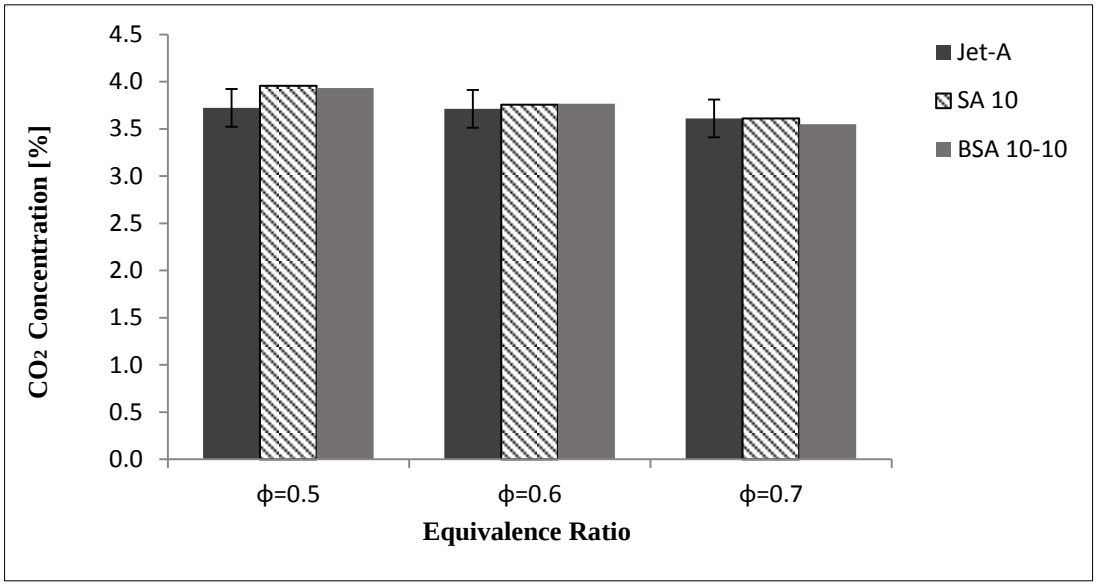

Figure 4.6: CO_2 global emission concentration for all flames for each equivalence ratio.

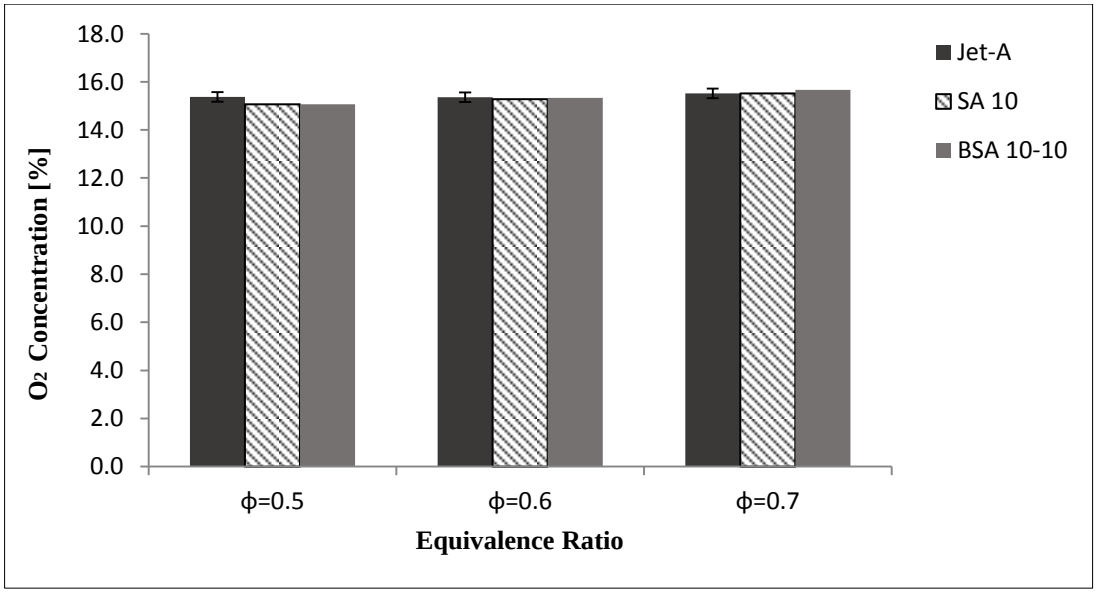

Figure 4.7: O_2 global emission concentration for all flames for each equivalence ratio.

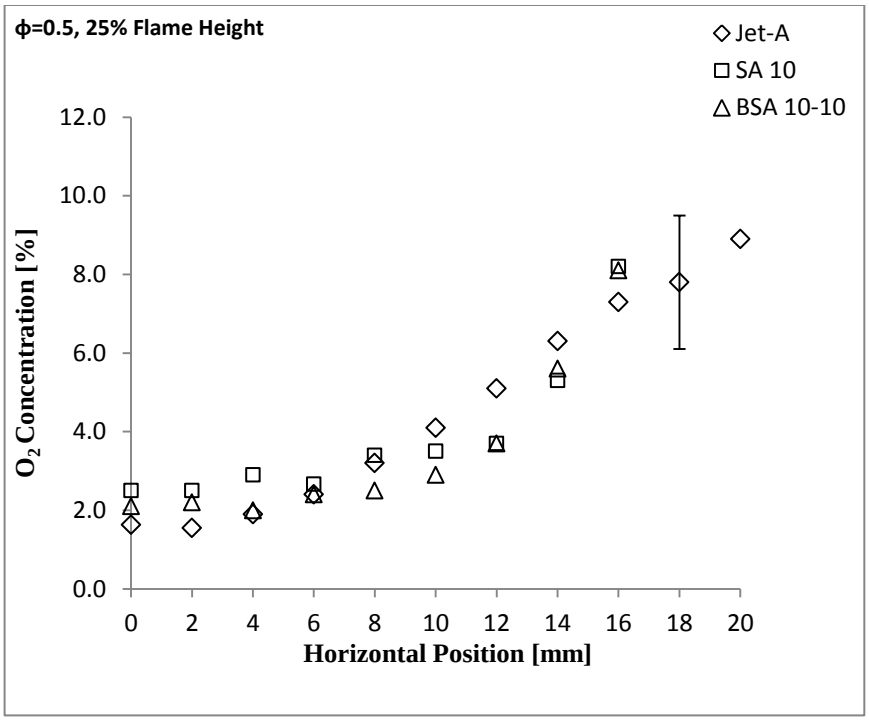

Figure 4.8: Radial in-flame O_2 concentration profiles at ϕ=0.5 and 25% flame height.

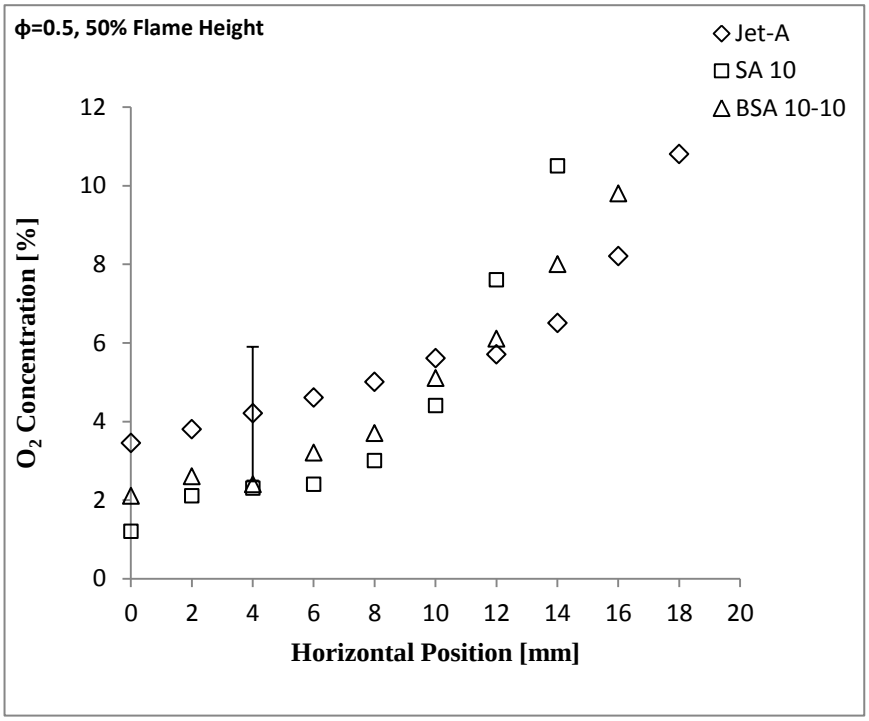

Figure 4.9: Radial in-flame O_2 concentration profiles at ϕ=0.5 and 50% flame height.

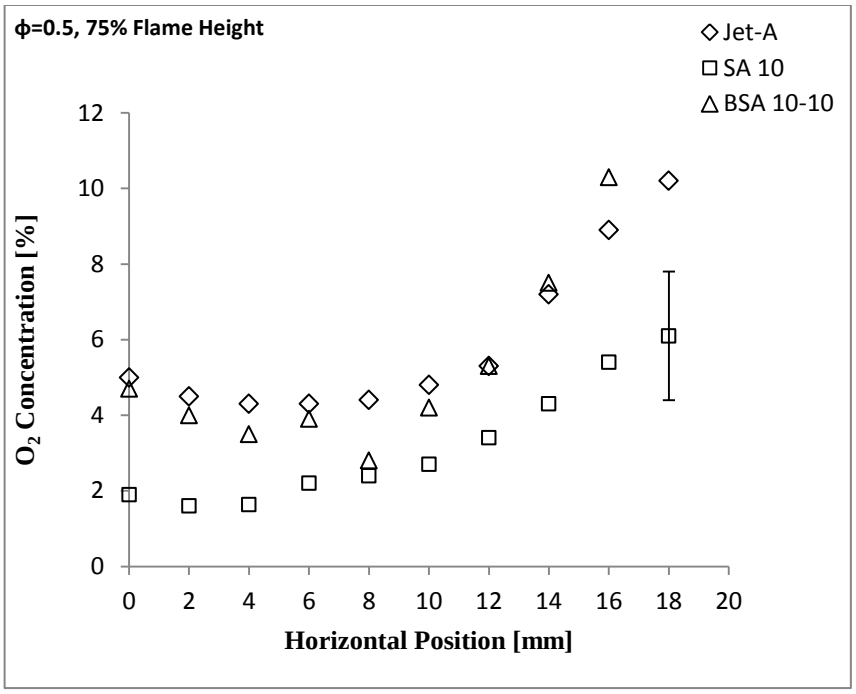

Figure 4.10: Radial in-flame O_2 concentration profiles at ϕ=0.5 and 75% flame height.

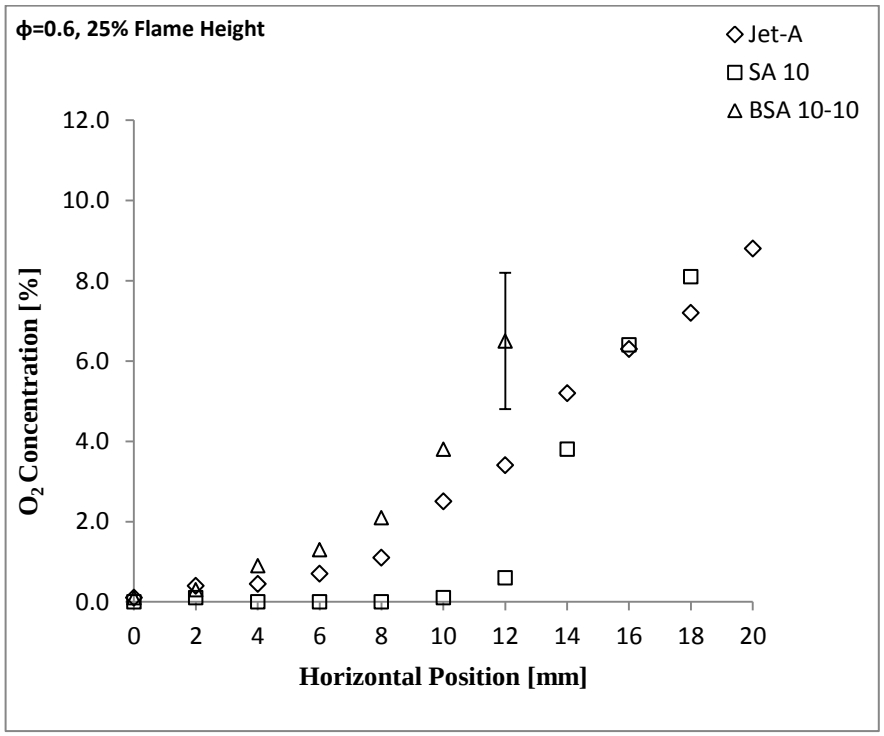

Figure 4.11: Radial in-flame O_2 concentration profiles at ϕ=0.6 and 25% flame height.

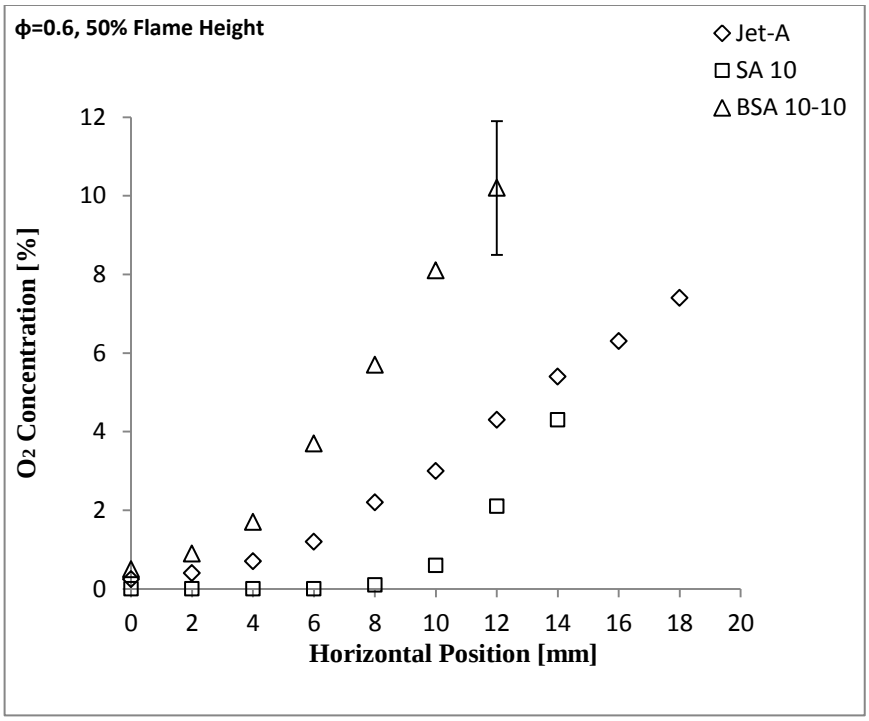

Figure 4.12: Radial in-flame O_2 concentration profiles at ϕ=0.6 and 50% flame height.

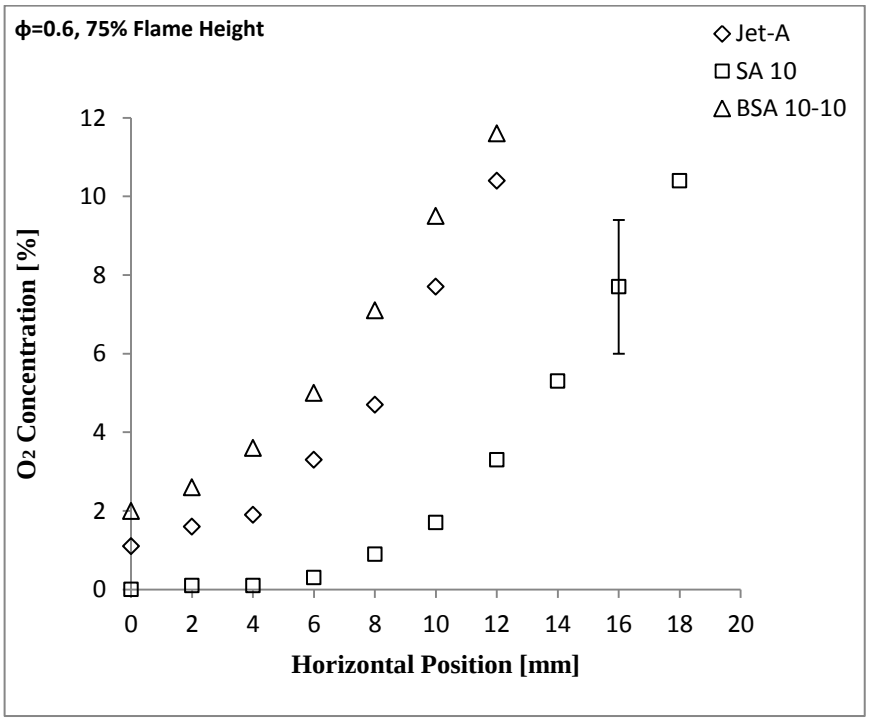

Figure 4.13: Radial in-flame O_2 concentration profiles at ϕ=0.6 and 75% flame height.

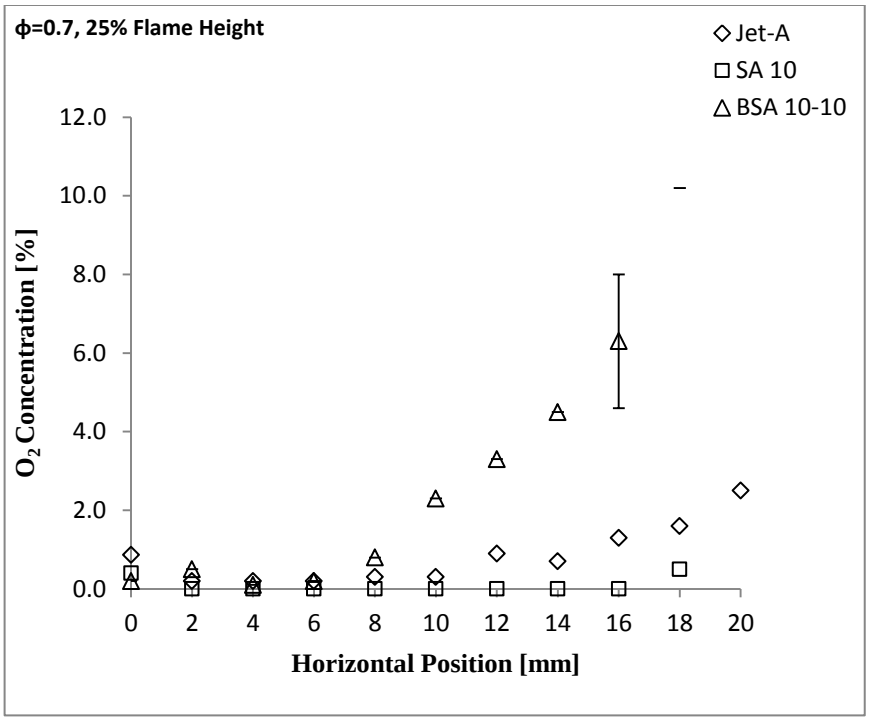

Figure 4.14: Radial in-flame O_2 concentration profiles at ϕ=0.7 and 25% flame height.

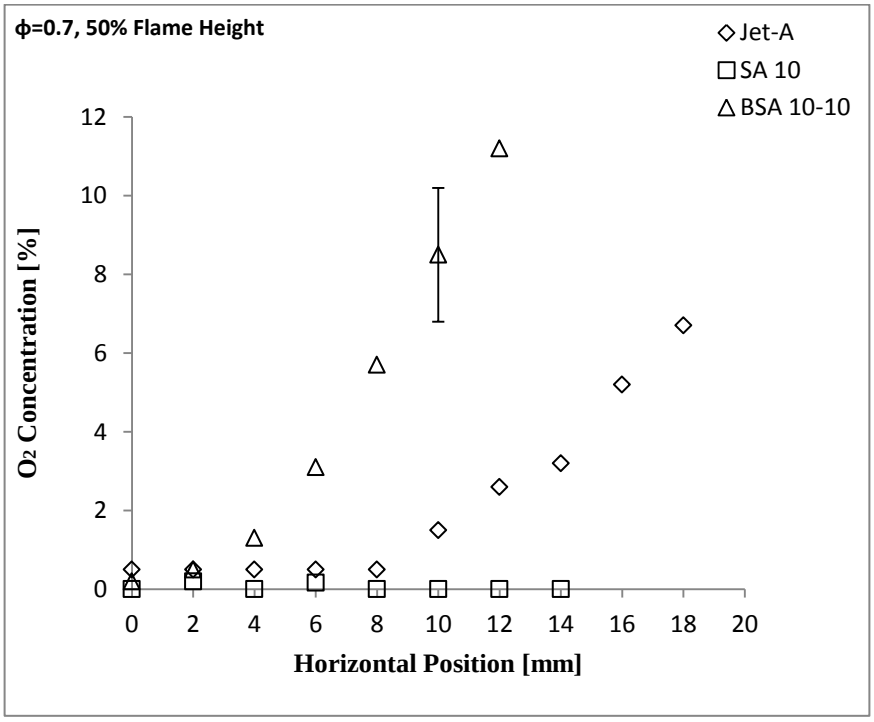

Figure 4.15: Radial in-flame O_2 concentration profiles at ϕ=0.7 and 50% flame height.

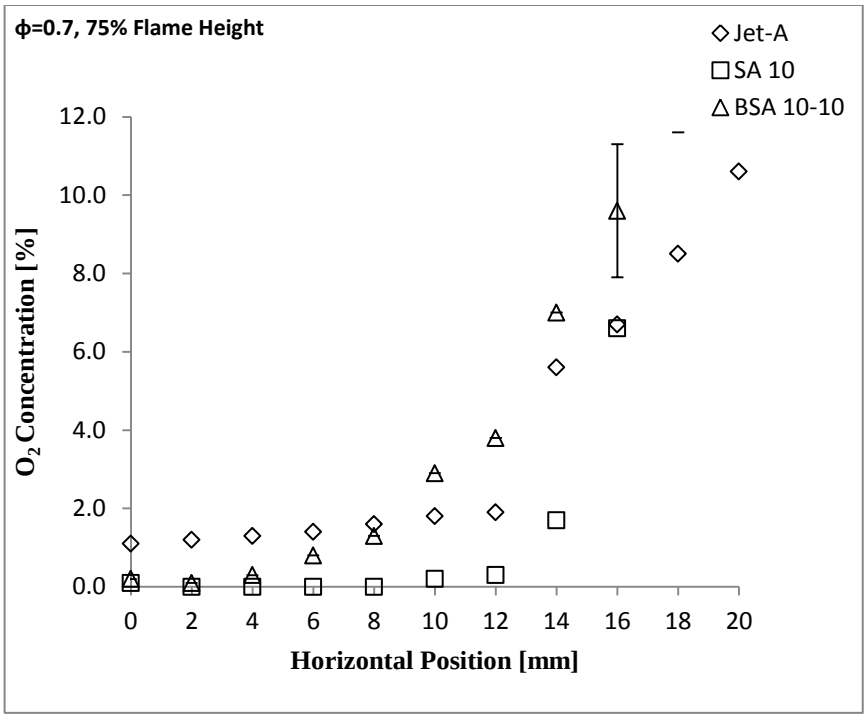

Figure 4.16: Radial in-flame O_2 concentration profiles at ϕ=0.7 and 75% flame height.

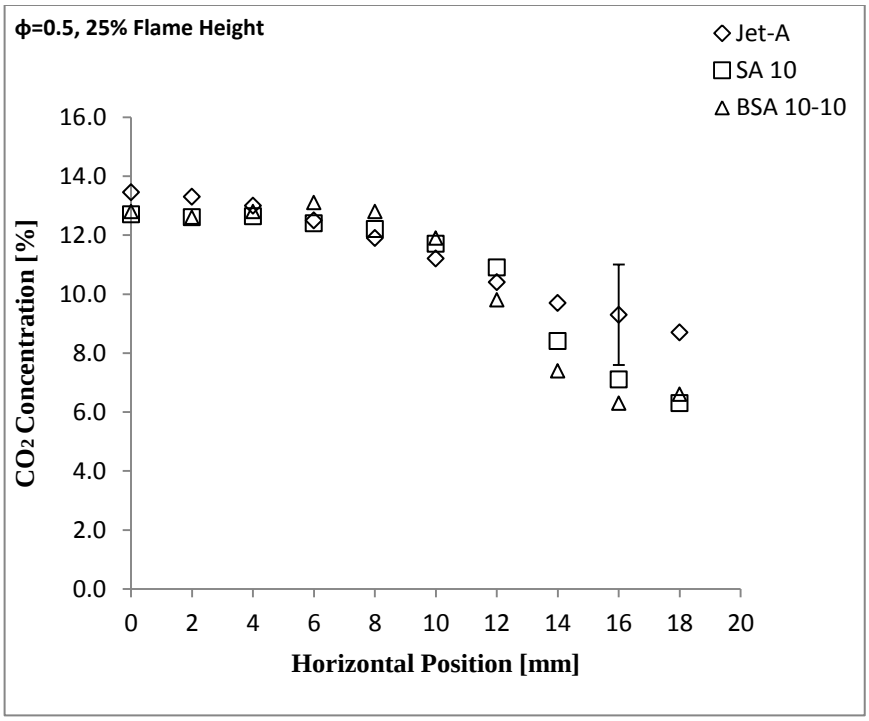

Figure 4.17: Radial in-flame CO_2 concentration profiles at ϕ=0.5 and 25% flame height.

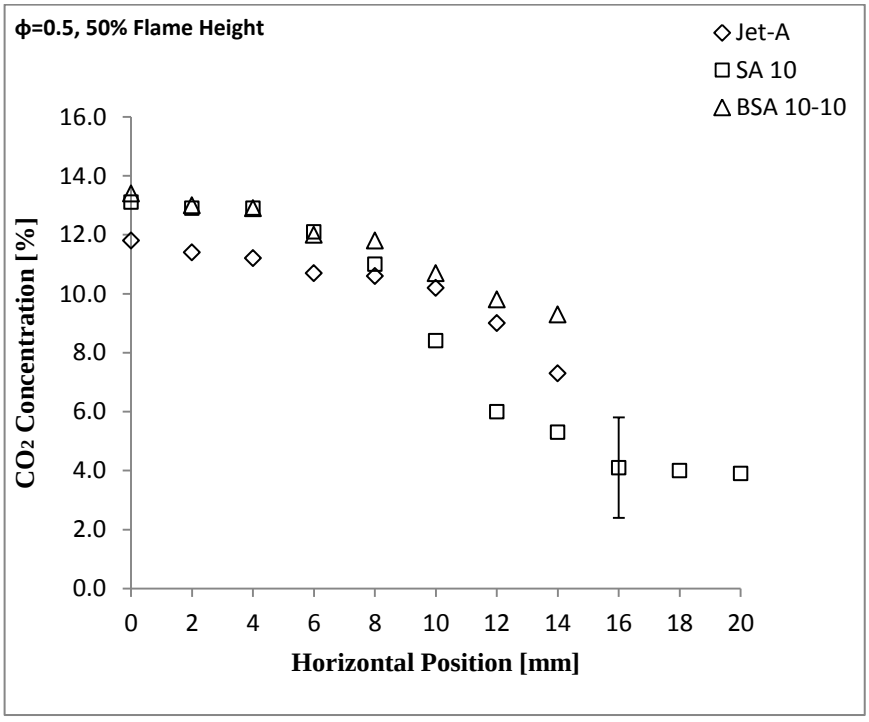

Figure 4.18: Radial in-flame CO_2 concentration profiles at ϕ=0.5 and 50% flame height.

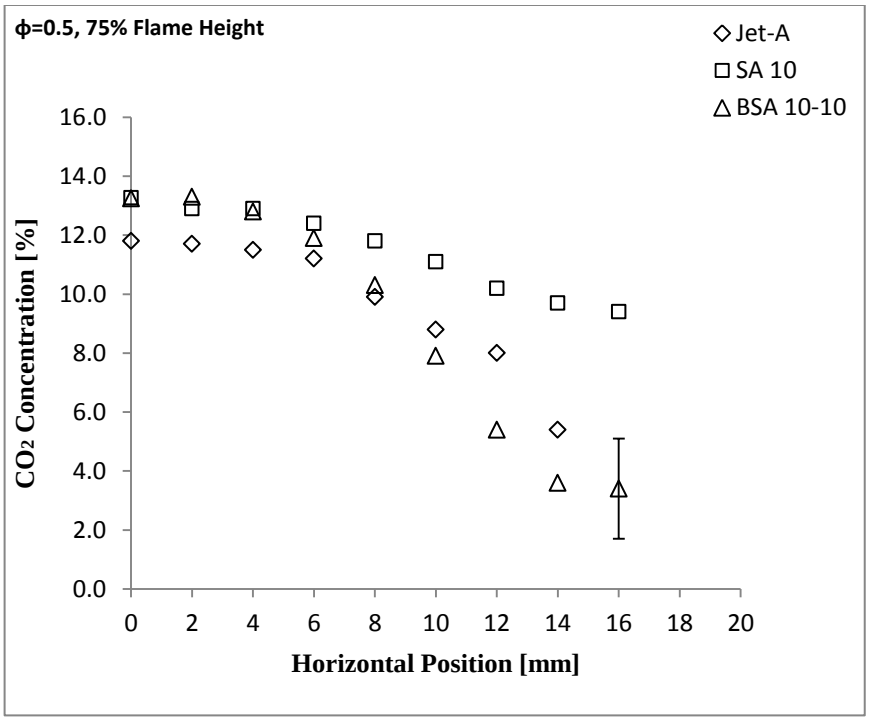

Figure 4.19: Radial in-flame CO_2 concentration profiles at ϕ=0.5 and 75% flame height.

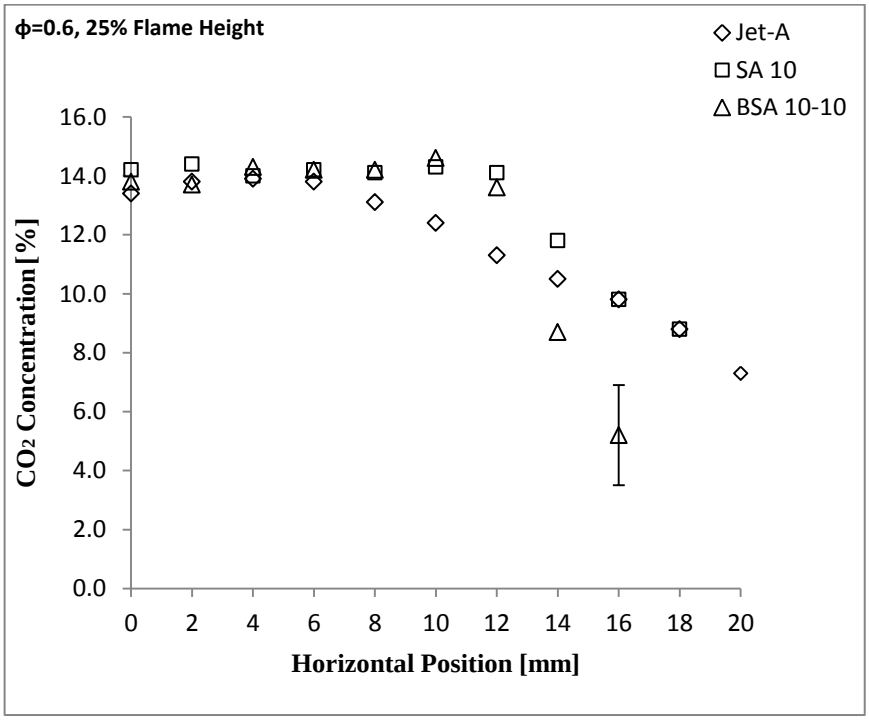

Figure 4.20: Radial in-flame CO_2 concentration profiles at ϕ=0.6 and 25% flame height.

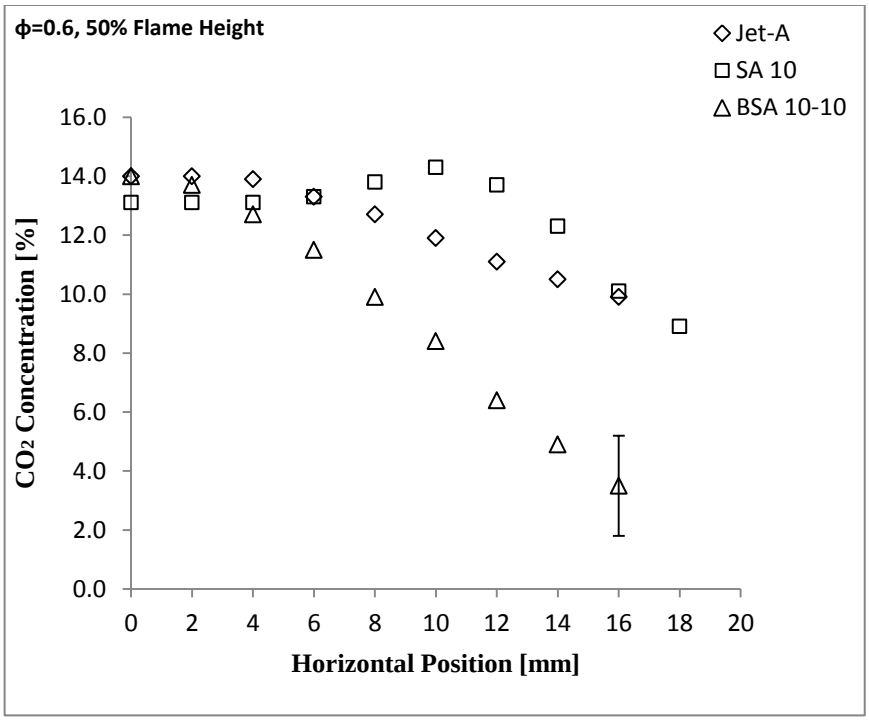

Figure 4.21: Radial in-flame CO_2 concentration profiles at ϕ=0.6 and 50% flame height.

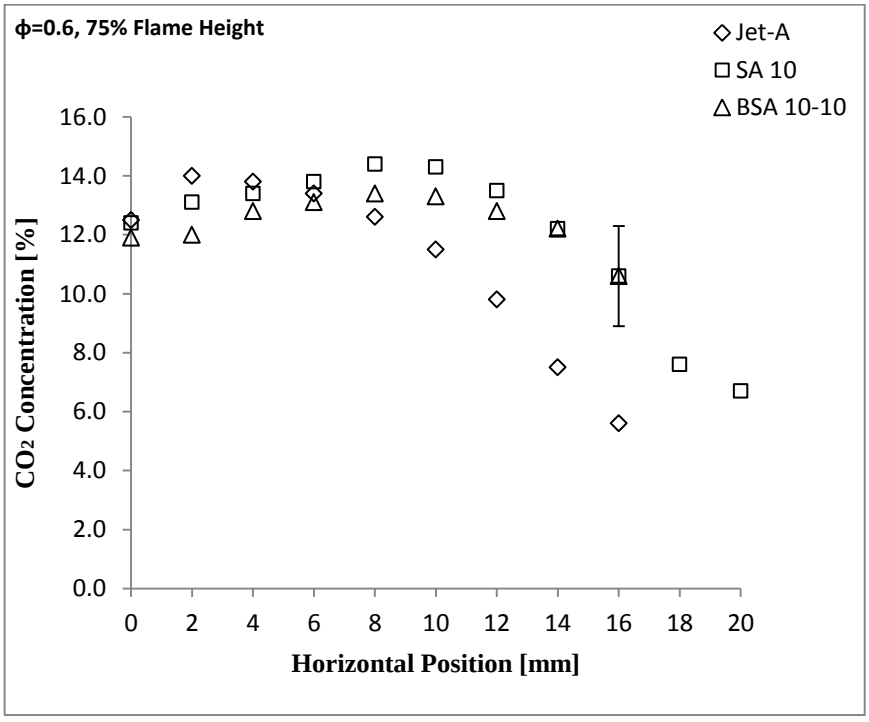

Figure 4.22: Radial in-flame CO_2 concentration profiles at ϕ=0.6 and 75% flame height.

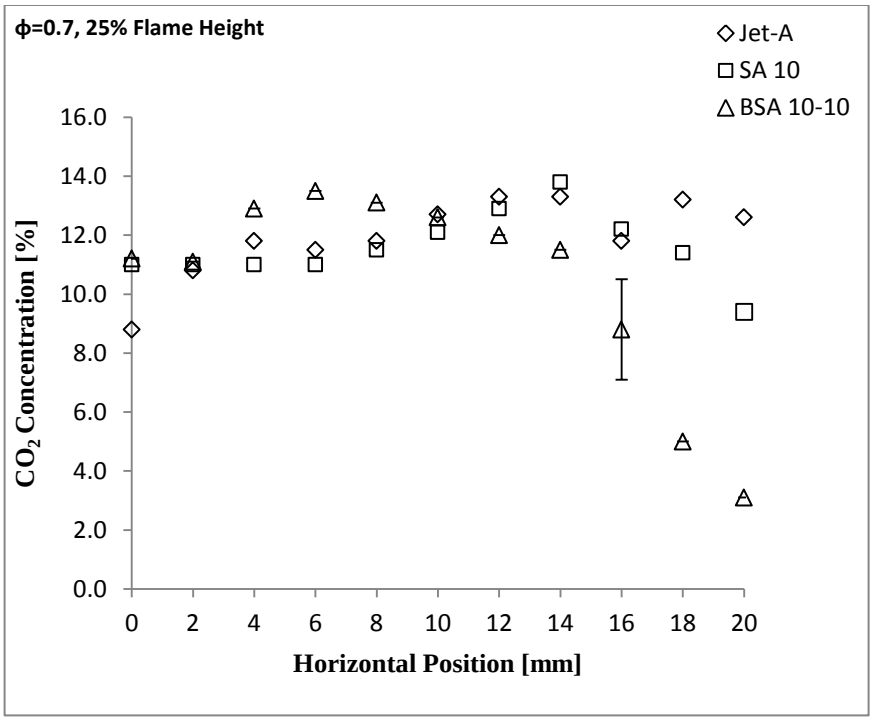

Figure 4.23: Radial in-flame CO_2 concentration profiles at ϕ=0.7 and 25% flame height.

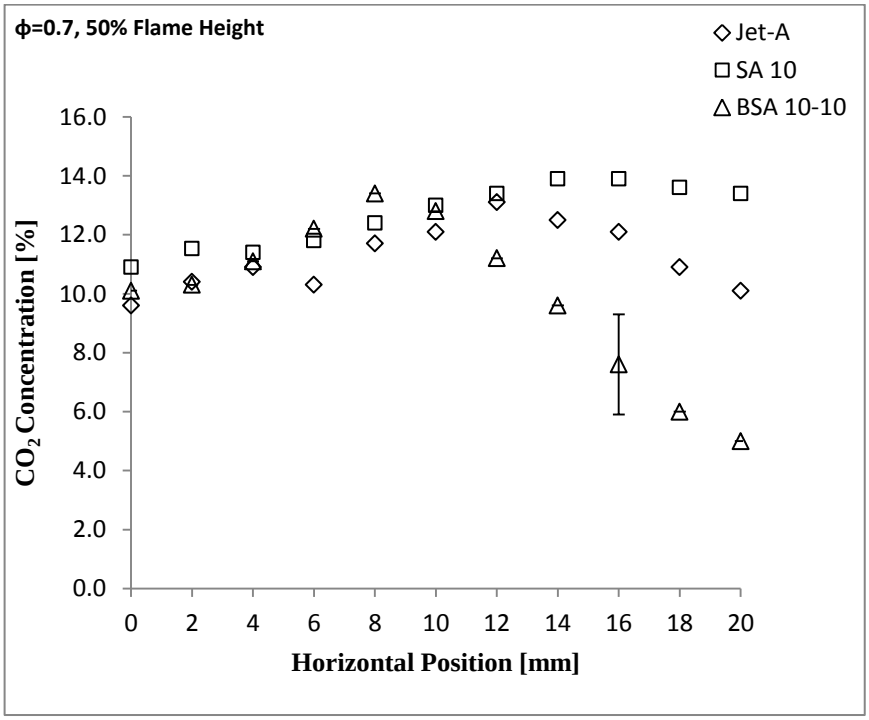

Figure 4.24: Radial in-flame CO_2 concentration profiles at ϕ=0.7 and 50% flame height.

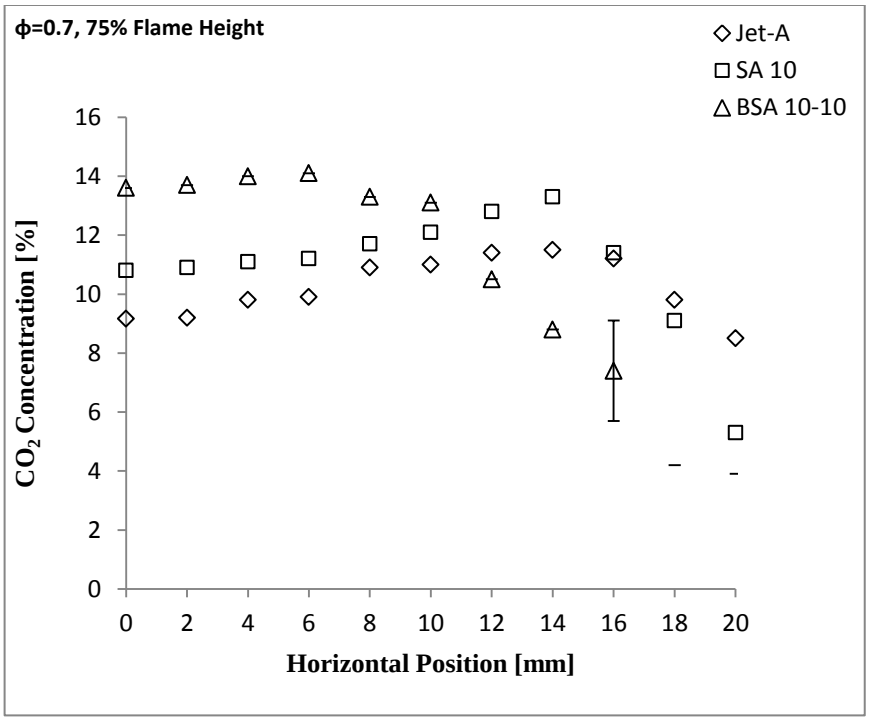

Figure 4.25: Radial in-flame CO_2 concentration profiles at ϕ=0.7 and 75% flame height.

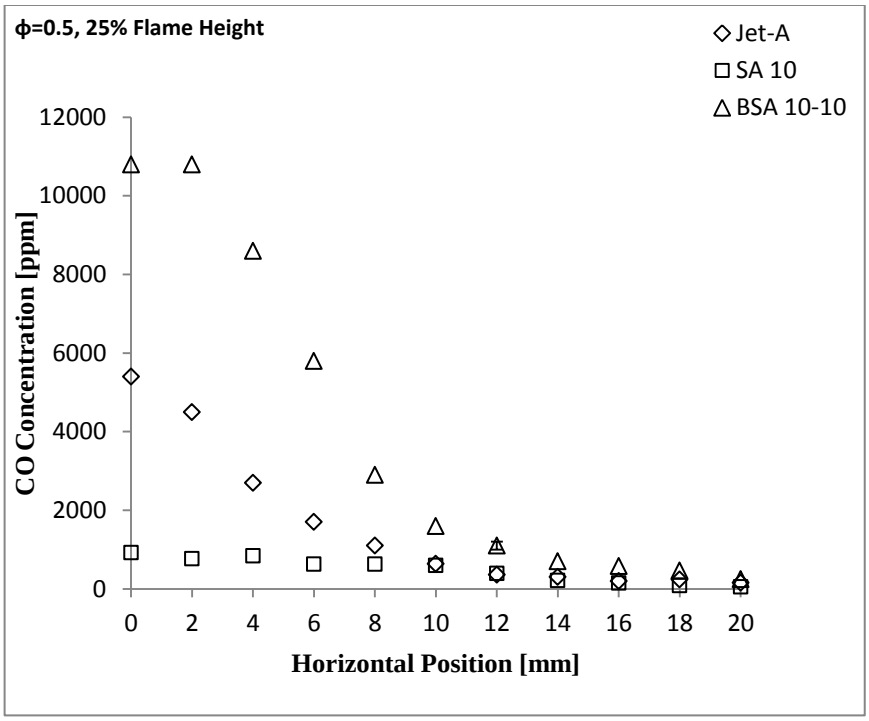

Figure 4.26: Radial in-flame CO concentration [ppm] profiles at ϕ=0.5 and 25% flame height.

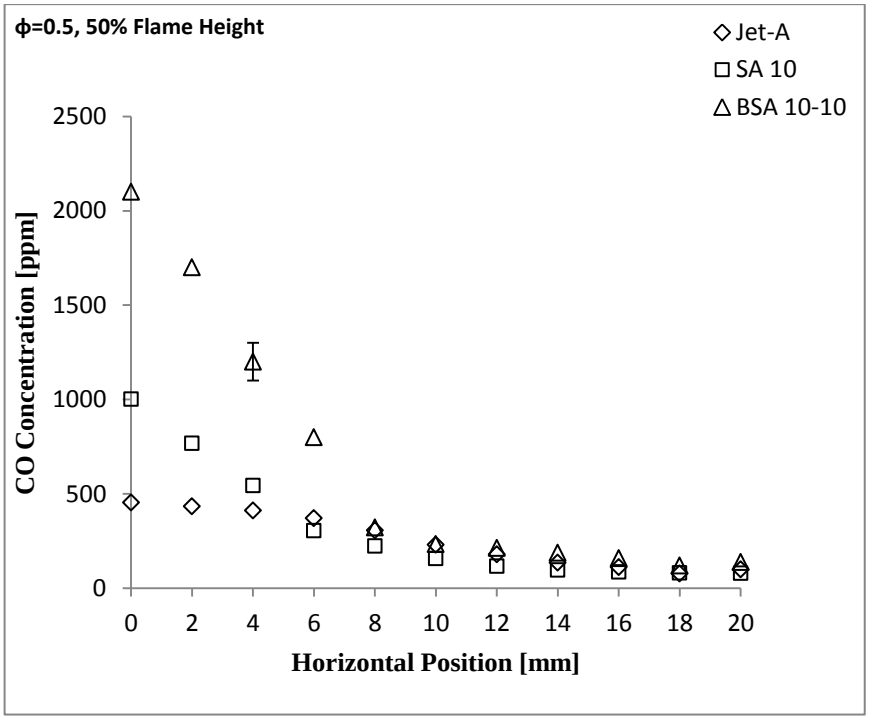

Figure 4.27: Radial in-flame CO concentration [ppm] profiles at ϕ=0.5 and 50% flame height.

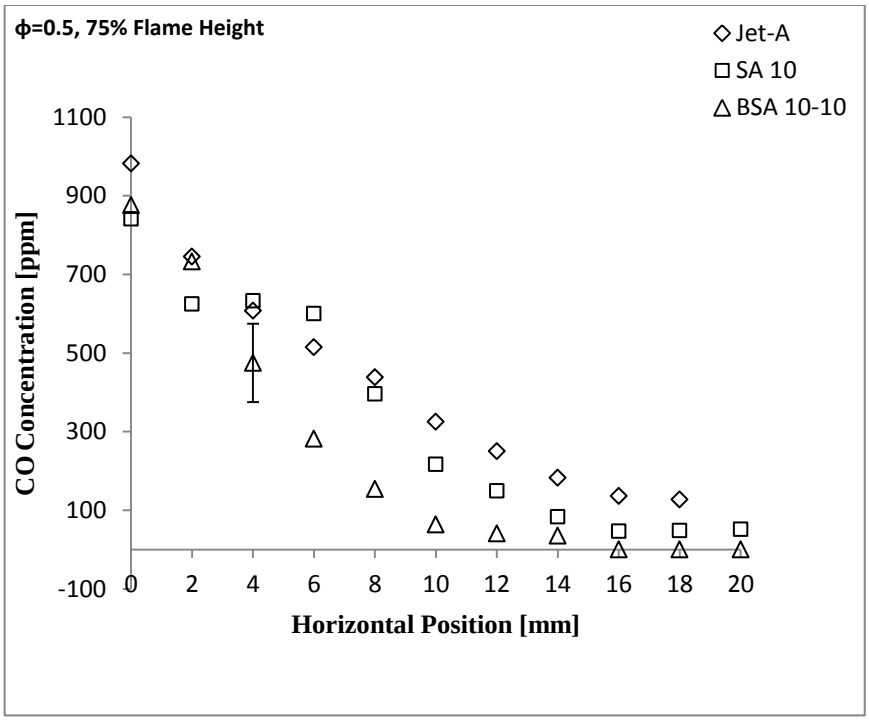

Figure 4.28: Radial in-flame CO concentration [ppm] profiles at ϕ=0.5 and 75% flame height.

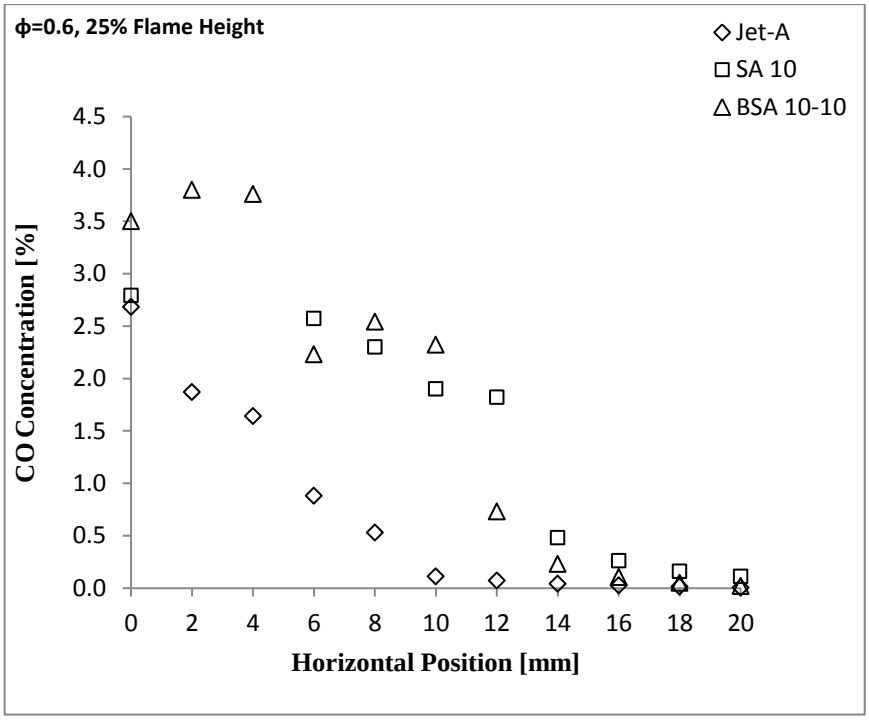

Figure 4.29: Radial in-flame CO concentration [%] profiles at ϕ=0.6 and 25% flame height.

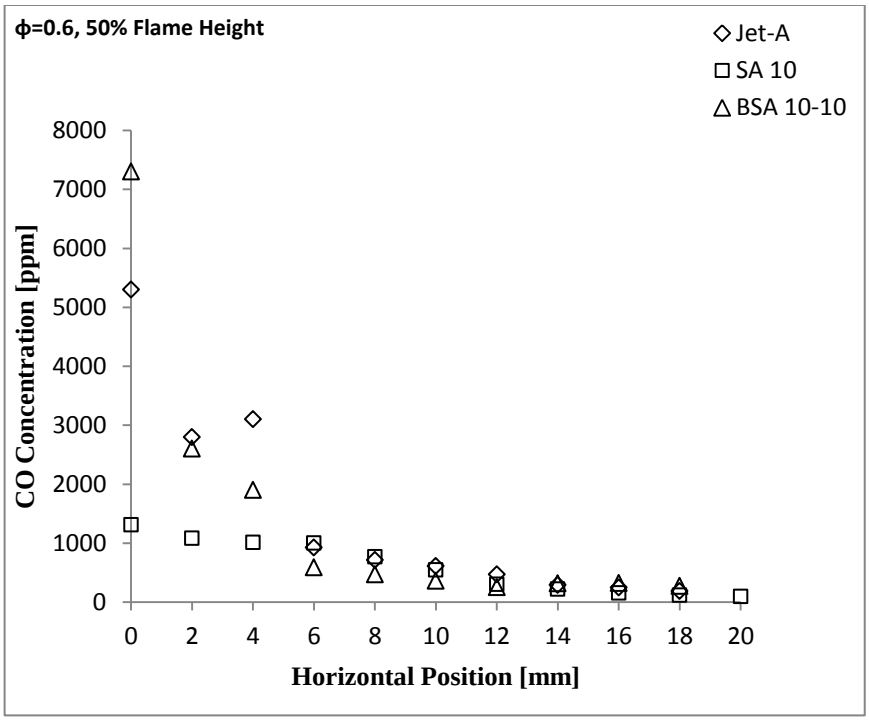

Figure 4.30: Radial in-flame CO [ppm] concentration profiles at ϕ=0.6 and 50% flame height.

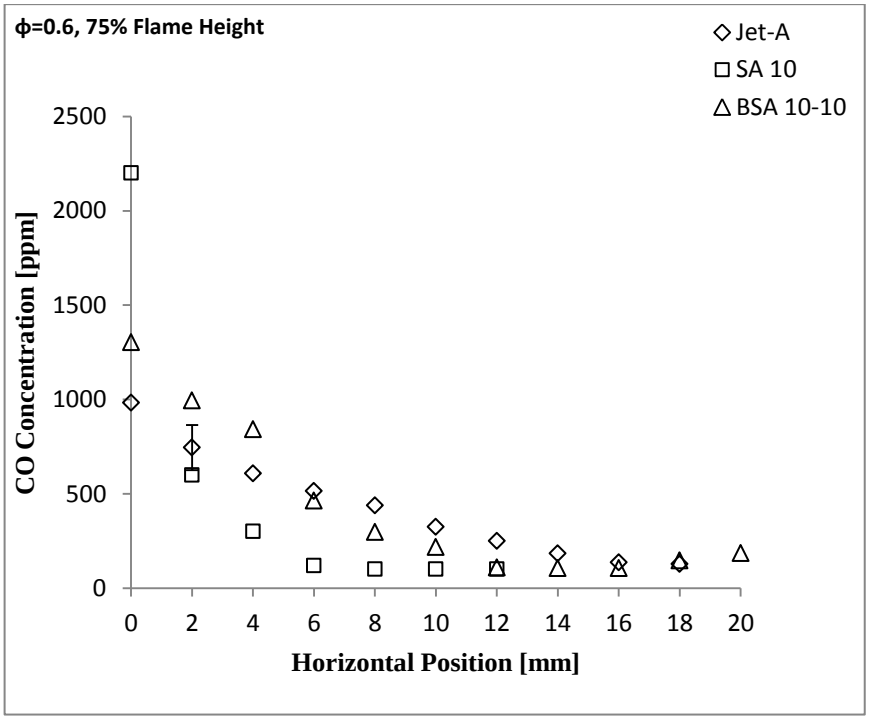

Figure 4.31: Radial in-flame CO [ppm] concentration profiles at ϕ=0.6 and 75% flame height.

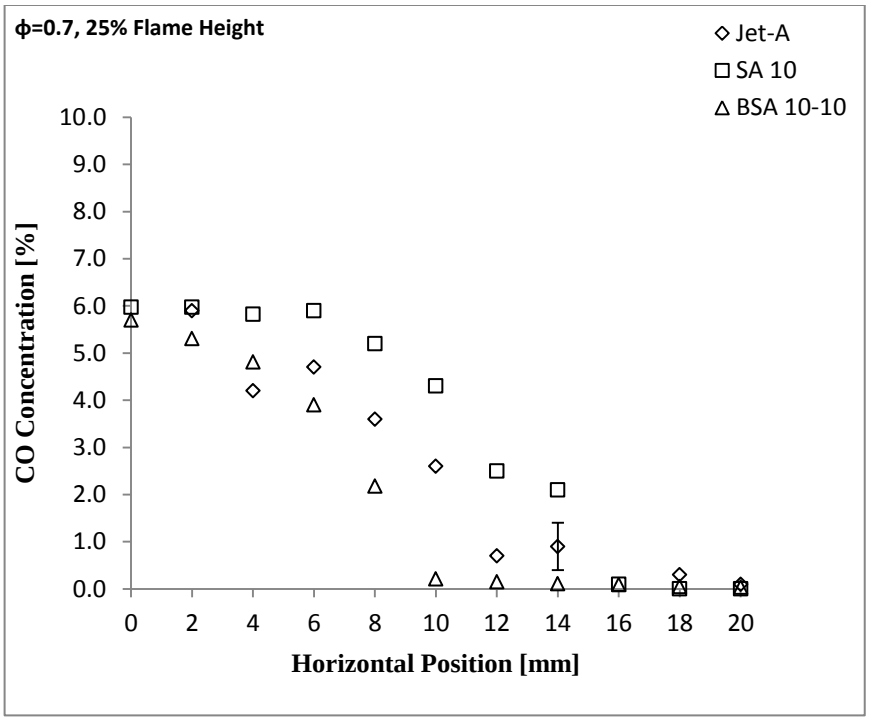

Figure 4.32: Radial in-flame CO concentration[%] profiles at ϕ=0.7 and 25% flame height.

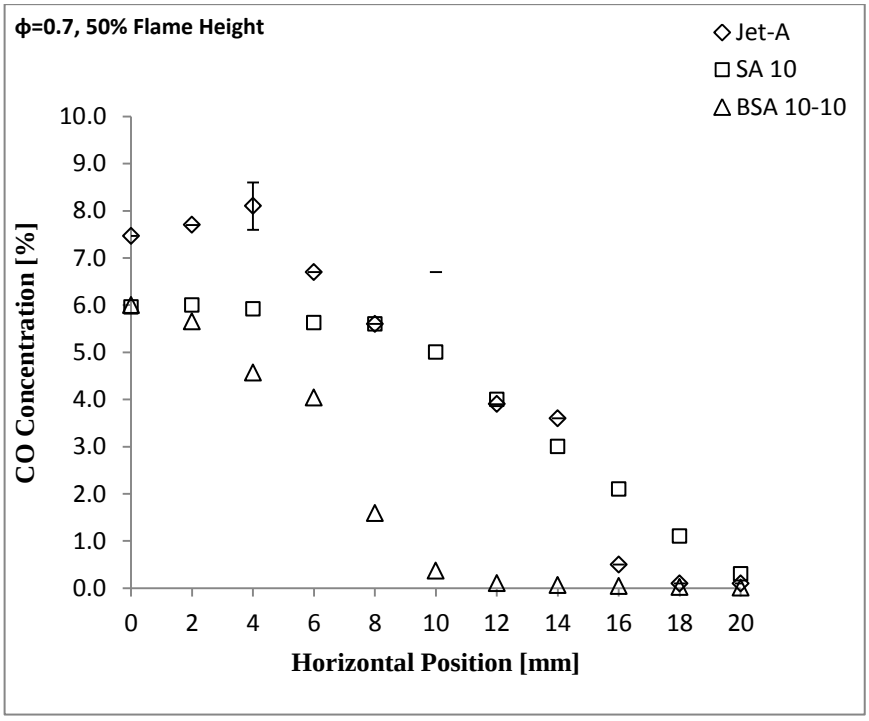

Figure 4.33: Radial in-flame CO concentration [%] profiles at ϕ=0.7 and 50% flame height.

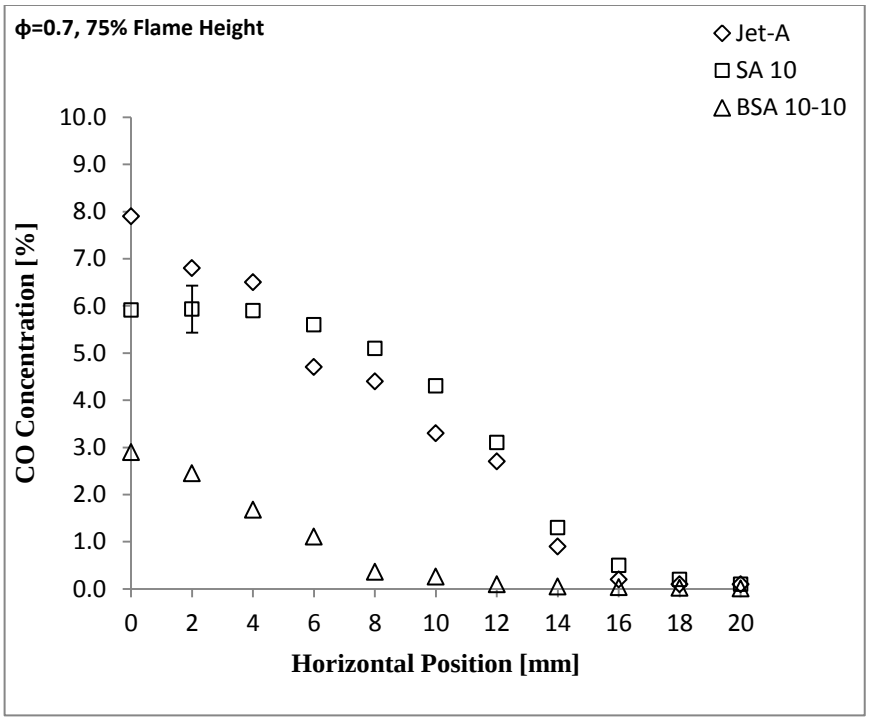

Figure 4.34: Radial in-flame CO concentration [%] profiles at ϕ=0.7 and 75% flame height.

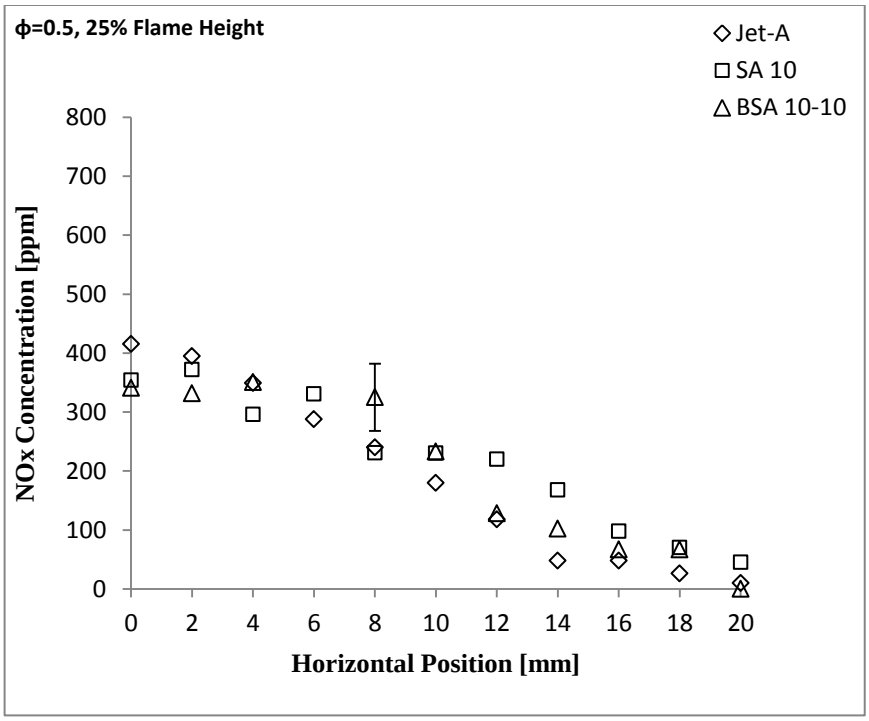

Figure 4.35: Radial in-flame NOx concentration profiles at ϕ=0.5 and 25% flame height.

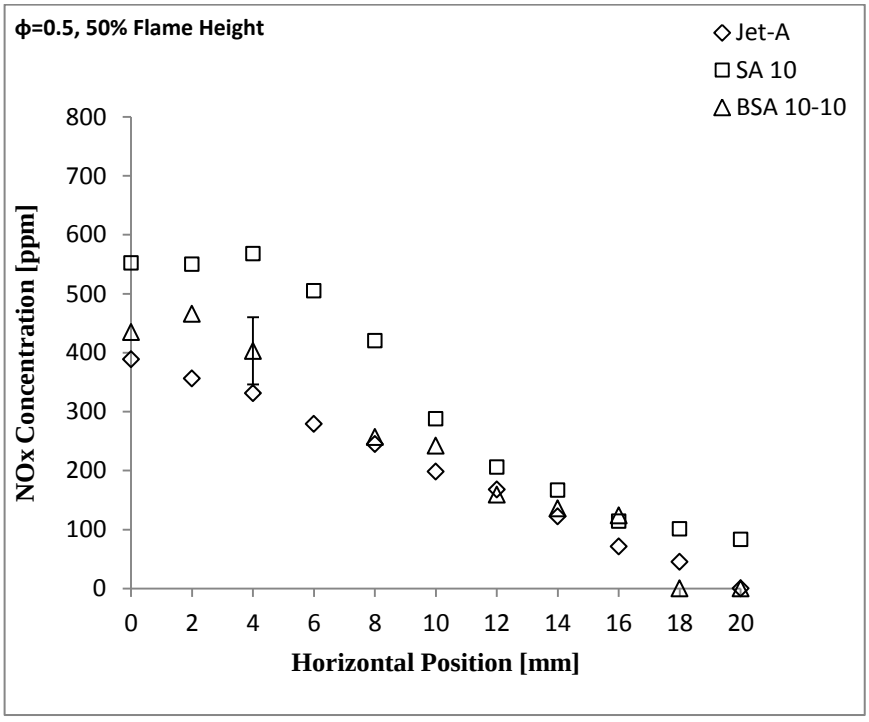

Figure 4.36: Radial in-flame NOx concentration profiles at ϕ=0.5 and 50% flame height.

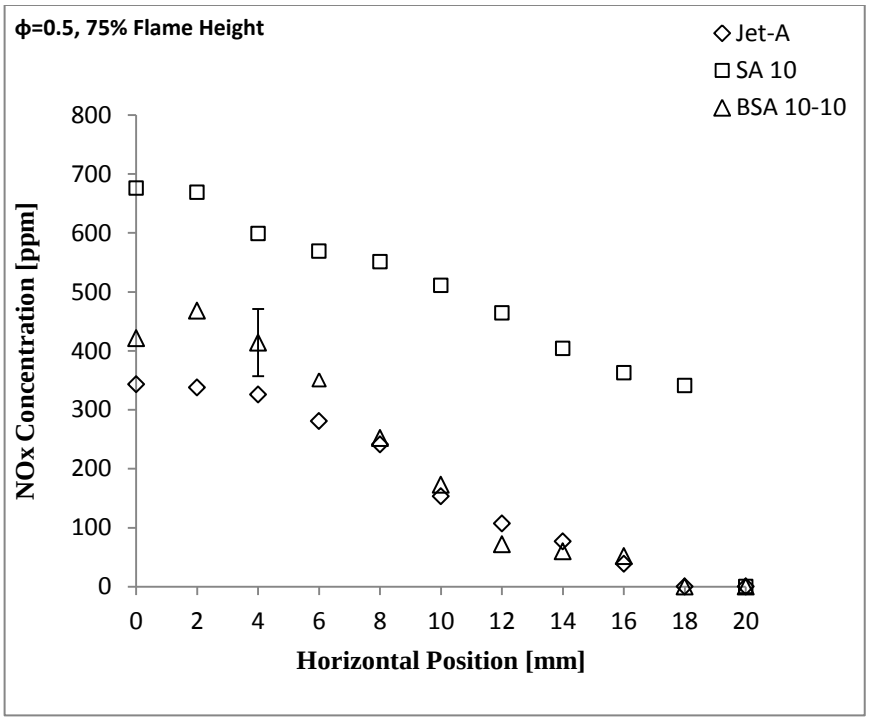

Figure 4.37: Radial in-flame NOx concentration profiles at ϕ=0.5 and 75% flame height.

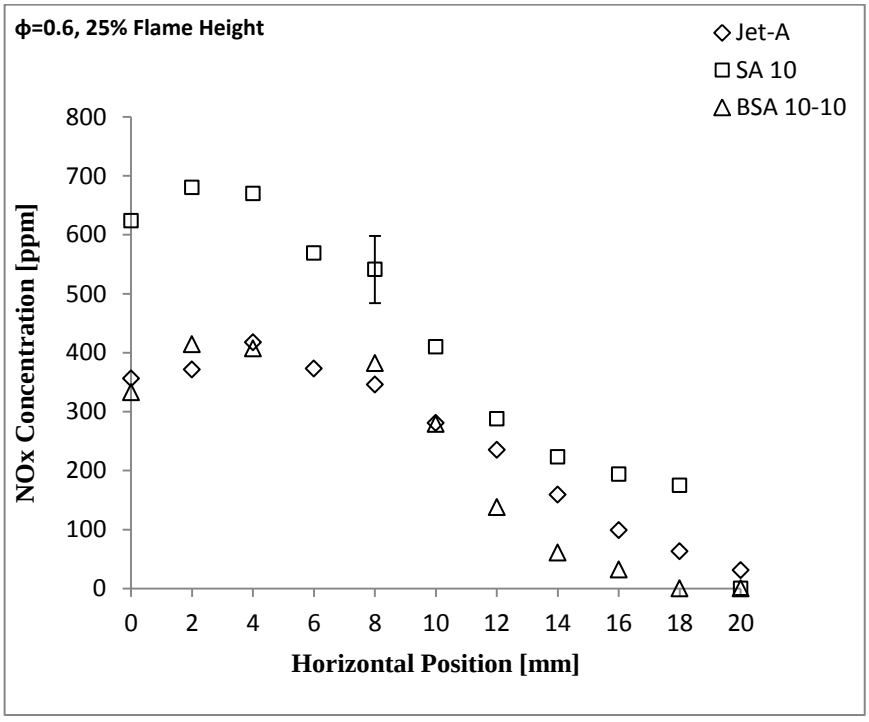

Figure 4.38: Radial in-flame NOx concentration profiles at ϕ=0.6 and 25% flame height.

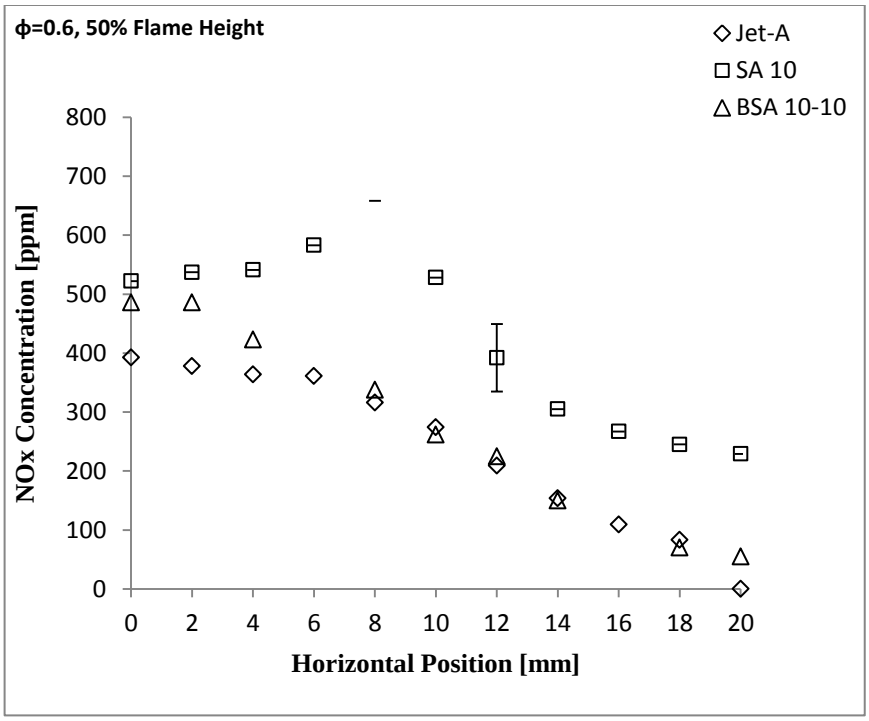

Figure 4.39: Radial in-flame NOx concentration profiles at ϕ=0.6 and 50% flame height.

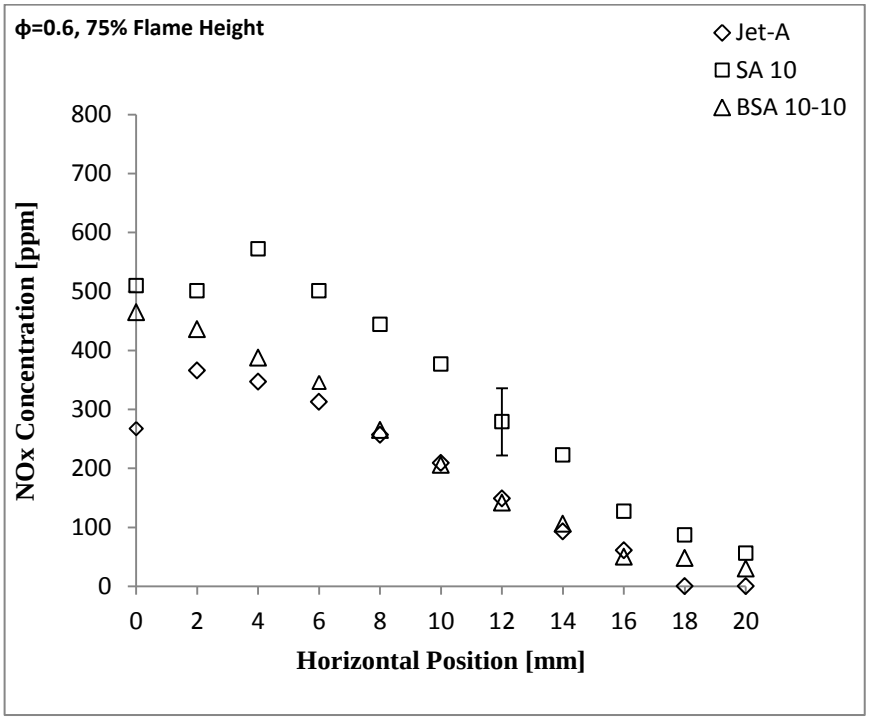

Figure 4.40: Radial in-flame NOx concentration profiles at ϕ=0.6 and 75% flame height.

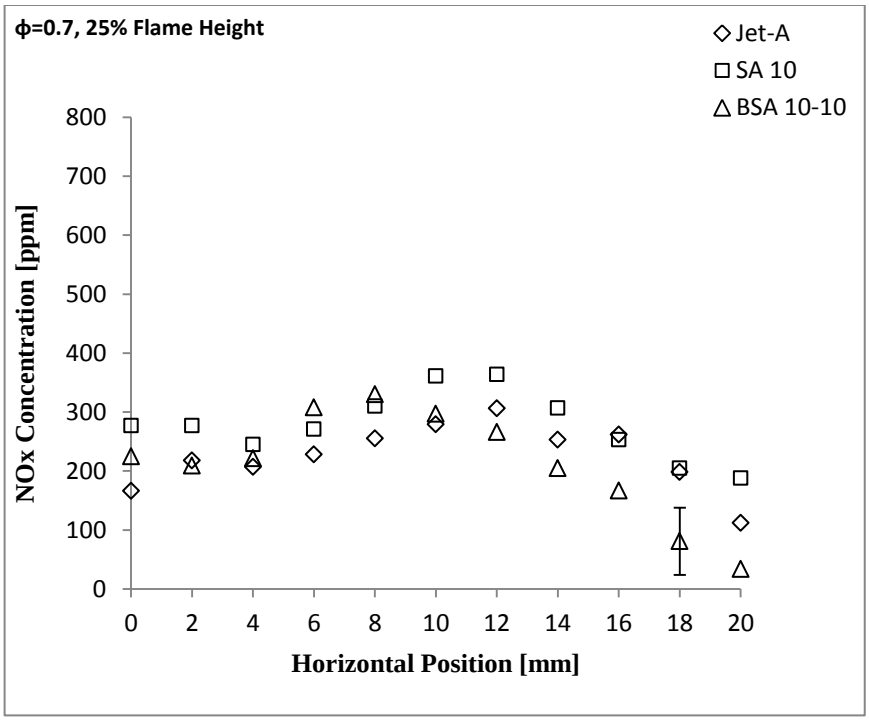

Figure 4.41: Radial in-flame NOx concentration profiles at ϕ=0.7 and 25% flame height.

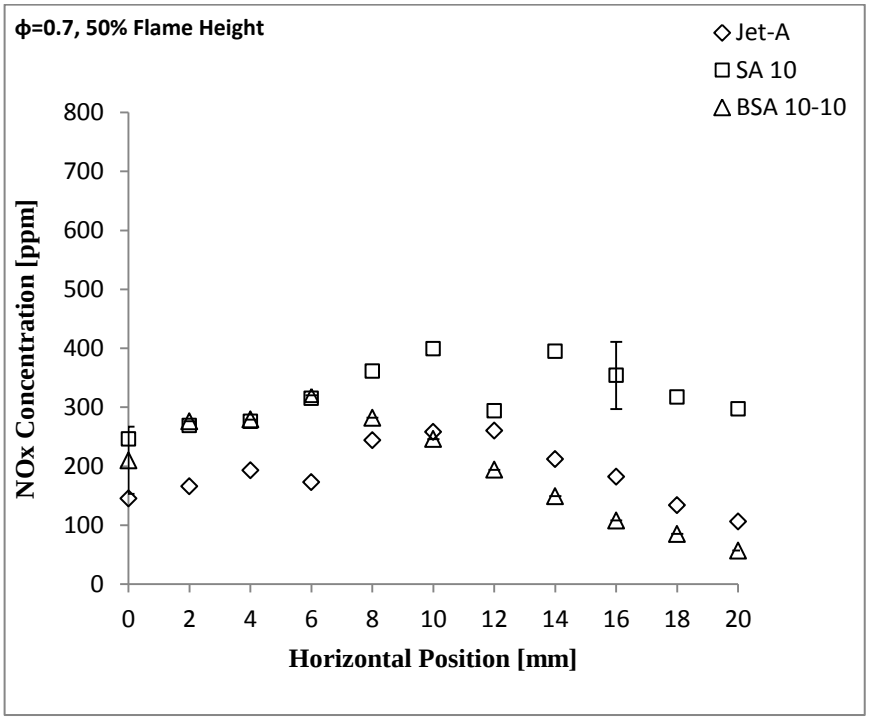

Figure 4.42: Radial in-flame NOx concentration profiles at ϕ=0.7 and 50% flame height.

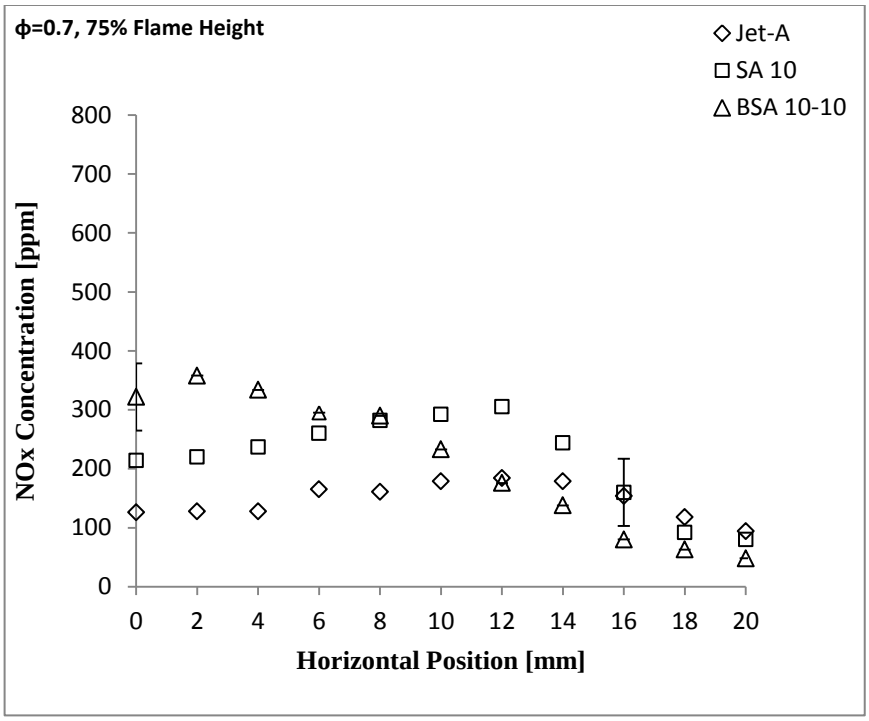

Figure 4.43: Radial in-flame NOx concentration profiles at ϕ=0.7 and 75% flame height.

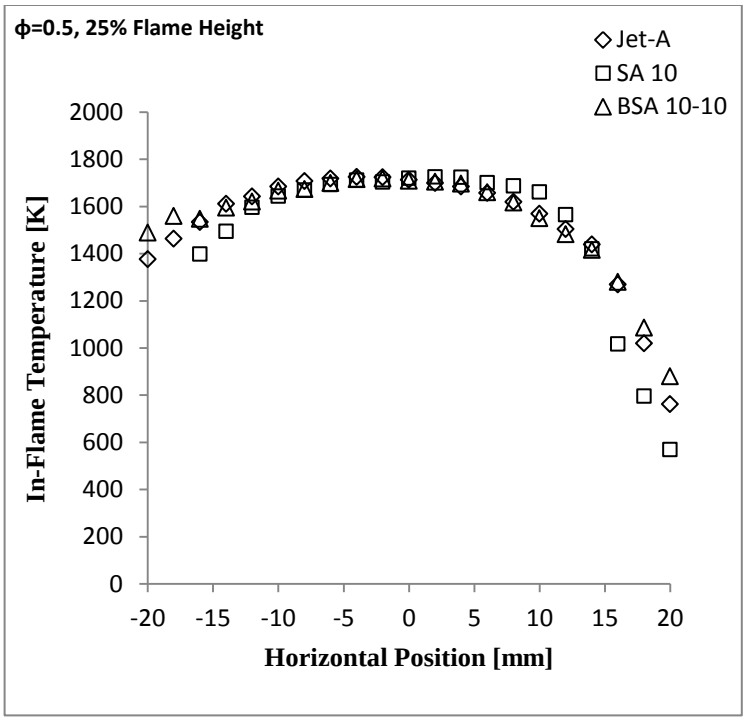

Figure 4.44: In-flame temperature radial profiles at ϕ=0.5 and 25% flame height.

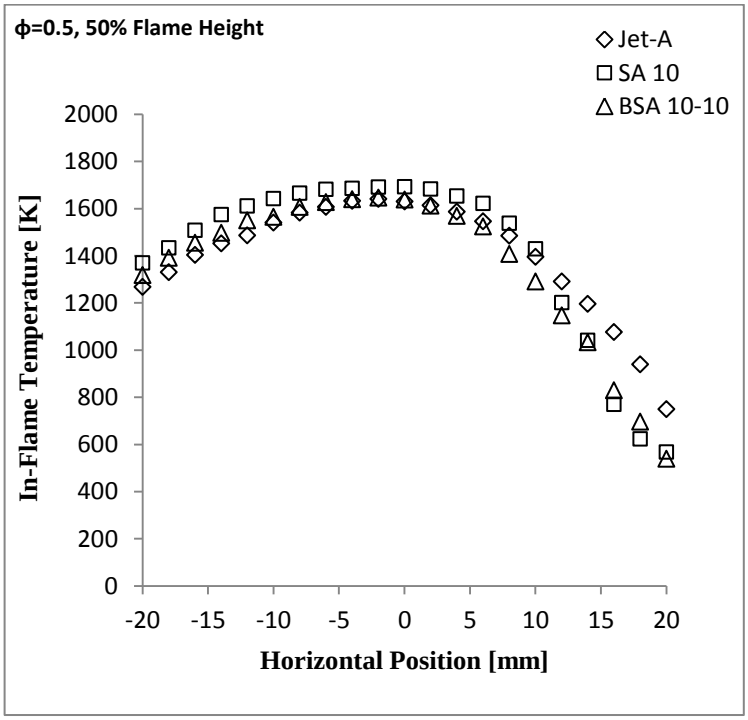

Figure 4.45: In-flame temperature radial profiles at ϕ=0.5 and 50% flame height.

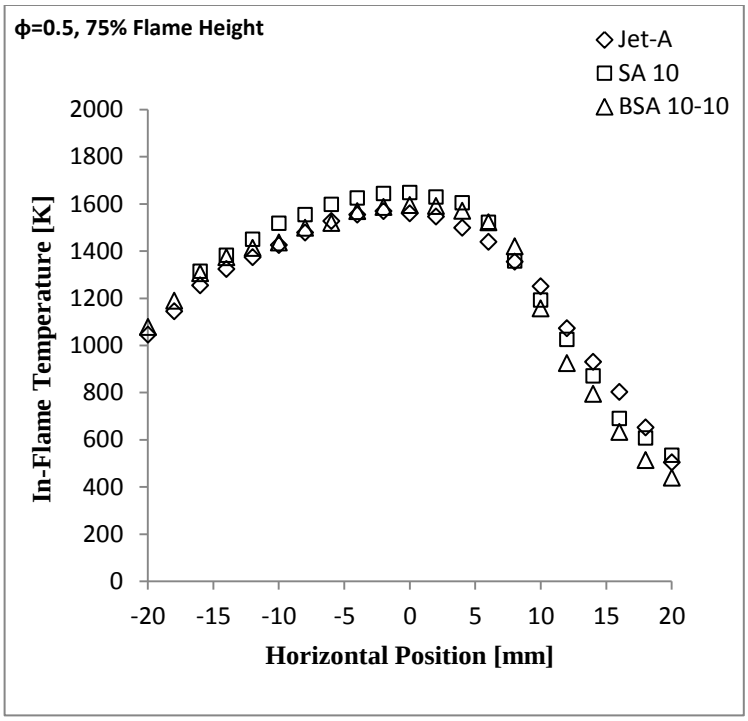

Figure 4.46: In-flame temperature radial profiles at ϕ=0.5 and 75% flame height.

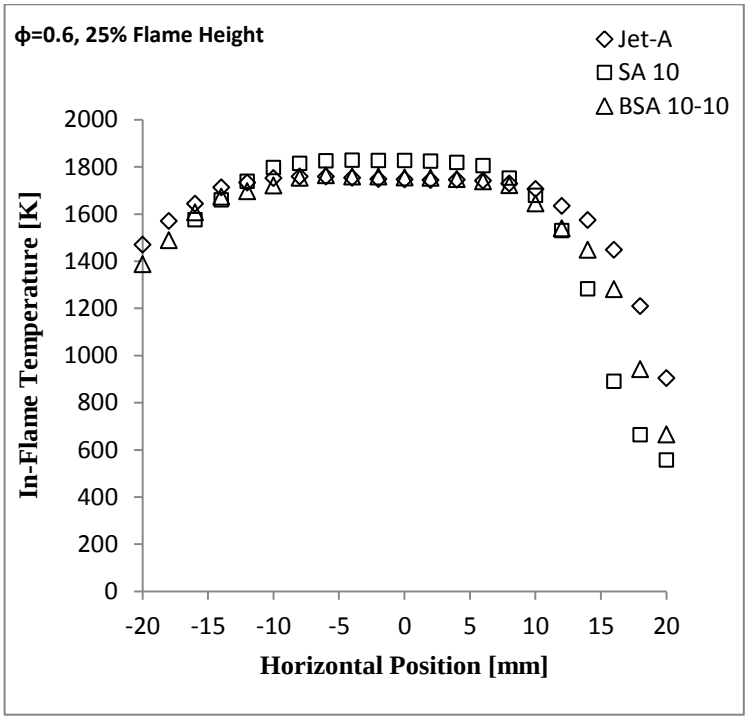

Figure 4.47: In-flame temperature radial profiles at ϕ=0.6 and 25% flame height.

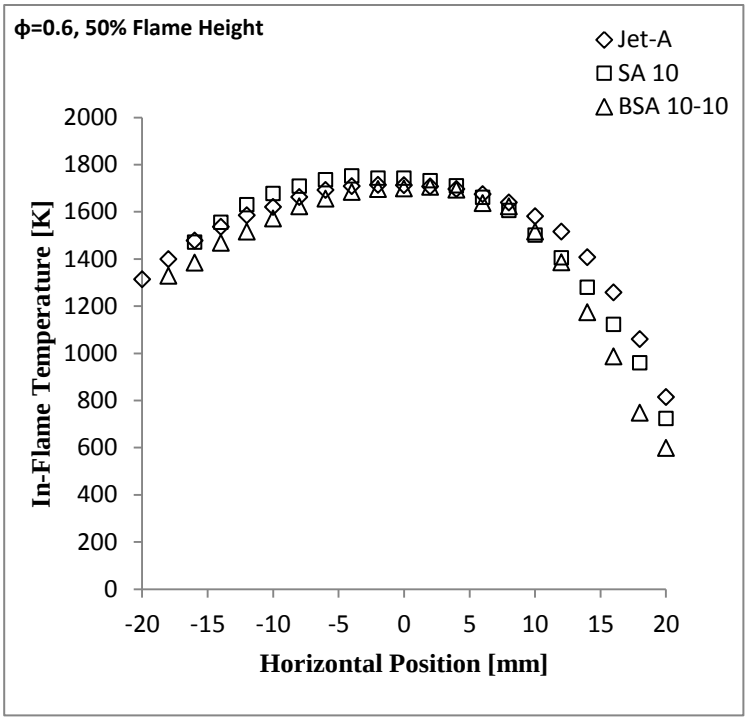

Figure 4.48: In-flame temperature radial profiles at ϕ=0.6 and 50% flame height.

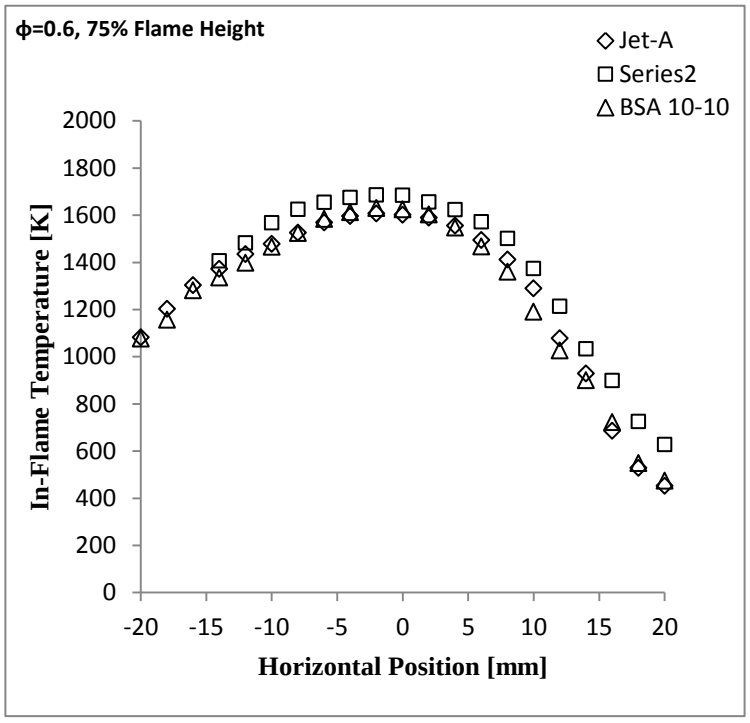

Figure 4.49: In-flame temperature radial profiles at ϕ=0.6 and 75% flame height.

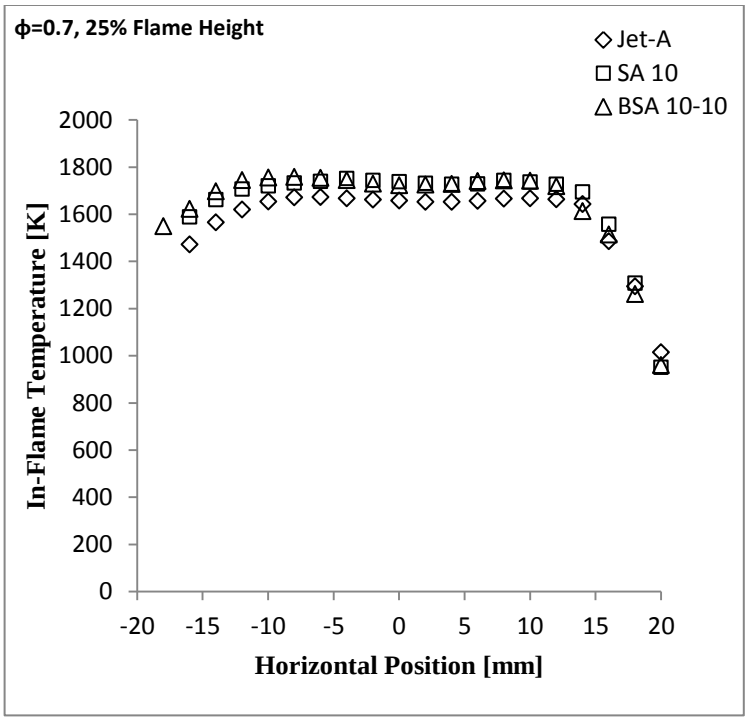

Figure 4.50: In-flame temperature radial profiles at ϕ=0.7 and 25% flame height.

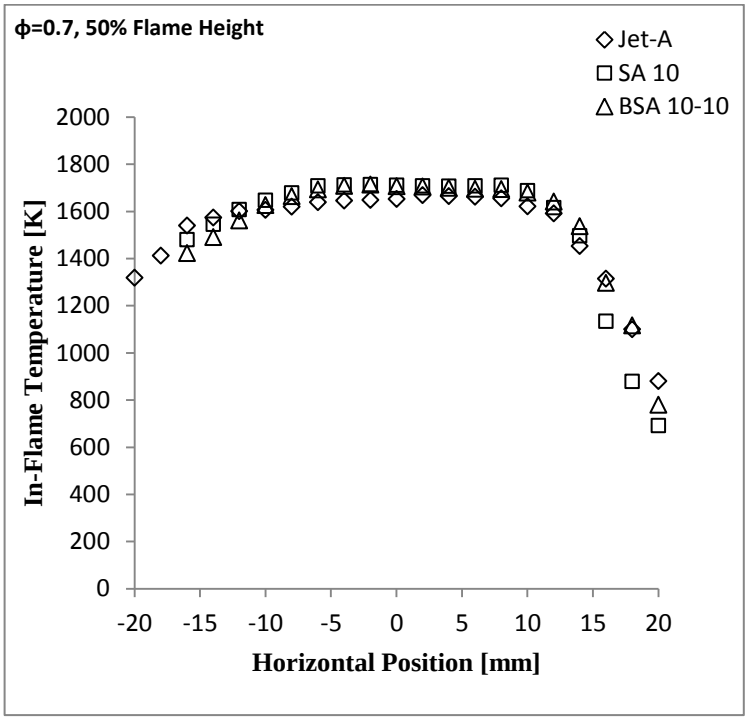

Figure 4.51: In-flame temperature radial profiles at ϕ=0.7 and 50% flame height.

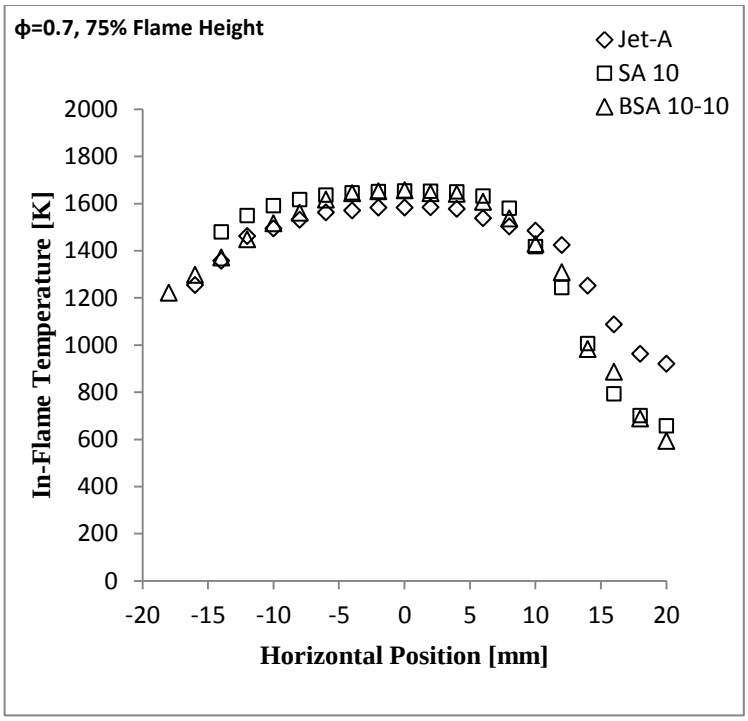

Figure 4.52: In-flame temperature radial profiles at ϕ=0.7 and 75% flame height.

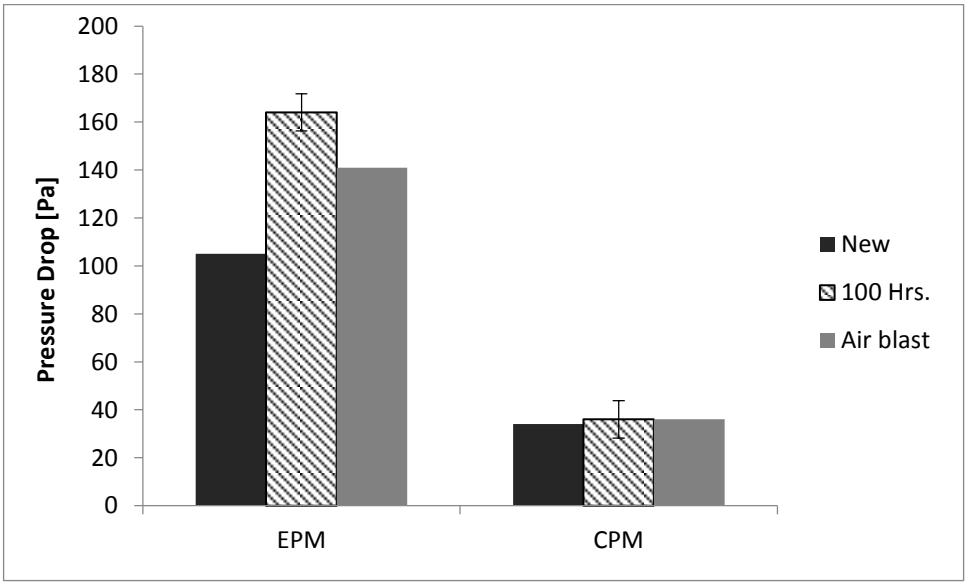

Figure 4.53: Pressure drop across porous media using new PM, after 100 hours of use, and after air blast maintenance

Chapter 5: Summary and Conclusions

In summary, the combustion characteristics and behavior were studied for nine different flames. The flames were studied at three different lean equivalence ratios (ϕ= 0.5, 0.6, 0.7), and the fuels used for the present study were pure Jet-A, SA 10 (Jet-A 90% - SME 10%), and a three component fuel BSA 10-10 (Jet-A 80% - SME 10% - butanol 10%). Flame appearance, visible flame height, global emissions indices for CO, and NOx, radial in-flame temperature profiles, radial in-flame species concentration profiles, and soot volume fraction at the centerline were measured and documented to comprehensively analyze the flame characteristics. A final assessment on the porous media status was carried out in order to measure the impact of the blends combustion on the blockage of porous media burner.

5.1 Conclusions

Based on the measured results the following can be concluded:

1. The flames generated in the porous media burner were all non-luminous, and blue in appearance. This effect is due the lean combustion conditions, enhanced evaporation of the reactants, and mixing mechanisms attributed to the porous media. The presence of fuel-bound oxygen in the blend affected the luminosity and visible height of the flames. As the amount of molecular-bound O_2 increased in the blend, the flames were less luminous and shorter, indicating a faster oxidization of the fuel. Axial measurements of soot volume fraction confirmed these claims as the measured results yielded zero ppm of soot, or amounts smaller than the calculated uncertainty.

2. The emission indices of NOx, were comparable for the all the fuel blends at a given equivalence ratio. Peak emission index for NOx were found to occur at ϕ= 0.6. It can be concluded that the thermal NOx formation mechanism is the dominant mechanism in all cases studied since the highest peak in-flame temperatures for all fuels were recorded at ϕ=0.6. Additionally, the in-flame concentration profiles of NOx were similar to those of in-flame temperature highlighting the relationship between the two. The NOx emission indices found during this study suggest that EI_{NOx} for porous media burner are comparable or lower than those measured at open spray flames, and open flames.

3. In-flame peak temperatures were found to be the highest at 25% flame height for all flames at all conditions. This suggests that the reaction stabilized close to the downstream surface of the porous media. Radial in flame temperature profiles were mostly uniform as a consequence of the enhanced mixing, and homogeneous reaction produced by the presence of the porous media. Peak temperatures were similar for all flames, at all conditions, on every flame height recorded, which was expected since the adiabatic flame temperatures of the blends do not vary more than 1% between each other.

4. The emission indices of CO, were comparable for the all the fuel blends at any given equivalence ratio. Peak emission index for CO were found to occur at ϕ= 0.6. CO in-flame concentration values corresponded to CO_2 concentration values suggesting that all carbon was present in either form. CO emission indices were significantly lower than those of open spray flames, and open flames which demonstrate the effects of the porous media burner in suppressing CO emissions. The relationship between EI_{CO} and equivalence ratio has to be further studied in order to fully comprehend the observed behavior.

5. After 100 hours of testing the pressure drop across the EPM increased by 59 Pa, while pressure drop increased 2 Pa for the CPM. Porous media degradation was mainly due to solid residues depositing on the PM, which caused pore blockages, and clogging. Blasting pressurized air through the porous media was found to be an effective way to give maintenance to the PM. After the procedure pressure drop of the EPM improved by 16%.

5.2 Recommendation for Future Studies

The use of porous media burner technology, paired with the combustion of ternary blends offers a high potential in the use of alternative energy sources. Based on the experience gained on this study research on this field can be further extended by considering different combination of testing conditions.

Varying the parameters that were kept constant such as co-flow temperature, total air flow rate, velocity at the spray, among others, may give an insight on how the conditions affect the combustion characteristics of the fuels being tested. Ambient and injection conditions might have significant effects on the overall combustion characteristics of the blends used. Additionally it is necessary to modify the setup by expanding the length of the flame chamber in order to prevent air entrainment on the study of longer flames.

Changing the porous media characteristics can expand the understanding of this technology. Studying the effects of thickness of each of the porous matrices, the material composition, pore density, and even the type of porous media used (honeycombs, beads, lattices, etc.), would give a deep understanding on the effect that the design of the burner has on combustion.

Varying the flame stabilization region presents an interesting study. Documenting the emissions, and performance of flame stabilized inside the porous media would give insights into the optimal flame configuration for a variety of applications, including those exclusive to inside flames such as thermophotovoltaic, and thermoelectrical energy generation.

Finally, it is necessary to explore the behavior of different ternary blends. Changing the biodiesel feedstock, or altering the composition ratios of the blend, will significantly alter the amount of fuel-bound oxygen. It is clear that molecular-bound oxygen has an effect on the flame characteristics; having a wider sample would give a better understanding on the effects that oxygen content has on combustion characteristics.

References

Aldana, C., Parthasarathy, R.N., Gollahalli, S.R. "Combustion properties of spray flames of canola methyl ester and diesel blends at lean inlet equivalence ratios", ***Journal of Petroleum Science Research,*** Vol. 3, issue 4, 2014. pp. 167-175.

Armas O., García-Contreras, R., Ramos, Á., "Pollutant emissions from New European Driving Cycle with ethanol and butanol diesel blends", ***Fuel Processing Technology***, Vol. 122, 2014. pp. 64-71.

Atmanli A., Ileri E., Yuskel B., Ylmaz N., "Extensive analyses of diesel-vegetable oil-n-butanol ternary blends in a diesel engine", ***Applied Energy***, Vol. 145, 2015. pp. 155-162.

Atmanli A., Ileri E., Yüksel B., "Effects of higher ratios of n-butanol addition to diesel-vegetable oil blends on performance and exhaust emissions of a diesel engine", ***Journal of the Energy Institute***, Vol. 88, 2015. pp. 209-220.

Balakrishnan A., Parthasarathy R.N., Gollahalli, S.R., "A review on the effects of biodiesel blends on compression ignition engine NOx emissions", ***Journal of Energy and Environmental Sustainability***, Vol. 1, 2016. pp. 67-76.

Barajas, P., "Combustion characteristics of biodiesel fuel with porous media burner", M.S. thesis, School of Aerospace and Mechanical Engineering, University of Oklahoma, Norman, Oklahoma, USA, 2009.

Baukal, C., John Zink Hamworthy Combustion, ***The John Zink Combustion Handbook Vol 1-3***, CRC Press, 2nd Edition, 2013.

Carter,F. L., Parthasarathy, R.N. and Gollahalli, S.R., "Emissions and performance of a gas turbine engine with two and three component blends of petroleum and biofuels", ***Proceedings of the Australian Combustion Symposium***, 2015. pp. 208-211.

Coordinated Research Council Inc., ***Hanbook of aviation fuel properties***, Society of Automotive Engineers, Inc., 1983.

Dahifale, B. S., "Flame characteristics of biodiesel blends in a porous-medium burner", M.S. thesis, School of Aerospace and Mechanical Engineering, University of Oklahoma, Norman, Oklahoma, USA, 2010.

Gao H.B., Qu Z.G., Tao W.Q., Feng X. "Combustion of methane/air mixtures in a two-layer porous burner: a comparison of alumina foams, beads, and honeycombs" ***Experimental Thermal and Fluid Science***, Vol. 52, 2014. pp. 215-220.

Gao H.B., Qu Z.G., Feng X, Tao W.Q., “Methane/air premixed combustion in a two-layer porous burner with different foam materials”, ***Fuel***, Vol. 115, 2014. pp. 154-161.

Gómez, A., Soriano, J.A, Armas O., “Evaluation of sooting tendency of different oxygenated and paraffinic fuels blended with diesel fuel”, ***Fuel***, Vol. 184, 2016. pp. 536-543.

Howell J.R, Hall M.J, Ellzey J.L. “Combustion of hydrocarbon fuels within inherent porous media”, ***Progress in Energy Combustion Science***, Vol. 22. 1996. pp. 121-145.

Imran, M., "Combustion characteristics of butanol and Jet-A blends in porous media burners", M.S. thesis, School of Aerospace and Mechanical Engineering, University of Oklahoma, Norman, Oklahoma, USA, 2015.

Imtenan, S., Masjuki, H., Varman, M., Arbab, M., Sajjad, H., Rizwanul Fattah, I., Abedin, M., Hasib, A., “Emission and performance improvement analysis of biodiesel-diesel blends with additives”, ***10th International Conference on Mechanical Engineering, ICME 2013, Procedia Engineering***, Vol. 90, 2014. pp. 472-477.

Jugjai, S., Polmart, N., “Enhancement of evaporation and combustion of liquid fuels through porous media”, ***Experimental Thermal Fluid Science***, Vol. 27, 2013. pp. 901-909.

Keramiotis, C., Stelzner, B., Trimis, D., Founti, M., “Porous burners for low emission combustion: An experimental investigation”, ***Energy***, Vol. 45, 2012. pp. 213-219.

Lapirattanakun, A., Charoensuk, J., “Development of porous media burner operating on waste vegetable oil”, ***Applied Thermal Energy***, Vol. 110, 2017. pp. 190-201.

Lovins, A.B., Rocky Mountain Institute, ***Reinventing Fire: Bold Business Solutions for the New Energy Era***, Chelsea Green Publishing Company, 1st Edition, 2011.

Mendes, M., Pereira, J.M., Pereira, J.C., “A numerical study of the stability of one-dimensional laminar premixed flames in inert porous media”, ***Combustion and Flame***, Vol. 153, 2008. pp. 525-539.

Mujeebu, M. A., and Abdul, M., "Applications of porous media combustion technology- a review", ***Journal of Applied Energy***, Vol. 86, 2009. pp. 1365-1375.

Mustafa, K., Abdullah, S., Abdullah, M., Sopian, K., “Comparative assessment of a porous burner using vegetable cooking oil–kerosene fuel blends for thermoelectric and thermophotovoltaic power generation”, ***Fuel***, Vol. 180, 2016. pp. 137-147.

Pan, J., Wu, D., Liu, X., Zhang, H., Tang, A., Xue, H., “Hydrogen/oxygen premixed combustion characteristics in micro porous media combustor”, ***Applied Energy***, Vol. 61, 2014. pp. 1279-1285.

Periasamy, C., "An experimental and numerical study of evaporation enhancement and combustion in porous media", Doctoral Dissertation, School of Aerospace and Mechanical Engineering, University of Oklahoma, Norman, Oklahoma, USA, 2007.

Probstein, R.F., Hicks, R.E., ***Synthetic Fuels***, Dover Publications Inc., 3rd Edition, 2006.

Ratul, T. H. "Combustion characteristics of spray flames of Jet-A/butanol blends" M.S. Thesis, School of Aerospace and Mechanical Engineering, University of Oklahoma, Norman, Oklahoma, USA, 2012.

Renewable Fuel Assiciation. "Statistics". Renewable Fuels Association. http://www.ethanolrfa.org/pages/statistics, 2010.

Szulczyk, K. R. "Which is a better transportation fuel – butanol or ethanol", ***International Journal of Energy and Environment (IJEE),*** Vol. 1, Issue 1, 2010. pp. 501-512.

Tsai, J., Chen, S., Huang, K., Lin, Y., Lee, W., Lin, C., and Lin, W. "PM, carbon and PAH emissions from a diesel generator fueled with soy-biodiesel blends", ***Journal of Hazardous Materials***, Vol. 179, 2010. pp. 237-243

Tuccar, G., Ozgur, T., Aydin, K., "Effect of diesel–microalgae biodiesel– butanol blends on performance and emissions of diesel engine, ***Fuel***, Vol. 132, 2014. pp. 47-52.

Turns, S.R., ***An Introduction to Combustion: Concepts and Applications***, McGraw-Hill Higher Education, 3rd Edition, 2011.

Weinberg, F. J., "Combustion Temperatures: The future?", ***Nature***, Vol. 233, 1971. pp. 239-241.

Yagi, S., & Iino, H., "Radiation from Soot Particles in Luminous Flames", ***Eighth International Symposium on Combustion***, The Combustion Institute, 1962. pp. 288-293.

Yilmaz N., "Performance and emission characteristics of a diesel engine fueled with biodiesel–ethanol and biodiesel–methanol blends at elevated air temperatures", ***Fuel***, Vol. 94, 2012. pp. 440-443.

Zhang, L., "Multicomponent drop vaporization modeling of petroleum and biofuel mixtures", Doctoral Dissertation, Department of Mechanical Engineering, Iowa State University, Ames, Iowa, USA, 2011.

Appendix A: Rotameter Calibration Charts

A.1 Rotameter Calibration for Jet-A

Rotameter: Ametek Lo-Flo
Tube: SK 1/8”-25-G-5
Float: Black Glass

Table A.1: Rotameter calibration values for Jet-A.

Rotameter Scale	Flow Rate (ml/min)
1	0.38
2	2.24
3	3.71
4	7.65
5	13.40
6	20.44
7	27.71
8	33.81
9	40.75
10	45.30

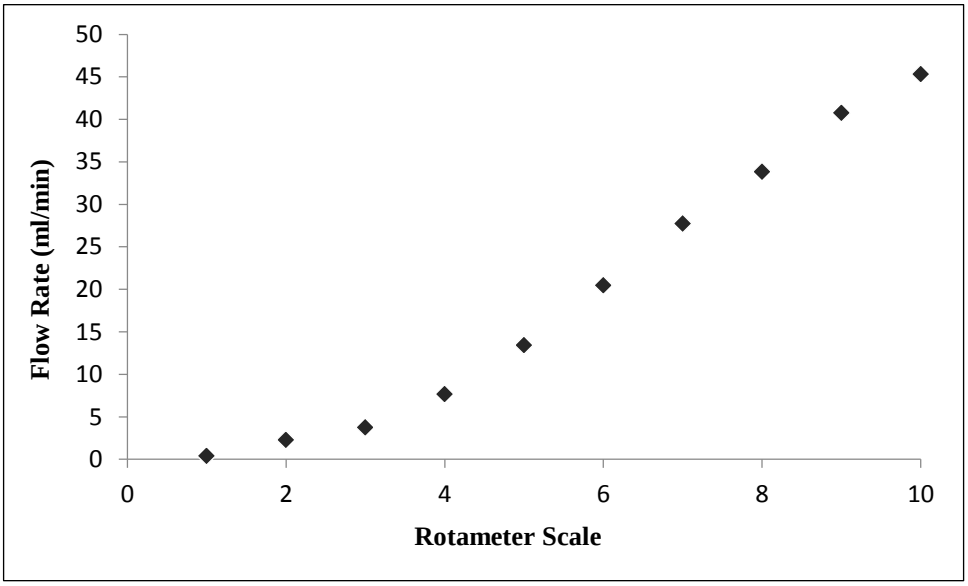

Figure A1: Rotameter calibration curve for Jet-A.

A.2 Rotameter Calibration for SA 10

Rotameter: Ametek Lo-Flo
Tube: SK 1/8”-25-G-5
Float: Black Glass

Table A.2: Rotameter calibration values for SA 10.

Rotameter Scale	Flow Rate (ml/min)
1	0.31
2	1.70
3	3.31
4	6.60
5	11.30
6	18.24
7	23.79
8	31.47
9	38.97
10	41.30

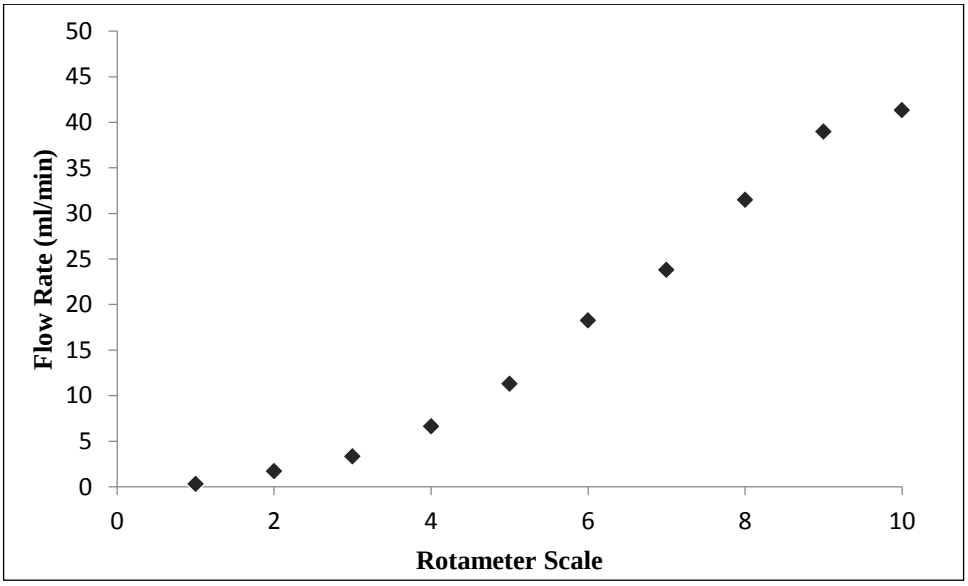

Figure A1: Rotameter calibration curve for SA 10.

A.3 Rotameter Calibration for BSA 10-10

Rotameter: Ametek Lo-Flo
Tube: SK 1/8”-25-G-5
Float: Black Glass

Table A.3: Rotameter calibration values for BSA 10-10.

Rotameter Scale	Flow Rate (ml/min)
1	0.42
2	1.76
3	3.25
4	6.52
5	11.36
6	18.03
7	24.86
8	31.49
9	38.13
10	41.66

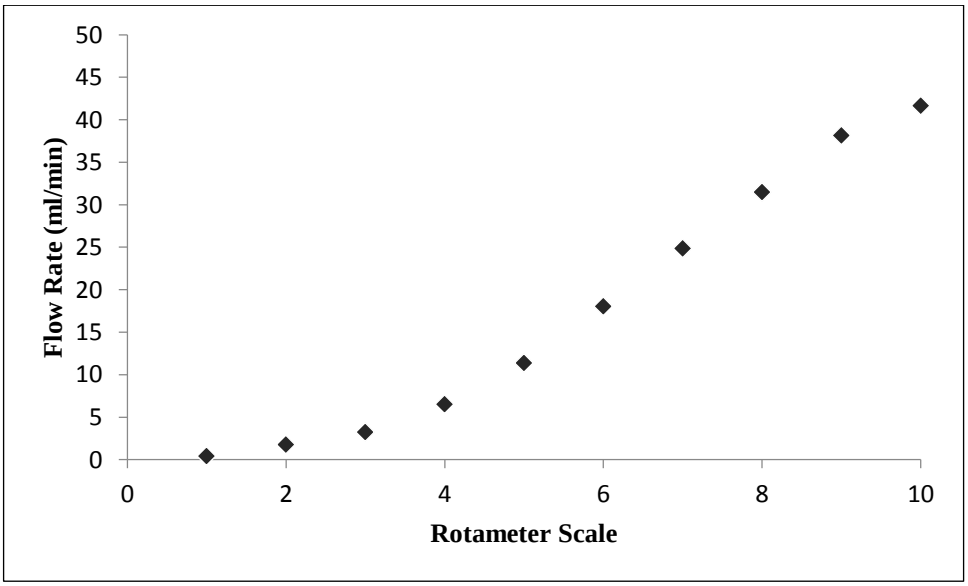

Figure A3: Rotameter calibration curve for BSA 10-10.

Appendix B: Sample Calculations

B.1 Stoichiometric Combustion Calculations

B.1.1 Jet-A

The stoichiometric combustion of Jet-A ($C_{13}H_{23}$) is given as:

$$C_{13}H_{23} + 18.75\ (O_2 + 3.76\ N_2) \rightarrow 13\ CO_2 + 11.5\ H_2O + 70.5\ N_2$$

With a stoichiometric air-to-fuel ratio, A/F, of:

$$\frac{A}{F}_{stoic} = 4.76 * a * \frac{MW_{air}}{MW_{fuel}}$$

For Jet-A, *a* has a value of 18.75, which yields a A/F_{stoic} of 14.38.

B.1.2 SA 10

The stoichiometric combustion of SA 10 ($C_{13.41}H_{23.81}O_{0.14}$) is given as:

$$C_{13.4}H_{23.8}O_{0.1} + 19.29\ (O_2 + 3.76\ N_2) \rightarrow 13.4\ CO_2 + 11.9\ H_2O + 72.5\ N_2$$

With a stoichiometric A/F of:

$$\frac{A}{F}_{stoic} = 4.76 * a * \frac{MW_{air}}{MW_{fuel}}$$

For Jet-A, *a* has a value of 19.29, which yields a A/F_{stoic} of 14.17.

B.1.3 BSA 10-10

The stoichiometric combustion of BSA 10-10($C_{11.3}H_{20.8}O_{0.3}$) is given as:

$$C_{11.3}H_{20.8}O_{0.3} + 16.4\ (O_2 + 3.76\ N_2) \rightarrow 11.37\ CO_2 + 10.4\ H_2O + 61.7\ N_2$$

With a stoichiometric A/F of:

$$\frac{A}{F}_{stoic} = \ 4.76 * a * \frac{MW_{air}}{MW_{fuel}}$$

For Jet-A, a has a value of 16.4, which yields a A/F_{stoic} of 13.85.

B.2 Emission Index and Uncertainty Sample Calculation

The calculation of the emission index is an effective method to account for the dilution of the species being measured from the ambient air entrainment (Turns, 2011). Emission index expresses the amount of pollutant formed per unit mass of fuel burnt [$g_{species}/kg_{fuel}$]. Emission index is calculated as follows:

$$EI_i = \left(\frac{X_i}{X_{CO}+X_{CO_2}}\right) * \left(x * \frac{MW_i}{MW_F}\right) \quad \text{(B1)}$$

Where EI_i, is the emission index for the species being recorded in [$g_{species}/kg_{fuel}$], X_i is the mole fraction of the species being measured, X_{CO} , and X_{CO2} are the mole fractions of carbon monoxide, and carbon dioxide respectively, x is the number of moles of carbon in a mole of fuel, MW_i [g/mol], and MW_F [kg/kmol] are the molar weights of the measured species and the fuel, respectively.

The following example on EI_{NOx} calculation corresponds to data measured for a BSA 10-10 flame at ϕ=0.6.

The average concentration values after three independent measurements are given in Table B.1

Table B.1: Average concentration values for global emissions measurements for BSA 10-10 at ϕ=0.6

O_2 (%)	15.3
CO_2 (%)	3.8
CO (PPM)	107.7
NO_x (PPM)	106.3

For BSA 10-10, the amount of carbon moles per mole of fuel (x) was 11.3, and the molecular weight of the fuel (MW_f) was 162.73 kg/kmol.

MW_{NOx} was taken as 30 kg/kmol, MW_{CO} as 28 kg/kmol, and MW_{CO2} as 44 kg/kmol.

Then, EI_{NOx} can be calculated as:

$$\mathrm{EI_{NOx}} = 1000 * \left(\frac{106.3 * 10^{-6}}{107.7 * 10^{-6} + .038}\right) * \left(11.3 * \frac{30}{162.73}\right)$$

$$\mathrm{EI_{NOx}} = 5.92 \frac{\mathrm{g_{NOx}}}{kg_{BSA\ 10-10}}$$

Uncertainty for the measurements was calculated accounting for precision or random error (P), and biased or fixed error (B). Precision error was statistically determined based on the sample size, and standard deviation of repeated samples. Biased error was accounted by the calibration error, or the least count of the instrument used. Overall uncertainty (w) can be calculated as the square root of the sum of the squares of both errors.

$$w = \sqrt{(P^2 + B^2)} \quad \text{(B2)}$$

Where precision error is calculated as,

$$P = t_{\nu,95\%} * \frac{S_x}{\sqrt{n}} \quad \text{(B3)}$$

Where $t_{\nu,95\%}$ is the Student's t-distribution value for 95% confidence interval, S_x is the standard deviation of the mean of the sample, and *n* is the sample size. Typical $t_{\nu,95\%}$ values are presented below.

Table B.2: Typical values of t-distribution confidence intervals at 95%.

n	**υ**	$\boldsymbol{t_{\nu,95\%}}$
3	2	4.303
4	3	3.182
5	4	2.776

Precision errors tended to be larger than the corresponding biased errors, and most of the uncertainty for this study is attributed to such. Measurements were repeated a minimum of three times in order to reduce precision errors, and the measurement instruments were periodically re calibrated to ensure accurate readings.

For certain calculations, where the final value depended on several independently measured quantities and multiple uncertainties were present, as in the case of *EI* calculations, the errors propagated. Below is an example of how the error propagation was accounted for while calculating emission indices.

$$w_{EI_{NOx}} = \sqrt{\left(\frac{\partial EI_{NOx}}{\partial X_{NOx}} * w_{X_{NOx}}\right)^2 + \left(\frac{\partial EI_{NOx}}{\partial X_{CO}} * w_{X_{CO}}\right)^2 + \left(\frac{\partial EI_{NOx}}{\partial X_{CO_2}} * w_{X_{CO_2}}\right)^2} \quad \text{(B4)}$$

Where;

$$\mathrm{EI_{NO_x}} = \left(\frac{\mathrm{X_{NOx}}}{\mathrm{X_{CO}+X_{CO_2}}}\right) * \left(\mathrm{X} * \frac{\mathrm{MW_{NO}}}{\mathrm{MW_F}}\right) \quad \text{(B5)}$$

$$\frac{\partial EI_{NOx}}{\partial X_{NOx}} = \left(\frac{1}{\mathrm{X_{CO}+X_{CO_2}}}\right) * \left(\mathrm{X} * \frac{\mathrm{MW_{NO}}}{\mathrm{MW_F}}\right) \quad \text{(B6)}$$

$$\frac{\partial EI_{NOx}}{\partial X_{CO}} = -\left(\frac{\mathrm{X_{NOx}}}{(\mathrm{X_{CO}+X_{CO_2}})^2}\right) * \left(\mathrm{X} * \frac{\mathrm{MW_{NO}}}{\mathrm{MW_F}}\right) \quad \text{(B7)}$$

$$\frac{\partial EI_{NOx}}{\partial X_{CO_2}} = -\left(\frac{\mathrm{X_{NOx}}}{(\mathrm{X_{CO}+X_{CO_2}})^2}\right) * \left(\mathrm{X} * \frac{\mathrm{MW_{NO}}}{\mathrm{MW_F}}\right) \quad \text{(B8)}$$

Where,

$w_{X_{NOx}}$ is the uncertainty associated with the NOx measurements

$w_{X_{CO}}$ is the uncertainty associated with the CO measurements

$w_{X_{CO_2}}$ is the uncertainty associated with the CO_2 measurements

The uncertainty associated with the Emission Index of NOx is then expressed as:

$$EI_{NO_x} \pm w_{EI_{NO_x}}$$

B.4 In-flame Temperature Measurements Correction

It was determined that the thermocouple used in the in-flame temperature measurements recorded a smaller temperature than the real temperature due to conductive, convective, and radiative heat losses. The methodology to address these offset in temperature is described by Jha (2008). The procedure involved the calculation of Reynolds number, Re, of the thermocouple bead, an approximation of the Nusselt number, Nu, and finally the radiation calculation which yielded the corrected values for temperature.

$$Re = \frac{u * d_{bead}}{\nu_{air}} \tag{B10}$$

$$Nu = \frac{hc * d_{bead}}{k_{air}} = 2 + (0.4Re^{0.5} + 0.06Re^{0.667}) * Pr^{0.4} \tag{B11}$$

$$T_{corrected} = \frac{\sigma * \epsilon}{h} * (T_{recorded}^4 - T_{\infty}^4) + T_{recorded} \tag{B12}$$

Where u [m/s^2] is the exit air velocity, d_{bead} [m] is the diameter of the thermocouple bead, ν_{air} [m^2/s] is the kinematic viscosity of air at the measured flame temperature, hc [W/m^2*K] is the convective heat transfer coefficient, k_{air} [W/m*K] is the thermal conductivity of air, Pr is the Prandtl number, T [K] is the temperature at the condition specified, σ [W/m^{2}K^4] is the Stefan-Boltzmann constant, and ϵ is the emissivity of the thermocouple wire. Thermal conductivity of air, and emissivity varied with measured flame temperature. The values for the constants used are as follows:

$d_{bead} = 0.2\ mm\ (measured)$

$\sigma = 5.67 * 10^{-8} \frac{W}{m^2 K^4}$

$k_{air} = (-2 * 10^{-8}) T_{recorded}^2 + (8 * 10^{-5}) T_{recorded} + 0.0042$
For temperatures between 300 K-1200 K

$k_{air} = (1 * 10^{-10}) T_{recorded}^3 - (5 * 10^{-7}) T_{recorded}^2 + 0.0009 T_{recorded} - 0.4868$
For temperatures between 1200 K-2500 K

$\nu_{air} = (1 * 10^{-9}) T_{recorded}^{1.6836}$
For temperatures between 300 K-2500 K

$\nu_{air} = (1 * 10^{-9}) T_{recorded}^{1.6836}$
For temperatures between 300 K-2500 K

$\epsilon = (1 * 10^{-7}) T_{recorded}^2 - 0.0004 T_{recorded} + 0.5605$
For temperatures between 300 K-2500 K

Pr = 0.68
Prandtl number is fairly constant over a wide range of temperatures

B.3 Adiabatic Temperature Calculation

The adiabatic temperature for each fuel was calculated using the methodology described by Turns (2011). Constant pressure adiabatic temperatures were calculated considering a stoichiometric reaction at the conditions in which the experiment was carried; reactants initial temperature, T_i = 463 K and atmospheric pressure. For adiabatic combustion of a fuel/air mixture the enthalpy of the reactants at the initial state ($T=T_0$) must equal the enthalpy of the products at the final state ($T=T_{ad}$).

$$\sum_{reactants} N_i\{\bar{h}^o_{f,i} + [\bar{h}^o_i(463\ K) - \bar{h}^o_{f,i}\ (298\ K)]\} = \sum_{products} N_j\{\bar{h}^o_{f,j} + \bar{c}_{p,i}[T_{ad} - 298\ K]\} \quad \text{(B9)}$$

Where N is the number of moles of a species, $\bar{h}^o_f$ [kJ/kmol] is the enthalpy of formation at 298 K of a species, $\left[\bar{h}^o_i(463\ K) - \bar{h}^o_{f,i}(298\ K)\right]$ [kJ/kmol] is the sensible enthalpy at 463 K of a species, $\bar{c}_{p,i}$ [kJ/kmol-K] is the specific heat of a species, T_{ad} [K] is the adiabatic flame temperature; i and j denote a reactant or a product.

Adiabatic temperature was found by solving equation B9 numerically since the heat capacity of the products varied with temperature. Tables B3a-c display the values corresponding to the properties involved in the equation at the specified conditions.

Table B.3a: Enthalpy of formation, sensible enthalpy, and specific heat capacity of the fuels.

Fuel	Enthalpy of Formation at 298 K [kJ/kmol]	Sensible Enthalpy at 463 K [kJ/kmol]	Specific heat capacity [kJ/kmol-K]
Jet-A	-349300	65863	399.2
SA 10	-391492	65679	398.1
BSA 10-10	-391492	62212	377.0

Table B.3b: Enthalpy of formation, and sensible enthalpy of air components.

Reactant	Enthalpy of Formation at 298 K [kJ/kmol]	Sensible Enthalpy at 463 K [kJ/kmol]
O_2	0	5071
N_2	0	4815

Table B.3c: Enthalpy of formation, and specific heat capacity of the combustion products.

Product	Enthalpy of Formation at 298 K[kJ/kmol]	Specific heat capacity at T_{ad} [kJ/kmol-K]
H_2O	-238302	58.7
CO_2	-393401	47.1
N_2	0	34.6

B.5 Soot Volume Fraction

The soot volume fraction measurements were calculated using the relationship from the application of Beer's Law and Mie's theory as described by Yagi and Iino (1962). Soot voulme fraction, $F_{v,}$ [ppm] is calculated by:

$$F_v = -\frac{\ln\left(\frac{I_o}{I_s}\right)\lambda}{k_\lambda \delta} \tag{B13}$$

Where I_s is the incident laser intensity [mW], I_o the attenuated laser intensity [mW], k_λ the spectral extinction coefficient based on the refractive indices of the soot, λ the laser wavelength [m], and δ the laser beam path (flame thickness) [m].

This relationship has been used by various authors such as Romero et al. (2013) who studied the soot distribution in laminar premixed flames of palm methyl ester and diesel blends, and Imran (2015) who did the same for butanol/Jet-A blends in a porous media combustor.

As described in Chapter 4, the soot volume fraction measurements for the flames of the study yielded 0 ppm of soot, or quantities smaller than those of the uncertainty calculated for the measurements. In order to attest for the validity of the method two measurements were taken for Jet-A flames at 60% flame height for equivalence ratio 1.0, and 1.2. Photographs of the flames at these conditions are shown in Figures B4a, and B4b.

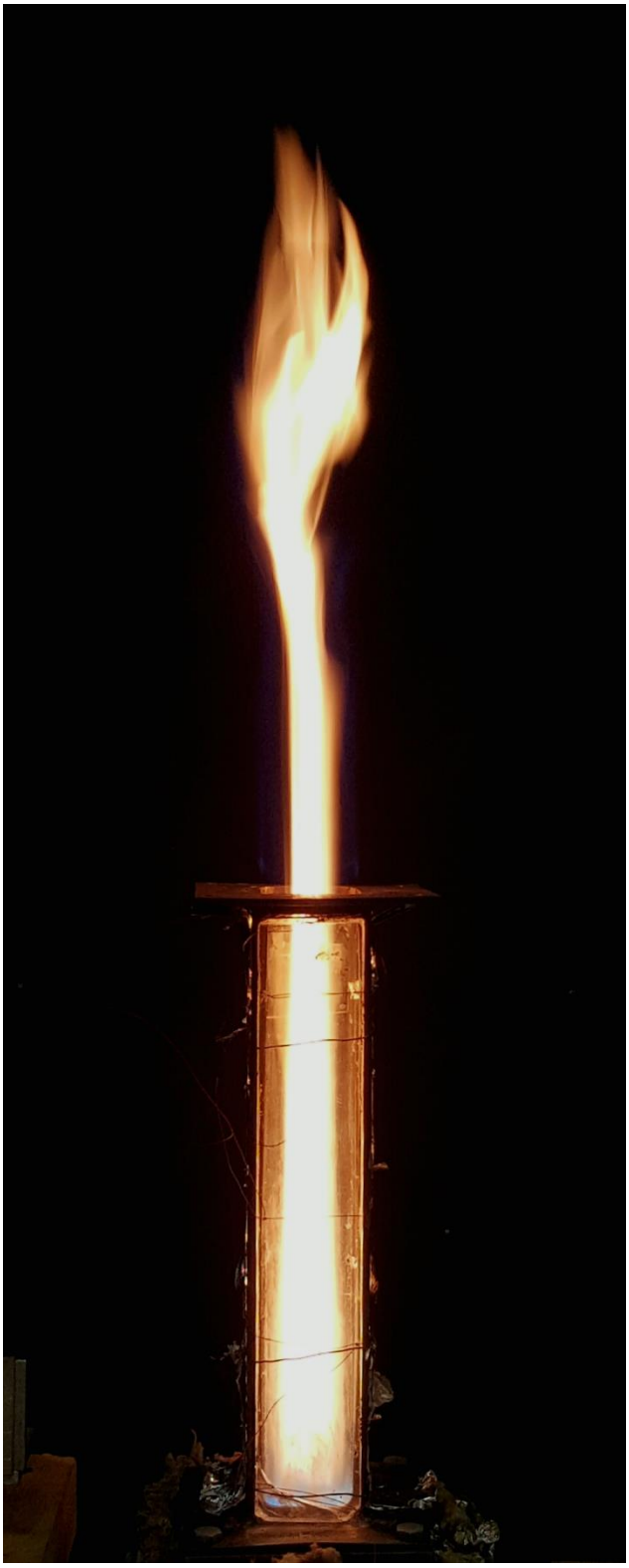

Figure B5a: Photograph of Jet-A flame at ϕ=1.0.

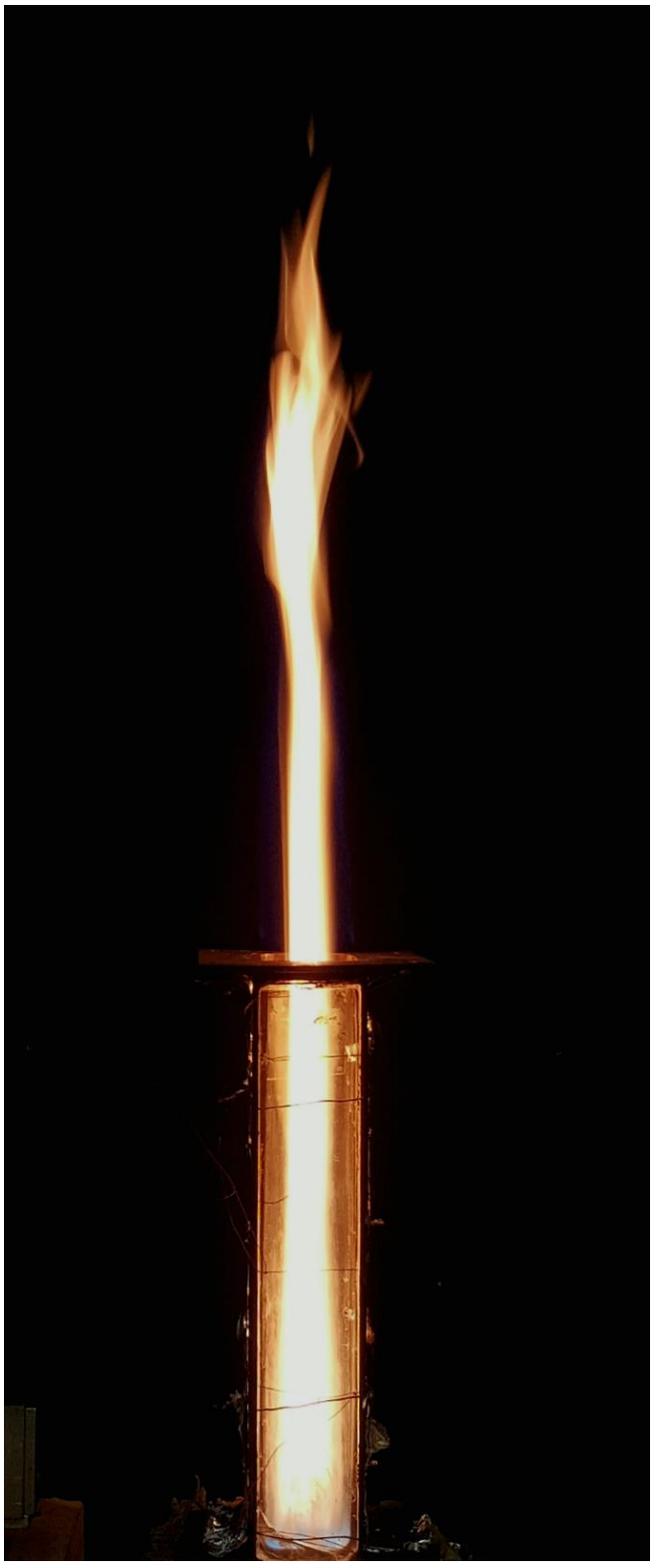

Figure B5b: Photograph of Jet-A flame at ϕ=1.2.

From the photographs, it can be clearly appreciated that the flame appearance is significantly different than the appearance of the flames described in previous chapters. Where the flames investigated for the study were all entirely blue indicating low soot formation, the flames of richer equivalence ratio show a yellow appearance; the color hueof the flame can be directly attributed to the prescence of radiating soot particles.

For the Jet-A flame at ϕ=1.0, at 60% of the flame height, the following results were found:

I_s = 2.64 mW

I_o = 2.59 mW

λ = 6.33*10^{-7} m

k_λ = 4.16

δ = 0.03 m

$$F_v = -\frac{\ln\left(\frac{2.59}{2.64}\right) * 6.33 * 10^{-7}}{4.16 * 0.03}$$

$$F_v = 0.096\ ppm\ \pm 0.07\ ppm$$

Similarly, for the Jet-A flame at ϕ=1.2 yielded a soot volume concentration of $0.110\ ppm\ \pm 0.07\ ppm$.

As suggested by the photographs, the soot concentration of the flames is larger than that of the flames investigated in the study.

From these observations, it can be concluded that if the flames investigated in the study have minimal soot formation, and instrumentation with a higher resolution will have to be used to obtain a better idea of the soot formation mechanisms occurring at lean equivalence ratios.

B.6 Equivalence Ratio and Flow Rate Calculation

The process of finding overall equivalence ratio for a fuel at a given condition is as illustrated below, to perform these calculations BSA 10-10 at ϕ=0.6 will be used as an example.

Knowing:

Volume of butanol: 0.1%

MW_b : 74kg/kmol

ρ_b : 805 kg/m^3

Volume of SME: 0.1%

MW_{SME} : 292.2kg/kmol

$\rho_{SME:}$: 881 kg/m^3

Volume of Jet-A: 80%

$MW_{JetA:}$ 179kg/kmol

$\rho_{JetA:}$: 795 kg/m^3

Then the number of moles of butanol in the blend for one m^3, N_b can be determined as,

$$N_b = 0.1\left(\frac{\rho_b}{MW_b}\right) = 0.1 * \left(\frac{804}{74}\right) = 1.09\ kmol$$

Similarly for number of moles of SME, and Jet-A;

$$N_{SME} = 0.3\ kmol;$$

$$N_{JetA} = 3.55\ kmol$$

The mole fractions, X, corresponding to these values are:

$$X_b = \frac{N_b}{N_b + N_{SME} + N_{JetA}} = 0.22$$

$$X_{SME} = 0.06\ ;$$

$$X_{JetA} = 0.72$$

The molecular weight of the blend, $MW_{BSA1010}$, can be estimated as:

$$MW_{BSA1010} = MW_b X_b + MW_{SME} X_{SME} + MW_{JetA} X_{JetA} = 156.95\ kg/kmol$$

The stoichiometric reaction for BSA 10-10 is given by:

$$C_{11.3} H_{20.8} O_{0.3} + 16.4\ (O_2 + 3.76\ N_2) \rightarrow 11.37\ CO_2 + 10.4\ H_2O + 61.7\ N_2$$

Which yields an air-to-fuel ratio, A/F of:

$$A/F_{stoic} = \frac{4.76 * a * MW_{air}}{MW_{Fuel}} = \frac{16.4 * 4.76 * 28.8}{156.95} = 13.95$$

Since the actual combustion condition is given by ϕ=0.6, the actual A/F ratio can be determined by using the definition for equivalence ratio:

$$\phi = \frac{A/F_{stoich}}{A/F_{actual}} \qquad \text{(B14)}$$

Then;

$$A/F_{actual} = \frac{A/F_{stoich}}{\phi} \tag{B15}$$

$$A/F_{actual} = \frac{13.85}{0.6} = 23.08$$

Which can be expressed as;

$$A/F_{actual} = \frac{\rho_{air} * \dot{Q}_{air}}{\rho_{fuel} * \dot{Q}_{fuel}}$$

For a given air volumetric flow rate, $\dot{Q}_{air}$, of 124.1 l/min, the corresponding fuel flow rate would be (if standard density of air is assumed) :

$$\dot{Q}_{fuel} = \frac{A/F_{actual} * \rho_{air} * \dot{Q}_{air}}{\rho_{fuel}}$$

$$\dot{Q}_{fuel} = \frac{23.08 * 1.2 * 124.1}{805 * 1000} = 8.0\ ml/min$$

The ratio of fuel flow rate and atomizing air flow rate was kept constant at 0.6 [$(l/min_{air})/(ml/min_{fuel})$] through all the experiments. For a fuel flow rate of 8.0 ml/min the corresponding atomizing air flow rate is set to be 4.8 l/min. Subsequently the total air flow rate (atomizing + co-flow) was kept constant through all the experiments; the corresponding co-flow air flow rate was 119.3 l/min.

B.7 Carbon Input Rate

Carbon input rat was kept relatively constant for a given equivalence ratio, to calculate the amount of carbon brought into the reaction an example calculation for a BSA 10-10 flame at ϕ=0.6 is presented below.

Taking the molecular formula of BSA 10-10, $C_{11.3}H_{20.8}O_{0.3}$, and the fuel flow rate calculated in the previous section (8.0 ml/min) the carbon input rate is given as:

$$CIR = Y_{carbon} * \dot{m}_{fuel} \tag{B16}$$

or,

$$CIR = Y_{carbon} * \dot{Q}_{fuel} * \rho_{fuel} \tag{B17}$$

where Y_{carbon} is the mass fraction of carbon in the fuel, $\dot{m}_{fuel}$ is the mass flow rate of fuel [kg/s], $\dot{Q}_{fuel}$ is the volumetric flow rate of fuel [m^3/s] and ρ_{fuel} is the density of the fuel [kg/m^3].

Then for BSA 10-10 at ϕ=0.6;

$$CIR = \frac{11.3 * 12}{11.3 * 12 + 20.8 * 1 + 0.3 * 16} * 1.34 * 10^{-7} * 805$$

$$CIR = 9.05 * 10^{-5} kg/s$$

Appendix C: Nomenclature

English Symbols

A	Surface area	[m^2]
A/F	Air to fuel ratio	[kg_{air}/kg_{fuel}]
B	Bias error	[-]
EI_{CO}	Emission index of carbon monoxide	[g_{co}/kg_{fuel}]
EI_{NOx}	Emission index of nitric oxides	[g_{NOx}/kg_{fuel}]
F_V	Soot volume fraction	[ppm]
h	Flame Length	[cm]
hc	Convective heat transfer coefficient	[W/m^2*K]
I_o	Attenuated laser intensity	[mW]
I_s	Incident laser intensity	[mW]
I_f	Flame intensity	[mW]
k	Thermal conductivity	[W/m*K]
k_λ	Spectral extinction coefficient	[-]

LHV	Lower heating value	[J/kg]
MW	Molecular weight	[kg/kmol]
m	Mass	[kg]
$\dot{m}$	Mass flow rate	[kg/s]
Nu	Nusselt number	[-]
P	Precision error	[-]
Pr	Prandtl number	[-]
$\dot{Q}$	Volumetric flow rate	[l/min]
Re	Reynolds number	[-]
S_X	Standard deviation	[-]
T	Temperature	[K]
T_0	Initial temperature	[K]
T_{ad}	Adiabatic flame temperature	[K]
w	Uncertainty in a parameter	[-]
x	Axial distance	[mm]

Greek Symbols

δ	Flame thickness	[cm]
ϵ	Emissivity	[-]
λ	Wavelength	[nm]
μ	Dynamic viscosity	[$N*s/m^2$]
ρ	Density	[kg/m^3]
σ	Stefan Boltzmann constant	[$5.67*10^{-8}$ W/m^2K^4]
υ	Kinematic viscosity	[m^2/s]
ϕ	Equivalence ratio	[-]
χ	Mole fraction	[-]

Chemical Symbols

C	Carbon
CO	Carbon monoxide
CO_2	Carbon dioxide
H	Hydrogen
N	Nitrogen
NO	Nitric oxide
NOx	Nitric oxide (NO + NO2)
O	Oxygen
O_2	Oxygen (molecule)

List of Abbreviations

AME	Aerospace and Mechanical Engineering
BSA 10-10	80% Jet A, 10% SME, and 10% n-Butanol blend (by volume)
CIR	Carbon input rate
CPM	Combustion porous medium
EPM	Evaporation porous medium
PM	Porous Media
ppcm	Pores per centimeter
ppi	Pores per inch
SA10	90% Jet A and 10% SME (by volume)
SME	Soy methyl ester